The Role of Voltage-Gated Sodium Channel Gene *Scn1b* in the Developing Pediatric Heart

by

Nnamdi E. Edokobi

A dissertation submitted in partial fulfillment
of the requirements for the degree of
Doctor of Philosophy
(Pharmacology)
in the University of Michigan
2021

Doctoral Committee:

Professor Lori L. Isom, Chair
Associate Professor Arun Anantharam
Assistant Professor David Jones
Associate Research Scientist Luis Lopez-Santiago
Professor Jack Parent
Research Investigator Roberto Ramos-Mondragon

Nnamdi E. Edokobi

nedok@umich.edu

ORCID iD: 0000-0002-7253-2503

Acknowledgments

I first want to thank my mentor, Dr. Lori Isom, for believing in me even when I had failed to do so for myself. She has given me an extraordinary amount of support and guidance for over half a decade which has reshaped my mentality into a better student, a better researcher, and a better person. I met Lori during the 2013 summer research program as a student researcher. Through her patience and passion, I learned so much about cardiac physiology and pharmacology that this sparked my interest in becoming a researcher. However, I did not think I could ever be smart, wise, or disciplined enough to successfully complete a PhD. Nearing the end of summer, Lori mentioned that I should consider completing a doctorate degree to which I candidly responded, "I am not smart enough." In an instant she replied, "stop selling yourself short and trust me." Up until that point, I had not met an academic professor that juggled home responsibilities, lab, and professorship duties, while also managing to stay accessible and available to those they mentored. That day I knew that if I wanted the most out of life, I must complete a PhD under her guidance. Lori's influence on my research path does not stop with me, because of her guidance and my experiences my younger sisters are pursuing careers in medicine and clinical research. My family is forever thankful to Lori Isom.

I am extremely grateful for my thesis committee members: Drs. Arun Anantharam, David Jones, Luis Lopez-Santiago, Jack Parent, and Roberto Ramos-Mondragon. Their immense expertise in neuronal and cardiac physiology was vital in shaping my projects to adequately address my research questions.

My time in graduate school has been spent being pruned by many remarkable scientists: Dr. Luis Lopez-Santiago, Dr. Roberto Ramos-Mondragon, Dr. Yukan Yuan, Dr. Jacob Hull, Dr. Yanting Zhao, Dr. Rene Caballero-Floran, and Nick Denomme have all been critical to my

development as a scientist, and I am thankful for the time they spent training me. In addition, I need to recognize Dr. Alexandra Bouza, Dr. Samantha Hodges, Dr. Heather O'Malley, Dr. Chunling Chen, Yan Chen, Veronica Beck, Larissa Robinson-Cooper, Caroline Scheuing and the rest of the Isom lab for their dependability and friendship.

I would like to acknowledge my collaborators who either directly trained me on specialized techniques or assisted in completing vital experiments for my thesis. For that I thank: Dr. Sami Noujaim, Dr. Erica Levitt, Dr. Chandrika Canugovi, Dr. Tracy Qiao, Dr. Louis Dang, the University of Michigan Bioinformatics Core, Dr. Julie Philippe, Dr. Peng Li, Dr. Yao-Chang Tsan, Dr. Adam Helms, and Dr. Sarah Weckhuysen.

I am also grateful for assistance from the administration staff at the University of Michigan and their support in all aspects of graduate school those including Lisa Garber, Josh Daniels, Ingrid Shriner-Ward, Dar-Weia Liao, Dennis Ondreyka, Audrey Morton-Dziekan, Elizabeth Oxford, Michelle Melis, Michelle Dimondo, Edmund Graham, and Dr. Cherie Dotson.

As a graduate student, I have had the pleasure of mentoring William Anderson, William Abel, and Lena Juratli. They were remarkably talented undergraduate trainees, and I was fortunate to have them assist in the development or progression of my thesis work.

Service was a major aspect of my graduate education. I am thankful to the University of Michigan for funding which allowed me to help mentor children. Additionally, I am appreciative for my friendship with Sierra Nance and Tony Larkin. Since meeting them on a sponsored recruiting trip, we three have been involved in several Diversity, Equity, and Inclusion initiatives together. That friendship has now blossom into us starting a company, HBCU-DAP, which has opened my horizon to mentoring students nationwide.

I cannot forget the people that have guided me in the years before coming to Michigan and helped me form the basis of the person I have become. For their support, guidance, and faith

in me I want to mention: Lydia Laidlow, Matthew Quinn, Matt Miller, Breslaw, Peter Koumlelis, the MARC U*STAR and Meyerhoff program, Keith Harmon, Dr. Jacqueline King, Dr. Cynthia Wagner, Dr. Stephen Miller, and Dr. Laundette Jones. During different parts of my life these individuals have stepped up to help me achieve my dreams.

Finally, I would like to thank my family and the many friends for their support throughout my life and during my graduate career. I was born into a family that has endlessly supported my goals, path, and way of life. Mom and Dad, you have been my inspiration to see this degree through. You have worked painstakingly hard to carve a life in America for my sisters and me. You have made countless sacrifices that I can only now truly appreciate as an adult. Thank you, Mom and Dad, for being amazing and loving parents. My sisters, Nneoma and Ozioma, you both are wonderful women that inspire me. Anytime I think I am doing something impressive; you both find a way to top it! I am a proud older brother and continue to be amazed at the things you accomplish in life. Kristy, Tim, Jordan, Jess, Dawn, Emma, Dennis, and Adam thank you for accepting me into your wonderful family. To my fiancée, Madison Hanson, you are my rock. You have been so patient and loving with me during this journey. You never fail to make me laugh and enjoy living life. I am so grateful to have you in my life!

Table of Contents

List of Tables

List of Figures

Abstract

Sudden Unexpected Death in Epilepsy (SUDEP) is the most devastating consequence of epilepsy, yet little is understood about its causes and no biomarkers exist to identify at-risk patients. Although the underlying mechanism(s) of SUDEP are unclear, evidence suggests that in addition to the seizures, breathing abnormalities, autonomic dysfunction, and cardiac arrhythmias may all play a role. Variants in *SCN1B*, encoding voltage-gated sodium channel (Na_v) β1/β1B subunits, are linked to neurological and cardiovascular diseases that predispose patients to sudden premature death, including developmental and epileptic encephalopathy type 52 (DEE52, OMIM 617350), Brugada Syndrome 5 (OMIM 612838), and Atrial Fibrillation Familial 13 (OMIM 615377). Several studies published by our laboratory and others have demonstrated, using heterologous and native cells, that β1/β1B subunits are multi-functional proteins that play critical roles in cellular excitability, cell adhesion, and transcriptional regulation. The *Scn1b*-null mouse model exhibits neurological dysfunction, cardiac dysfunction, and premature death by the third week of life, highlighting the clinical relevancy of variants in this gene. The work presented in this thesis aimed to further our understanding about the role of *SCN1B* in cardiac pathophysiology. Although the mechanism of SUDEP is complicated, we hypothesize that *SCN1B* DEE52 variants predispose patients to underlying cardiac abnormalities, thereby, increasing their risk of SUDEP. This hypothesis is explored in the following chapters. The first chapter reviews Na_vs biochemistry and the role of α and β subunits in cardiac physiology. Chapter 2 focuses on the role of the *Scn1b* in the regulation of atrial physiology using the *Scn1b* null mouse model. We show differential expression of genes that are associated with atrial dysfunction in *Scn1b* null hearts. Remarkably, neonatal *Scn1b* null hearts showed a

significant accumulation of atrial collagen, increased susceptibility to pacing-induced AF *in vivo*, sinoatrial node dysfunction, and increased numbers of cholinergic neurons in ganglia that innervate the sinoatrial node. Administration of atropine reduced the incidence of AF in null mice, implicating autonomic influence. Finally, we found prolonged action potential duration and increased late sodium current density, with no change in transient sodium current density, in acutely isolated null atrial myocytes compared to wildtype. These results demonstrate a critical role for *Scn1b* in early postnatal atrial development. Chapter 3 presents work aimed to understand the mechanism of the *SCN1B*-linked DEE missense variant c.265c>T, predicting p.R89C, in heterologous cells and patient derived induced pluripotent stem cell cardiomyocytes (iPSC- CMs). In this detailed investigation, we determined that the patient iPSC- CMs have aberrant excitability, with similar properties as acutely isolated ventricular myocytes from *Scn1b*-null mice, including increased sodium current and action potential prolongation. Based on these findings, we concluded that the *SCN1B*-p.R89C variant may predispose patients to cardiac dysfunction in addition to severe epilepsy. This novel work provides important new insights into understanding the pathophysiological roles of Na_V-β1 subunits in human pediatric cardiac cells. Taken together, this work demonstrates that *SCN1B* loss of function significantly impacts the developing heart in addition to the developing brain.

Chapter 1. Voltage-Gated Sodium Channel β1/β1b Subunits Regulate Cardiac Physiology and Pathophysiology

(Portions of this chapter have been published in frontiers in Physiology 2018 doi: 10.3389/fphys.2018.00351. PMID: 29740331)

Nnamdi Edokobi and Lori L. Isom, PhD

Introduction

The heart is a rhythmic electromechanical pump facilitating the movement of blood, oxygen, and vital substances to the other body parts. It consists of excitable specialized cells called cardiomyocytes, which enable the heart to perform this vital physiological function. Cardiomyocyte electrical activity is attributed to the generation of cardiac action potentials, which are propagated through the coordinated signaling of ion channels (Nerbonne and Kass 2005). Changes in the expression, subcellular localization, or biophysical properties of ion channels can predispose the heart to potential life-threatening arrhythmias. Therefore, determining the mechanisms ion channels use to maintain normal cardiac rhythm is key to developing novel therapeutics for cardiac disorders.

Voltage-gated sodium channels (Na_vs) are essential for the initiation and propagation of action potentials in mammalian atrial myocytes, ventricular myocytes, and Purkinje cells (non-pacemaker cells) in the heart (Nerbonne and Kass 2005). Structurally, Na_vs are heterotrimeric

transmembrane proteins consisting of one pore-forming α subunit that is both covalently and non-covalently linked to two different β subunits (Isom, De Jongh et al. 1992, Catterall 2000, Morgan, Stevens et al. 2000, Calhoun and Isom 2014, O'Malley and Isom 2015) (Figure 1.1). Five β subunit proteins, encoded by four genes, have been identified in mammals (Isom, De Jongh et al. 1992, Makita, Bennett et al. 1994) and their functional loss can result in neuronal and cardiac channelopathies (O'Malley and Isom 2015). Originally, the β subunits were characterized as simple accessory proteins to α subunits. However, we now know that β subunits serve as critical links between the extracellular and intracellular signaling environments of cardiac and neuronal tissue through ion channel modulation, genetic regulation, and cell-cell adhesion. The aim of this chapter is to cover the current knowledge of β subunits in cardiac physiology and pathophysiology.

Na_v-α subunit

To understand β subunit physiology in heart, one must first consider the pore-forming α subunits. Mammalian genomes contain 9 Na_v-α subunits, encoded by the *SCN1-10A* genes (Catterall, Goldin et al. 2005). The α subunits contain all the machinery necessary for channel cell surface expression, ion conduction, voltage sensing, gating, and inactivation (Catterall 2012). The Na_v-α subunits transition between several conformations through the course of an action potential, including closed, open, and inactivated states (Savio-Galimberti, Gollob et al. 2012). At resting membrane potential, the channel is in the closed state, where no sodium ions are conducted. With sufficient depolarization, the channel can shift conformation to an open state. In this state sodium ions enter the cell and drive further depolarization of the membrane.

After transition to the open state, the channel rapidly inactivates. Fast inactivation, with a recovery time constant on the millisecond time scale, allows cells to repolarize and the channel to again become available for reactivation (de Lera Ruiz and Kraus 2015). Channels exposed to prolonged depolarization lasting seconds to minutes or following a long burst of high-frequency discharges can enter a slow inactivated state, with a recovery time constant from hundreds of milliseconds to tens of seconds, which regulates cellular excitability by reducing the number of channels available for activation (Silva 2014).

Na_v Structure

The Na_v-α subunit is a large protein, ~260kDa, consisting of 4 homologous domains (I-IV), each composed of 6 transmembrane segments (S1-S6) (Noda, Shimizu et al. 1984, Catterall 2000) (Figure 1.1). The S4 segment in each domain serves as a voltage sensor. These specialized transmembrane segments contain positively charge amino acids (arginine and lysine) in every third position (Catterall 2010). Neutralization of the positive charges in S4 transmembrane segments of all four domains results in altered channel gating (Stuhmer, Conti et al. 1989, , Kontis, Rounaghi et al. 1997, Marban, Yamagishi et al. 1998). At resting membrane potential, S4 segments are fixed in their inward position (Yang and Horn 1995, Yang, George et al. 1996, Bezanilla 2002). A depolarizing voltage pulse leads to a transient outward movement of the S4 in domains I-III (Yang and Horn 1995, Yang, George et al. 1996, Bezanilla 2002). The VSD is connected to the pore-forming module by an intracellular linker between transmembrane segments S4 and S5 of each domain. Motion of the S4 segments results in a conformational change that results in the opening of the channel pore (de Lera Ruiz and Kraus 2015). The S5

segment, S6 segment, and the extracellular connecting pore-loops (P-loops) of the four homologous domains have been shown to function together as the channel pore-forming module, containing the channel pore and the selectivity filter (Catterall 2012). A series of site-directed mutagenesis experiments showed that the selectivity filter, which distinguishes ions with similar charges and radii, is composed of 4 amino acid residues each contributed by the four homologous domains: aspartate (D) in DI, glutamate (E) in DII, lysine (K) in DIII, and alanine (A) in DIV (or DEKA) (Terlau, Heinemann et al. 1991, Heinemann, Terlau et al. 1992, Lipkind and Fozzard 2008). The outward movement of the voltage sensor opens the channel and exposes an intracellular binding site for the inactivation gate. Fast inactivation occurs through occlusion of the pore, thereby, blocking all ion conduction. The fast inactivation gate consists of a short loop on the intracellular side of the channel linking domains III and IV (Catterall 2000, Ulbricht 2005). The highly conserved hydrophobic amino acid motif isoleucine-phenylalanine-methionine (IFM) in the III-IV linker is essential for fast inactivation, as deletion of IFM resulted in a channel that failed to inactivate (Vassilev, Scheuer et al. 1988, Vassilev, Scheuer et al. 1989, West, Patton et al. 1992, Eaholtz, Colvin et al. 1999). Action potentials in nervous, cardiac, and skeletal muscle tissue are dependent on proper gating of Na_v-α subunits. Numerous gain- and loss-of-function variants in sodium channel α subunit genes have been linked to channelopathies, including epilepsy, cardiac arrhythmias, myotonia, and pain disorders. Thus, finding Na_v subtype-specific targeted therapies is currently an important area of research.

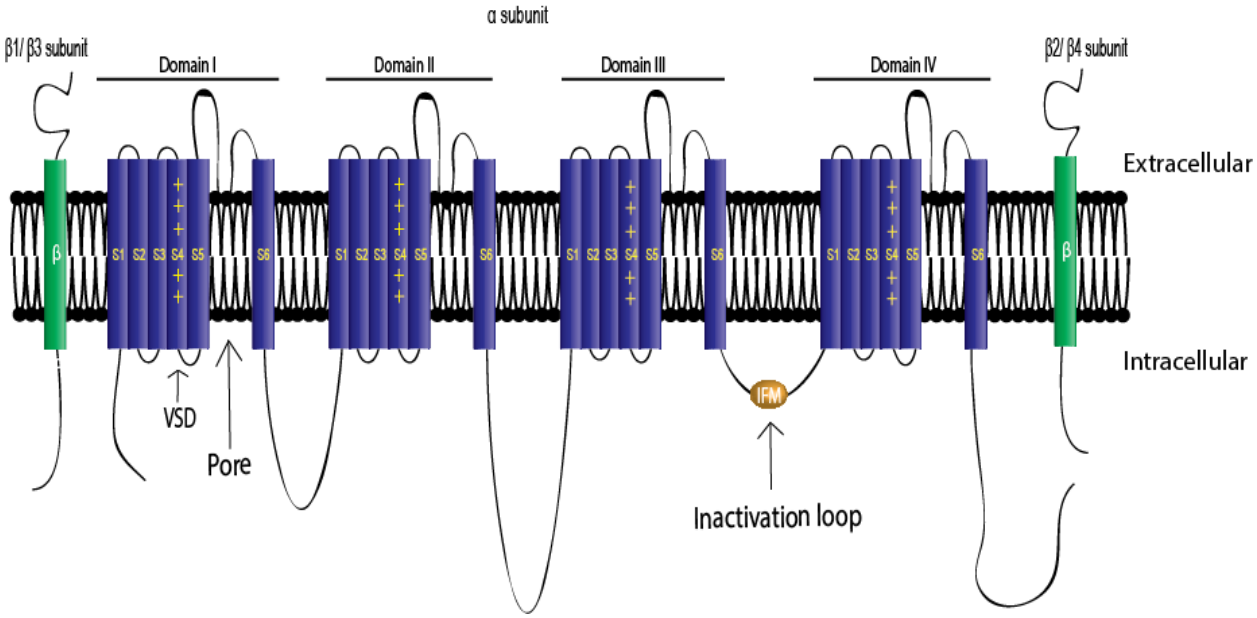

Figure 1.1 Topology of the Nav-α and -β subunits.

Na_vs contain a pore-forming α subunit consisting of four homologous domains of six transmembrane segments. The S4 segment of each Na_v-α subunit homologous domain forms the voltage sensing domain (VSD) and segments 5 and 6 in each domain create the ion-conducting pore. Three hydrophobic amino acids, IFM, form the inactivation gate (Catterall 2012). Na_vs also contain one or more β subunits. There are five β subunits, β1-β4, and the developmentally regulated β1B. β1-β4 all contain a large extracellular immunoglobulin (Ig) domain, single transmembrane domain, and an intracellular C-terminal domain. β1 and β3 are non-covalently linked to α, whereas β2 and β4 are covalently linked through disulfide bonds (Calhoun and Isom 2014).

Nine mammalin Na_v-α subunits subtypes have been identified and functionally characterized. The subtypes are highly identical in amino acid sequence and their functional properties are relatively similar (Catterall 2000). The α subunits subtypes can be catogorized by their sensitivy to tetrodoxin (TTX), a toxin isolated from the puffer fish. *SCN1A*/Na_v1.1, *SCN2A*/Na_v1.2, *SCN3A*/Na_v1.3, *SCN4A*/Na_v1.4, *SCN8A*/Na_v1.6 and *SCN7A*/Na_v1.7 are termed 'TTX-sensitive', as these channels are blocked by low nanomolar concentrations of TTX (Catterall 2012). In contrast, *SCN5A*/Na_v1.5, *SCN10A*/Na_v1.8, and *SCN9A*/Na_v1.9 require micromolar TTX concentrations for inhibition and are thus considered to be 'TTX-resistant' channels (Catterall 2012). TTX-resistant channels contain a cysteine residue in the selectivity filter at a position that is otherwise filled by an aromatic amino acid in TTX-sensitive channels (Satin, Kyle et al. 1992). Na_v-α subunits have been classified in the past by their tissue type expression, e.g. brain or heart, however, this type of classification is less useful as many Na_v-α subunits have been shown to be expressed in multiple tissue types. In addition, Na_v expression can change in pathophysiology. For example, in healthy cardiomyocytes, the TTX-resistant *SCN5A*/Na_v1.5 is the predominantly expressed α subunit and the primary contributor to recorded sodium current (I_{Na}) density (Rogart, Cribbs et al. 1989, Gellens, George et al. 1992, Kazen-Gillespie, Ragsdale et al. 2000, Maier, Westenbroek et al. 2002). In contrast, brain neurons predominantly express the TTX-sensitive Na_v-α subunits, *SCN1A*/Na_v1.1, *SCN3A*/Na_v1.3, and *SCN8A*/Na_v1.6. However, cardiomyocytes also express Na_v1.1, Na_v1.3, and Na_v1.6 (Dhar Malhotra, Chen et al. 2001, Maier, Westenbroek et al. 2002, Lopez-Santiago, Meadows et al. 2007, Auerbach, Jones et al. 2013) (Figure 1.2) in the transverse tubules (T-tubules) (Dhar

Malhotra, Chen et al. 2001, Lopez-Santiago, Meadows et al. 2007), where they are postulated to function in excitation-contraction coupling (Maier, Westenbroek et al. 2002). Likewise, Nav1.5 expression has been shown in the limbic system in brain (Hartmann, Colom et al. 1999). *SCN10A*/Na_v1.8, is an important contributor to Na_v conductance in dorsal root ganglia, nociceptive nerves, and cardiac nerves/ganglionated plexi (Odening 2019). In healthy cardiomyocytes it remains controversial whether *SCN10A*/Na_v1.8 is expressed in both cardiac neurons and cardiomyocytes (Odening 2019), however, in diseased hearts there is a significant upregulation of *SCN10A*/Na_v1.8 mRNA and protein in both cardiac tissue and cardiomyocytes (Dybkova, Ahmad et al. 2018, Odening 2019). In summary, the localization of Na_v-α subunits is highly regulated, and the fine-tuned control of Na_v expression is an important key in maintaining healthy tissue excitabilty.

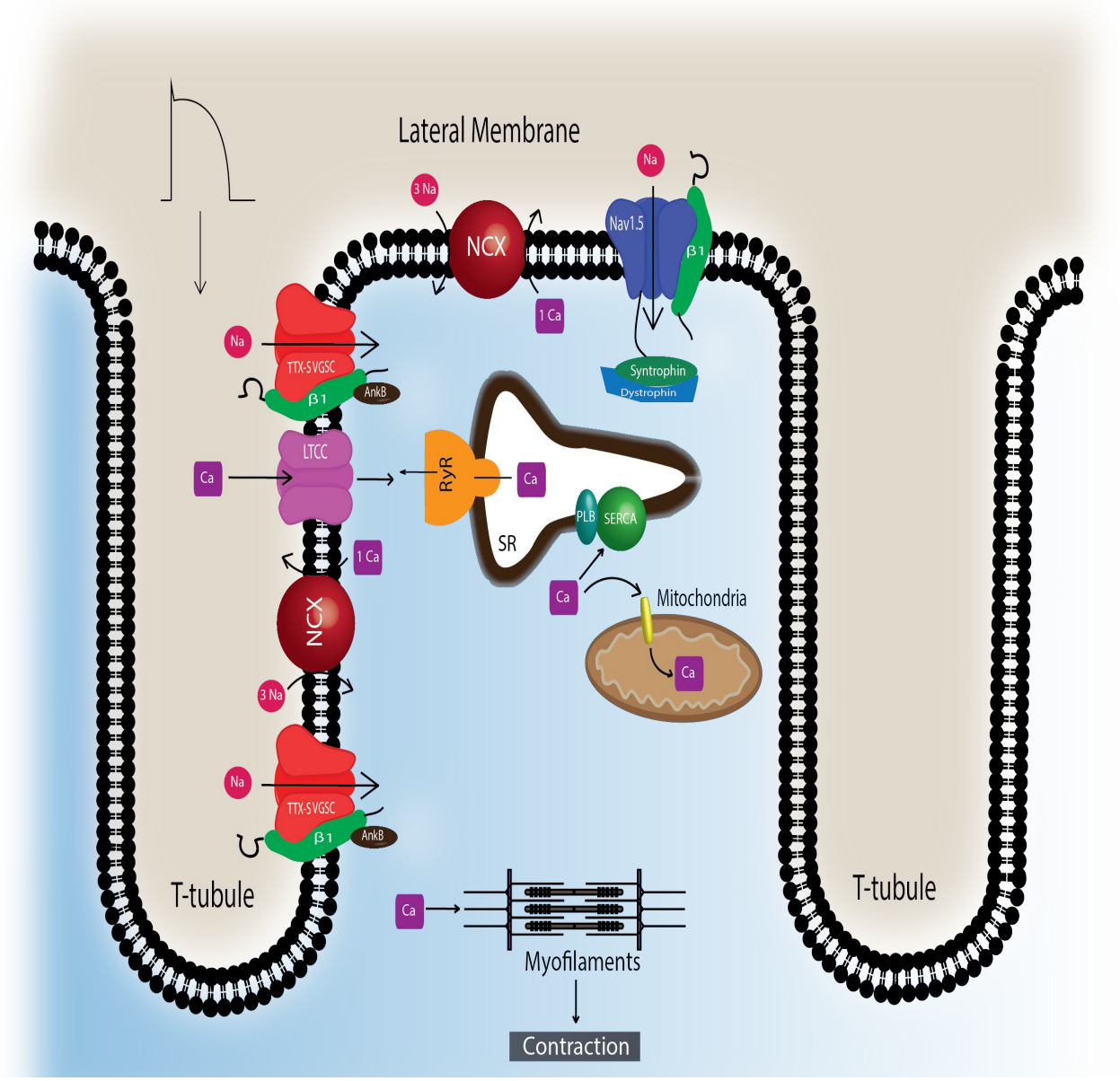

Figure 1.2 TTX-Sensitive Navs are localized to transverse tubules (T-tubules).

TTX-sensitive Na_vs, including $Na_v1.1$, $Na_v1.3$, and $Na_v1.6$, are located at the T-tubules of CMs where they are thought to participate in the regulation of excitation-contraction coupling. Non-phosphorylated Nav-β1 subunits are co-localized with TTX- sensitive Na_v-α subunits at the T-tubules where they play roles in calcium signaling and homeostasis. $Na_v1.5$ is localized at the lateral membrane as well as the ID (Figure 3). At the lateral membrane, $Na_v1.5$ is complexed with syntrophin and dystrophin. Abbreviations: L-type calcium channel (LTCC), phospholamban (PLB), ryanodine receptor (RyR), sarcoplasmic reticulum Ca2+-ATPase (SERCA), sodium-calcium exchanger (NCX), transverse tubules (T-tubule).

SCN5A/$Na_v1.5$: The predominant cardiac Na_v-α subunit

Cardiomyocytes associate at the intercalated disk (ID), where adherens junctions, gap junctions, and desmosomes participate in intercellular communication (Vermij, Abriel et al. 2017) (Figure 1.3A). $Na_v1.5$ channels cluster at cell-cell junction sites at the ID, where they co-localize with the cardiac gap junction (GJ) protein, connexin-43 (Cx43) (Maier, Westenbroek et al. 2002, Maier, Westenbroek et al. 2004) (Figure 1.3B). $Na_v1.5$ clustering is proposed to contribute to rapid AP conduction from cell-to-cell, similar to the node-to-node saltatory conducting function of TTX-sensitive Na_vs in myelinated nerves (Freeman, Desmazières et al. 2016).

Cytoskeletal integrity is a pre-requisite for normal electrical coupling. During cardiac development, GJ proteins and $Na_v1.5$ appear at the ID after formation of adherens junctions (Vreeker, van Stuijvenberg et al. 2014). The perinexus, a recently identified region of the ID, is defined as the area surrounding the plaque of functional GJs (Rhett, Veeraraghavan et al. 2013) (Figure 1.3B). Here, free connexons appear at the periphery of the GJ, after which they bind to zonula occludens1 (ZO-1). GJs form when ZO-1 free connexons from one cell associate with ZO-1 free connexons of a neighboring cell (Rhett, Jourdan et al. 2011). Disruption of Cx43/ZO-1 interactions increases GJ size (Hunter 2005), and in a ZO-1 null model, GJ plaques are larger (Palatinus, O'Quinn et al. 2010). Cx43 also interacts with $Na_v1.5$ in the perinexus (Rhett, Ongstad et al. 2012) (Figure 1.3B). The presence of $Na_v1.5$ at the perinexus may suggest that, in addition to GJ proteins, Na_vs may participate in coupling across the extracellular space, with increasing evidence supporting that both Cx43 and $Na_v1.5$ are necessary for cell-to-cell

transmission of Aps (Gutstein, Morley et al. 2001, Lin, Liu et al. 2011, Jansen, Noorman et al. 2012).

Ankyrin-G, a cytoskeletal adaptor protein, is necessary for normal expression of $Na_v1.5$ and coupling of the channel to the actin cytoskeleton (Mohler, Rivolta et al. 2004). A human *SCN5A* BrS variant eliminates $Na_v1.5$-ankyrin-G interactions (Mohler, Rivolta et al. 2004). This mutation, located in the $Na_v1.5$ DII–III loop, prevents channel cell surface expression in ventricular cardiomyocytes and alters channel properties. In agreement with this result, rat cardiomyocytes with reduced expression of ankyrin-G have reduced levels of $Na_v1.5$ expression and I_{Na} density. Abnormal $Na_v1.5$ localization can be rescued in ankyrin-G deficient cardiomyocytes through exogenous over-expression of ankyrin-G (Lowe, Palygin et al. 2008). Ankyrin-G recruits βIV spectrin, which forms important scaffolding structures and plays a role in the maintenance and integrity of the plasma membrane and cytoskeleton (Yang, Ogawa et al. 2007). βIV spectrin associates with and targets a subpopulation of Ca^{2+}/calmodulin-dependent protein kinase II (CaMKIIδ) to the ID to phosphorylate a critical serine residue in the $Na_v1.5$ I–II linker (Hund, Koval et al. 2010, Makara, Curran et al. 2014). Mouse cardiomyocytes expressing a mutant form of βIV spectrin show a positive shift in steady-state inactivation, elimination of late I_{Na}, shortened action potential duration (APD), and decreased QT intervals (Hund, Koval et al. 2010), confirming that formation of the $Na_v1.5$-ankyrin-G signaling complex is critical for maintaining normal cardiac excitability.

$Na_v1.5$ channels are also expressed at the cardiomyocyte lateral membrane, where they have distinct biophysical properties and binding partners from those at the ID. In ventricular

cardiomyocytes, $Na_v1.5$ at the lateral membrane forms a complex containing dystrophin and syntrophin (Figure 1.2), while $Na_v1.5$ at the ID complexes with the membrane-associated guanylate kinase (MAGUK) protein adapter protein, synapse-associated protein 97 (SAP97), and ankyrin-G (Petitprez, Zmoos et al. 2011) (Figure 1.3C). These results demonstrate that there are at least two distinct $Na_v1.5$ pools in cardiomyocytes. In heterologous cells, surface expression of $Na_v1.5$ is regulated by its interaction with SAP97 via a PDZ-domain (post-synaptic density protein-PSD95, disc large tumor suppressor-Dlg1, zonula occludens1-ZO1). Either the truncation of the fourth domain of $Na_v1.5$ (Shy, Gillet et al. 2014) or depletion of SAP97 (Matsumoto, Fujikawa et al. 2012) results in reduced channel cell surface expression, with a subsequent decrease of I_{Na}.

$Na_v1.5$ also interacts with fibroblast growth factor homologous factor 1B (FHF1B) (Liu, Dib-Hajj et al. 2003), calmodulin (Kim, Ghosh et al. 2004, Young and Caldwell 2005), Nedd4-like-ubiqutin-protein ligases (Van Bemmelen, Rougier et al. 2004, Rougier, van Bemmelen et al. 2005), and can be phosphorylated by Fyn (Ahern, Zhang et al. 2005), a src family tyrosine kinase. All of these interacting proteins are involved in the regulation of channel subcellular localization and activity. Taken together, these results accentuate the idea that Na_vs associate with protein complexes that are specific to subcellular domains, and these interactions are critical to cardiac physiology. Undoubtedly, changes in one component of a given complex results in significant consequences to overall cardiac excitability and synchrony.

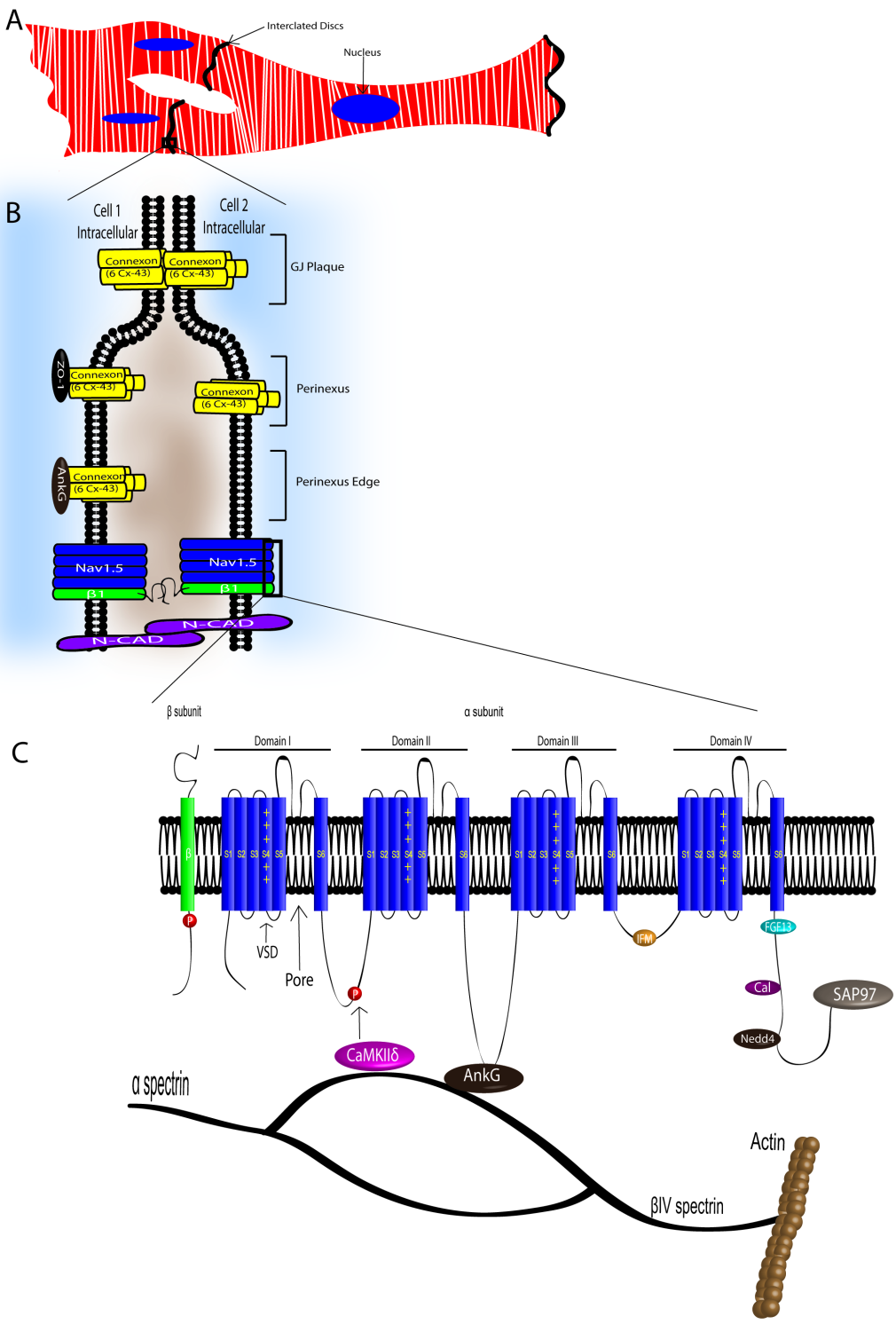

Figure 1.3. Nav complexes at the cardiac intercalated disk.

CMs associate at the ID, where $Na_v1.5$, Na_v-β1 subunits, adherens junctions, gap junctions, and desmosomes define intercellular communication. **(A)** Associated CMs. **(B)** Proposed model of the GJ plaque, perinexus, and perinexus edge. Na_v-β1 subunits at the ID are tyrosine phosphorylated, possibly through Fyn kinase activation, and may function in cell–cell adhesion in the perinexus and perinexus

edge. **(C)** At the ID, $Na_v1.5$ associates with a multi-protein complex. Abbreviations: Ankyrin-G (AnkG), Calmodulin (Cal), Ca2+/calmodulin-dependent protein kinase II (CaMKIIδ), Fibroblast growth factor homologous factor 1B (FHF1B), N-Cadherin (N-Cad), Nedd4-like-ubiqutin-protein ligases (Nedd4), Synapse-associated protein 97 (SAP97).

Interacting protein	**Effects on $Na_v1.5$**	**Reference(s)**
Ankyrin-G (AnkG)	Proper expression at plasma membrane and coupling to actin cytoskeleton	(Mohler, Rivolta et al. 2004)
Calmodulin (Cal)	Regulates biophysical properties	(Tan, Kupershmidt et al. 2002, Kim, Ghosh et al. 2004, Young and Caldwell 2005, Gabelli, Boto et al. 2014)
Ca^{2+}/calmodulin-dependent protein kinase II (CaMKIIδ)	Phosphorylation and modulates excitability	(Hund, Koval et al. 2010, Makara, Curran et al. 2014)
Fibroblast growth factor homologous factor 1B (FHF1B)	Modulate channel gating	(Liu, Dib-Hajj et al. 2003)
Nedd4-like-ubiqutin-protein ligases (Nedd4)	Ubiquitination and regulated internalization. Possible mechanism in modulation of channel density at the plasma membrane	(Van Bemmelen, Rougier et al. 2004, Rougier, van Bemmelen et al. 2005)
Synapse-associated protein 97 (SAP97)	Stability and anchoring to the cell membrane	(Petitprez, Zmoos et al. 2011, Matsumoto, Fujikawa et al. 2012)

Table 1.1. Nav1.5 Intercalated Disk interacting proteins.

Na_v-β subunits

Na_v heterotrimer complex consists of an Na_v-α subunit that is both covalently and non-covalently linked to two different Na_v-β subunits (Isom, De Jongh et al. 1992, Catterall 2000, Calhoun and Isom 2014, O'Malley and Isom 2015). Each Na_v-β subunit (*SCN1B*/β1 and β1B, *SCN2B*/β2, *SCN3B*/β3, *SCN4B*/β4) has been identified in mammalian heart in both chambers (atria and ventricle) (Zhu, Wang et al. 2021). Na_v-β1, -β2, -β3, and -β4 are transmembrane proteins with type 1 topology consisting of an extracellular N-terminus containing a heavily glycosylated immunoglobulin (Ig) domain that is approximately one-third of the total protein molecular mass, a transmembrane segment, and an intracellular C-terminus (Calhoun and Isom 2014) (Figure 1.4). Na_v-β1B, which was originally called β1A (Kazen-Gillespie, Ragsdale et al. 2000)), is a *SCN1B* splice variant formed through the in-frame retention of intron 3. This splice variant contains the Na_v-β1 N-terminal and Ig domains, but has a distinct C-terminal domain that lacks a transmembrane segment (Kazen-Gillespie, Ragsdale et al. 2000), resulting in a secreted cell adhesion molecule (Patino, Brackenbury et al. 2011). Na_v-β1, Na_v-β1B, and Na_v-β3 associate non-covalently with α subunits via their N- and C-termini (McCormick, Isom et al. 1998, Meadows, Malhotra et al. 2001). In contrast, Na_v-β2 and Na_v-β4 interact covalently with α subunits via a single cysteine located in the N-terminal, extracellular Ig loop (Chen, Calhoun et al. 2012, Gilchrist, Das et al. 2013). While the pore forming α subunits are sufficient for ion conduction, Na_v-β subunits regulate I_{Na} density, kinetics, voltage-dependence of activation and inactivation, and levels of Na_v-α subunit cell surface expression (Calhoun and Isom 2014). Heterologous expression systems and mouse models have shown that Na_v-β subunits modulate α

subunits in cell type specific manners, thus the Na_v-α/β subunit composition of a given cell confers unique biophysical properties that can be finely tuned.

Variants in *SCN1B* (Kazen-Gillespie, Ragsdale et al. 2000, Patino, Brackenbury et al. 2011), are implicated in a variety of inherited pathologies including developmental and epileptic encephalopathy (DEE) (O'Malley and Isom 2015), Brugada syndrome (BrS) (Watanabe, Koopmann et al. 2008, Hu, Barajas-Martínez et al. 2012), long-QT syndrome (LQTS) (Riuró, Campuzano et al. 2014), atrial arrhythmias (Watanabe, Darbar et al. 2009), and sudden infant death syndrome (SIDS) (Hu, Barajas-Martínez et al. 2012, Neubauer, Rougier et al. 2018) (Figure 1.4 and Table 1.2). Regardless of disease etiology, patients with *SCN1B* variants have an increased risk of sudden death. The reminder of this chapter will concentrate on *SCN1B*; however, it is important to understand that variants in *SCN2B, 3B, and 4B* are also linked to diseases such as cancer, cardiac conduction disorders, and neurological diseases, signifying the importance of Na_v-β subunits in physiology.

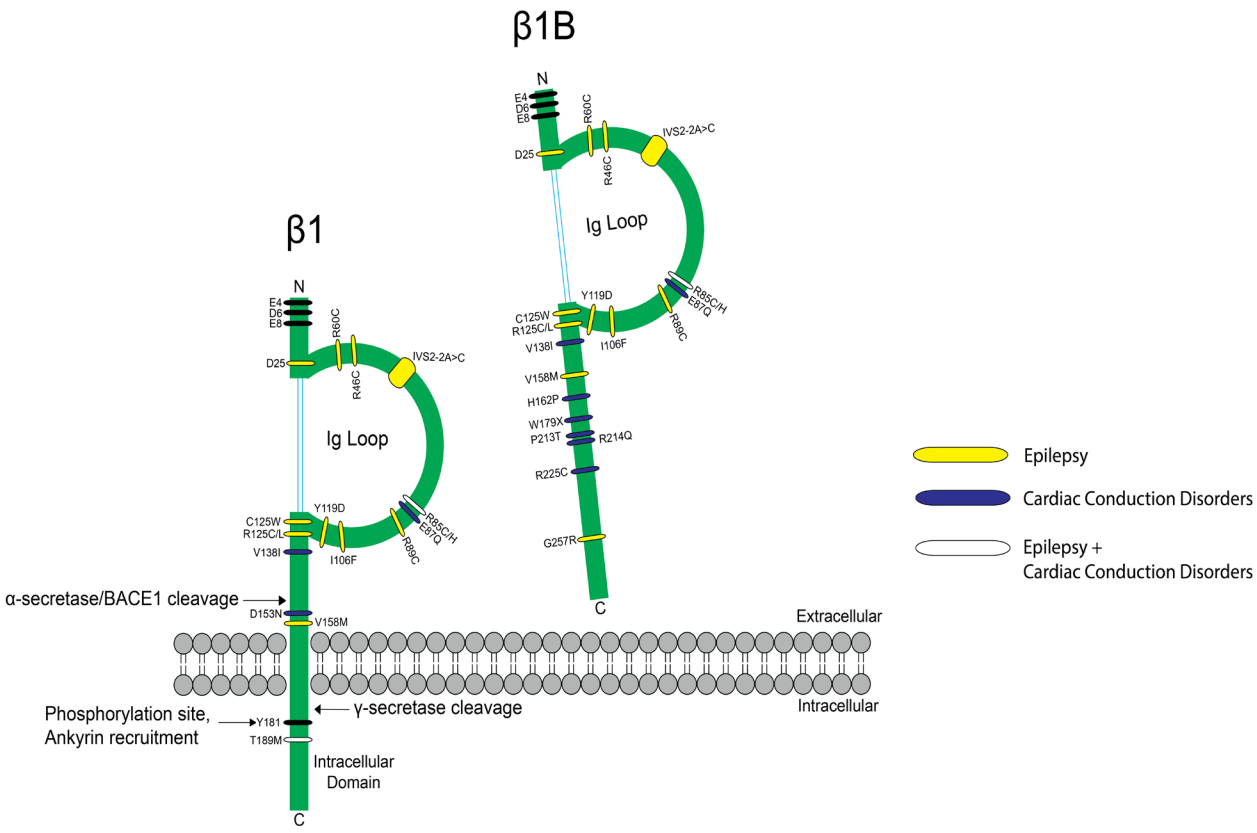

Figure 1.4. *SCN1B* variants are linked to epilepsy syndromes and cardiac conduction diseases.

SCN1B encodes Na_v-β1 (left) and its secreted splice variant Na_v-β1B (right). Sites for ankyrin binding, phosphorylation, and proteolytic cleavage are indicated. Ig: immunoglobulin. Human disease variants in β1 or β1B are indicated in yellow, blue, white and are described in Table 1. Adapted from (O'Malley and Isom 2015)

Disease	β1	β1B
Atrial fibrillation	R85H (Watanabe, Darbar et al. 2009), D153N (Watanabe, Darbar et al. 2009)	R85H (Watanabe, Darbar et al. 2009), D153N (Watanabe, Darbar et al. 2009)
Brugada syndrome	E87Q (Watanabe, Koopmann et al. 2008)	E87Q (Watanabe, Koopmann et al. 2008), H162P (Holst, Saber et al. 2012), W179X (Watanabe, Koopmann et al. 2008), R214Q (Holst, Saber et al. 2012, Hu, Barajas-Martínez et al. 2012)
Developmental and Epileptic Encephalopathy (DEE) /Dravet syndrome	I106F (Ogiwara, Nakayama et al. 2012), Y119D (Ramadan, Patel et al. 2017), C121W (Wallace, Wang et al. 1998), R125C (Patino, Claes et al. 2009), R85C (Aeby, Sculier et al. 2019), R89C (Darras, Ha et al. 2019), R46C (Scala, Efthymiou et al. 2021), R60C (Scala, Efthymiou et al. 2021)	I106F (Ogiwara, Nakayama et al. 2012), Y119D (Ramadan, Patel et al. 2017), C121W (Wallace, Wang et al. 1998), R125C (Patino, Claes et al. 2009), R85C (Aeby, Sculier et al. 2019), R89C (Darras, Ha et al. 2019), R46C (Scala, Efthymiou et al. 2021), R60C (Scala, Efthymiou et al. 2021)
Generalized Epilepsy with Febrile Seizures Plus (GEFS+)	D25N (Orrico, Galli et al. 2009), R85H (Scheffer, Harkin et al. 2006), R125L (Fendri-Kriaa, Kammoun et al. 2011), five amino acid deletions (IVS2-2A>C) (Audenaert, Claes et al. 2003)	D25N (Orrico, Galli et al. 2009), R85H (Scheffer, Harkin et al. 2006), R125L (Fendri-Kriaa, Kammoun et al. 2011), five amino acid deletions (IVS2-2A>C) (Audenaert, Claes et al. 2003)
Idiopathic epilepsy		G257R (Patino, Brackenbury et al. 2011)
Sudden Infant Death Syndrome		R214Q (Hu, Barajas-Martínez et al. 2012), R225C (Neubauer, Rougier et al. 2018)
Sudden Unexpected Nocturnal Death Syndrome	V138I (Liu, Tester et al. 2014), T189M (Liu, Tester et al. 2014)	V138I (Liu, Tester et al. 2014)
Long QT Syndrome		P213T (Riuró, Campuzano et al. 2014)

Table 1.2. *SCN1B* variants linked to human disease.

Na_v-β1 post-translational modifications

Na_v-β subunits undergo multiple post-translational modifications including glycosylation, phosphorylation, proteolytic cleavage, and palmitoylation. All Na_v-β subunits have highly glycosylated N-terminal domains, containing 3 to 4 N-linked glycosylation sites each (Isom, De Jongh et al. 1992, McCormick, Isom et al. 1998, Johnson, Montpetit et al. 2004). Na_v-β subunit glycosylation impacts their surface expression and channel modulatory properties (Johnson, Montpetit et al. 2004).

The Na_v-β1 intracellular domain is phosphorylated at tyrosine (Y) residue 181 (Figure 1.4). Using a fyn kinase assay with a peptide representing the β1 wild-type (WT) intracellular domain as substrate resulted in increased fyn kinase activity over the no-substrate control. In contrast, fyn kinase activity levels were not different from no-substrate control when a peptide representing the β1 phosphomimetic, β1-p.Y181E, intracellular domain was used as substrate (Bouza, Philippe et al. 2020). These results supported our hypothesis (Brackenbury, Davis et al. 2008) that fyn kinase directly phosphorylates the β1 intracellular domain at position Y181. Human Embryonic Kidney (HEK) cells stably expressing $Na_v1.5$ transiently transfected with β1-WT or the phosphomimetic constructs, β1-p.Y181A or β1-p.Y181E, increased I_{Na} compared to Na_v-α alone. Interestingly, despite normal membrane localization and cell adhesive activity, β1-p.Y181F did not increase I_{Na} over control levels. These results suggest that the ability of Na_v-β1 to increase $Na_v1.5$-generated $I_{Na,}$ occurs independently of the tyrosine phosphorylation state of Na_v-β1 intracellular domain. However, why β1-p.Y181F retains normal cell adhesive function

but not I_{Na} modulation remains unanswered. In cardiomyocytes, tyrosine-phosphorylated Na_v-β1 and non-phosphorylated Na_v-β1 are differentially localized to subcellular domains where they interact with specific cytoskeletal and signaling proteins (Malhotra, Thyagarajan et al. 2004). At the T-tubules, non-phosphorylated Na_v-β1 interacts with TTX-sensitive Na_vs and ankyrin-B (Malhotra, Thyagarajan et al. 2004). In contrast, tyrosine-phosphorylated Na_v-β1 is localized to the ID where it interacts with $Na_v1.5$ and N-cadherin (Malhotra, Thyagarajan et al. 2004). Phosphorylation may be a signaling mechanism by which cardiomyocytes regulate the density and localization of Na_v-β1 at specific subcellular domains. Whether phosphorylation targets Na_v-β1 to subcellular regions in cardiomyocytes or whether Na_v-β1 is differentially phosphorylated upon arrival to those subcellular regions is important to understand this signaling mechanism in cardiomyocytes.

Na_v-β subunits are targets for sequential proteolytic cleavage by BACE1 and γ-secretase, resulting in the release of N-terminal and C-terminal domains (Wong, Sakurai et al. 2005, Patino, Brackenbury et al. 2011, Bouza, Edokobi et al. 2021), a process referred to as Regulated Intramembrane Proteolysis (RIP) (Lal and Caplan 2011). These cleavage products have important physiological effects on transcriptional regulation of genes. For example, cleavage of Na_v-β2 in neurons *in vitro* leads to translocation of a soluble intracellular domain (ICD) to the nucleus, where it increases *SCN1A* mRNA and $Na_v1.1$ protein expression (Kim, Carey et al. 2007). Cleavage of Na_v-β1, results the similar generation of a soluble ICD that translocates to the nucleus (Bouza, Philippe et al. 2020, Bouza, Edokobi et al. 2021). Importantly, RIP of Na_v-β1 occurs independently of the phosphorylation state of Na_v-β1 residue Y181. In cardiomyocytes, it was determined that the β1-ICD may function as a molecular brake on the expression of genes

involved in excitation-contraction coupling (Bouza, Edokobi et al. 2021). The signaling mechanisms involved in regulating Na_v-β1 RIP-excitation coupling increases our knowledge of modulatory mechanisms of β1 function *in-vivo* and provides novel potential therapeutic targets for drug discovery to treat *SCN1B*-linked channelopathies.

Lastly, Na_v-β1 subunits are S-palmitoylated. Mutation of a single residue in Na_v-β1, cysteine (C) 162 to alanine (A), prevents palmitoylation, reduces the level of Na_v-β1 polypeptides at the plasma membrane, and results in a reduction in the extent of β1 RIP, suggesting that the plasma membrane is the site of Na_v-β1 proteolytic processing (Bouza, Philippe et al. 2020). Despite the biochemical changes, β1-p.C162A co-expression with Nav1.5 increased I_{Na}, similar to WT-β1 (Bouza, Philippe et al. 2020). Thus, some post-transcriptional modifications may not alter α-β1 subunit interactions, but instead affect Na_v-β1 membrane localization and downstream signaling in the absence of α subunit co-expression. It will be interesting to determine whether phosphorylation and palmitoylation alter WT-β1 interactions with Na_v-α subunit subtypes in addition to $Na_v1.5$.

Na_v-β1 is more than accessory

Na_v-β subunits are now recognized as multifunctional proteins (O'Malley and Isom 2015) that are involved in a variety of cellular functions. Na_v-β subunits are Ig superfamily cell adhesion molecules (CAMs) that facilitate cell-cell communication and initiate intracellular signaling cascades. Na_v-β1 and -β2 participate in *trans*-homophilic cell adhesion, resulting in the recruitment of ankyrin-G to the plasma membrane at sites of cell-cell contact (Malhotra, Kazen-

Gillespie et al. 2000). Importantly, at least *in vitro*, this occurs both in the presence and absence of α subunits. Na_v-β1 and -β2 also participate in cell–matrix adhesion, binding tenascin-R and tenascin- C to modulate cell migration (Srinivasan, Schachner et al. 1998, Xiao, Ragsdale et al. 1999). Na_v-β3 does not function as a *trans* homophilic CAM when expressed in non-adherent *Drosophila* S2 cells, as shown for Na_v-β1 and -β2 (McEwen, Chen et al. 2009). In contrast, Na_v-β3 does participate in cell adhesion when expressed in mammalian cells, where *trans* homophilic adhesion was shown to require an intramolecular Cys2–Cys24 disulfide bond that maintains the integrity of the Ig domain, suggesting that this bond may not be formed correctly in insect cells (Yereddi, Cusdin et al. 2013). Finally, the secreted Na_v-β1B *SCN1B* splice variant functions as a CAM ligand to promote signal transduction in cultured neurons (Patino, Brackenbury et al. 2011).

Na_v-β1 cell adhesive activity has been implicated in neuronal development *in vivo*. β1-β1 trans homophilic cell adhesion mediates neurite outgrowth in WT cerebellar granular neurons (CGNs) in culture (Davis, Chen et al. 2004). Neurite length was significantly longer when WT CGNs, expressing Na_v-β1, were grown on a monolayer of fibroblasts that also expressed β1, compared to WT neurons grown on a control fibroblast monolayer that did not express β1. Consistent with this result, *Scn1b* null CGN neurite length was not increased over controls, regardless of β1 expression in the cell monolayer. *Scn1b* null mouse optic nerve, spinal cord, and sciatic nerve nodes of Ranvier have abnormal architecture (Chen, Westenbroek et al. 2004). In WT mouse cerebellum, CGN axons project from the granule layer to the molecular layer, where they form parallel fibers. In contrast, *Scn1b* null mouse CGN axons are defasiculated and have aberrant pathfinding, forming a disrupted molecular layer (Brackenbury, Davis et al. 2008,

Brackenbury, Yuan et al. 2013). Abnormal pathfinding and defasiculation were also observed in the *Scn1b*-null corticospinal tract and hippocampus (Brackenbury, Davis et al. 2008, Brackenbury, Yuan et al. 2013). Thus, *Scn1b* plays a critical role in neuronal development and pathfinding.

In the heart, the subcellular localization of Na_v-β1 to the intercalated disk suggests a role for this subunit in cardiac cell–cell communication. *Scn1b* and *Scn5a* have overlapping, but not identical, temporal and spatial expression profiles during heart development (Domínguez, Navarro et al. 2005). In ventricular myocytes, Na_v-β1 is co-localized to the ID (Kaufmann, Westenbroek et al. 2010) with $Na_v1.5$ (Maier, Westenbroek et al. 2004), as well as to the T-tubules with TTX-sensitive Na_v-α subunits (Malhotra, Kazen-Gillespie et al. 2000, Lopez-Santiago, Meadows et al. 2007, Lin, O'Malley et al. 2015). More recent evidence showed that β1-mediated cell-cell adhesion occurs at the perinexal membrane, a specialized area of ID, and that this interaction can be acutely inhibited by βadp1, a novel peptide mimetic of the Na_v-β1 extracellular CAM domain (Veeraraghavan, Hoeker et al. 2018). Dose-dependent administration of βadp1 decreased cellular adhesion in heterologous Na_v-β1-overexpressing fibroblasts. 75% of βadp1-treated hearts exhibited spontaneous ventricular tachycardias, revealing preferential slowing of transverse conduction. Importantly, *Scn1b* null mouse ventricles displayed striking evidence of perinexal de-adhesion, similar to normal hearts treated with βadp1 (Veeraraghavan, Hoeker et al. 2018). These data support a role for *trans* β1-β1 mediated cell-cell adhesion in ventricular myocytes and suggest a mechanistic role for adhesion in AP conduction. Importantly, in addition to cardiomyocytes, Na_v-β1 subunits are expressed in cardiac fibroblasts and preliminary results suggest that Na_v-β1 is expressed in cardiac neurons (not shown). Thus,

because a large proportion of *SCN1B* variants affect the Ig domain (O'Malley and Isom 2015), it is likely that disruption of β1-β1 mediated cell-cell adhesion *in vivo* contributes to cardiac disease mechanisms and, if so, that restoring adhesion may be a future therapeutic target.

Na_v-β1 modulation of $Na_v1.5$

Na_v-β1 and -β1B modulation of $Na_v1.5$ varies depending on the model system studied. In *Xenopus* oocytes, the amplitude of $Na_v1.5$-expressed I_{Na} increases with increasing amounts of Na_v-β1 mRNA (Qu, Isom et al. 1995). Antisense-mediated post-transcriptional silencing of *Scn1b* in H9C2, a cardiomyocytes cell line, alters both TTX-sensitive and TTX-resistant Na_v-α mRNA and protein expression, resulting in decreased I_{Na} (Baroni, Picco et al. 2014). In contrast, *Scn1b* null ventricular mouse cardiomyocytes have increased expression of *Scn3a* and *Scn5a*, along with increased TTX-sensitive and TTX-resistant I_{Na} (Lopez-Santiago, Meadows et al. 2007, Lin, O'Malley et al. 2015, Bouza, Edokobi et al. 2021). These results suggest that Na_v-β1 subunits are involved in acute and long-term mechanisms that differentially control expression and function of Na_v-α subunits.

In heterologous cells, Na_v-β1 or -β1B co-expression with $Na_v1.5$ increases I_{Na} compared to Nav1.5 alone by increasing channel expression at the plasma membrane (Watanabe, Koopmann et al. 2008, Casini, Tan et al. 2010, Hu, Barajas-Martinez et al. 2012, Riuró, Campuzano et al. 2014, Yuan, Koivumaki et al. 2014, Bouza, Philippe et al. 2020, Martinez-Moreno, Selga et al. 2020, Wang, Han et al. 2020, Bouza, Edokobi et al. 2021). Thus far, *SCN1B* epilepsy or cardiac arrhythmia variants that alter the Na_v-β1 or -β1B coding sequence (Figure 1,

Table 1.2) generally result in loss-of-function in terms of the ability to increase I_{Na} density, with varying effects on channel gating and kinetic properties. While we have information on the loss-of-function effect of the β1-p.C121W mutation on cell-cell adhesion (Meadows, Malhotra et al. 2002), these experiments have not been performed for other variants. This functional information will be critical to understanding the disease phenotype in patients.

While the Na_v-α subunits are known to form and function as monomers, evidence suggests that $Na_v1.5$ can also form dimers under certain situations, and that dimerization is mediated through an interaction site within the first intracellular loop (Clatot, Hoshi et al. 2017). Na_v-α subunit dimers display coupled gating properties, which are mediated through the action of 14-3-3 proteins (Clatot, Hoshi et al. 2017). The 14-3-3 family of proteins is important for the regulation of cardiac I_{Na} and disrupted 14-3-3 expression may exert pro-arrhythmic effects on cardiac electrical properties (Allouis, Le Bouffant et al. 2006, Sreedhar, Arumugam et al. 2016). The functional importance of $Na_v1.5$ dimerization may be to target and enhance the density of channels at specific subcellular domains. Interestingly, $Na_v1.5$-R1432G, a surface localization defective *SCN5A* mutant, displays a dominant negative effect on WT $Na_v1.5$ only in the presence of the Na_v-β1 subunit (Mercier, Clément et al. 2012). Thus, Na_v-β1 may promote interactions between WT $Na_v1.5$ and mutant Na_v-α subunits, leading to a dominant negative effect. Importantly, interpretation of these data should be taken with caution as Na_v-β subunits are multifunctional proteins, and native tissue/cells express a variety of interacting proteins that are critical to Na_v-β subunits full function.

Na_v-β1 modulation of potassium channels

Cardiac potassium channels (K_vs) are vital in repolarizing non-pacemaker cells and in setting the resting membrane potential in all cardiac cells. During non-pacemaker cell APs in the heart, transient outward potassium current (I_{to}) contributes to rapid repolarization during phase 1 (Nerbonne and Kass 2005). The delay observed in rapid repolarization during phase 2 involves outward rectifying potassium currents (I_{Kur}, I_{Kr}, and I_{Ks}) and accelerated repolarization during phase 3 is mediated by inward rectifying potassium currents (I_{K1}, I_{KAch}, and I_{KATP}) (Nerbonne and Kass 2005). At the end of phase 3, inward rectifying potassium currents play an important role in setting the resting membrane potential (Nerbonne and Kass 2005). Interestingly, Na_v-β1 can interact with and modulate voltage gated K_vs in addition to Na_vs. Thus, Na_v-β1 subunit multifunctionality may allow for crosstalk between different ion channel types to regulate excitability in cardiomyocytes.

K_v-α subunits assemble as tetramers that normally associate with modulatory Kv-β subunits (Snyders 1999). The K_v4.x subfamily of channels express rapidly activating, inactivating, and recovering cardiac I_{to} (Snyders 1999). Heterologous co-expression of Na_v-β1 with K_v4.3 results in a ~four-fold increase in I_{to} density (Deschênes and Tomaselli 2002). Additionally, Na_v-β1 alters the voltage-dependence and kinetics of channel gating compared to K_v4.3 expressed alone (Deschenes and Tomaselli 2002). Na_v-β1B can also associate with K_v4.3 in heterologous systems, resulting in increased I_{to} (Hu, Barajas-Martinez et al. 2012). Importantly, Na_v-β1 associates with K_v4.2 and enhances its surface expression in heterologous systems (Marionneau, Carrasquillo et al. 2012). Whole-cell voltage-clamp recordings obtained

from cells expressing K_v4.2 with Na_v-β1 resulted in higher I_{to} densities compared to K_v4.2 alone (Marionneau, Carrasquillo et al. 2012). Na_v-β1 can also interact with and modulate K_v1 (K_v1.1, K_v1.2, K_v1.3, or K_v1.6) and K_v7 (K_v7.2) channels (Nguyen, Miyazaki et al. 2012). *In vivo*, K_v-α modulation by β1/β1B is cell type dependent. *Scn1b* null dorsal root ganglion (DRG) neurons are hyperexcitable and have decreased levels of I_{to} (Lopez-Santiago, Brackenbury et al. 2011). *Scn1b* null ventricular CMs exhibit increased I_{to}s, $I_{K\ slow}$, and I_{ss} as well as altered expression of K_v genes. Acute silencing of Na_v-β1 subunits in neonatal rat ventricular myocytes with siRNA targeting significantly reduced the expression of K_v4.x protein and reduced both I_{Na} and I_{to} (Deschênes, Armoundas et al. 2008). These data highlight the idea that acute vs. constitutive reduction of *Scn1b* expression *in vivo* will result in differential modulation of ionic currents.

Similar to Na_v1.5, Kir2.x channels, conducting the inward rectifier current I_{K1}, contain a C-terminal PDZ-binding domain which mediates interaction with SAP97 and syntrophin (Matamoros, Perez-Hernández et al. 2016). Data suggest that Kir2.x channels associate in microdomains that include caveolin 3, Na_v1.5, SAP97, and syntrophin (Vaidyanathan, Vega et al. 2013). Na_v1.5 interacts with α1-syntrophin via an internal N-terminal PDZ-like binding domain in addition to the C-terminal PDZ-binding domains (Matamoros, Perez-Hernández et al. 2016). Importantly, Na_v1.5-β1 co-expression increases Kir2.1 and Kir2.2, but not Kir2.3, currents, again suggesting that these channels are functionally linked and that β1 is critical to the formation of multi-ion channel complexes.

Scn1b-mediated regulation of cardiac physiology

Animal models have been instrumental in understanding the role of *Scn1b* in excitability. *Scn1b* deletion in mice results in severe seizures, ventricular arrhythmias, and sudden death prior to weaning (Chen 2004). *Scn1b* null ventricular cardiomyocytes exhibit prolonged AP repolarization, increased *Scn5a*/$Na_v1.5$ expression, increased *Scn3a*/$Na_v1.3$ expression, increased transient and persistent (late) I_{Na} density, and prolonged QT and RR intervals on the ECG (Lopez-Santiago, Meadows et al. 2007). Additionally, *Scn1b* null ventricular cardiomyocytes have increased I_K and decreased calcium currents (I_{Ca}), potentially mediated by a combination of changes in gene expression and loss of β1/β1B interaction with those ion channels (Bouza, Edokobi et al. 2021). Consistent with this, ventricular cardiomyocytes acutely isolated from cardiac-specific *Scn1b* null mice have increased I_{Na} density, increased susceptibility to polymorphic ventricular arrhythmias, and altered intracellular calcium handling (Lin, O'Malley et al. 2015). Cardiac specific *Scn1b* deletion also results in increased duration of calcium signaling in ventricular cardiomyocytes, resulting in delayed afterdepolarization (Lin, O'Malley et al. 2015). Thus, *Scn1b* deletion is clearly arrhythmogenic in mouse ventricular tissue. Until now, the atrial phenotype of *Scn1b* null mice has not been described. Chapter 2 provides a detailed investigation into the structural and functional consequences of *Scn1b* deletion in atrial physiology. Phenotyping the complex heterogenous specialized cells found in cardiac tissue is critical for determining the mechanisms promoting or sustaining arrhythmias, as well as discovering clinically relevant treatments for *SCN1B*-linked disease.

SCN1B and human channelopathies

DEE52, differentially diagnosed as Dravet Syndrome or Early infantile Developmental and Epileptic Encephalopathy (EIDEE), is linked to *SCN1B* biallelic loss-of-function variants (Patino, Claes et al. 2009, O'Malley and Isom 2015, Aeby, Sculier et al. 2019, Darras, Ha et al. 2019). Hallmarks of this disorder include onset before 12 months of age, frequent and prolonged febrile seizures, neurodevelopmental delays, and ataxia. Importantly, patients with DEE52 are at a higher incidence of sudden unexpected death in epilepsy or SUDEP (Bell and Sander 2001, Tomson, Nashef et al. 2008) . In these patients, SUDEP occurs predominately during sleep, but the exact mechanism of sudden death remains unclear (Elmali, Bebek et al. 2019, Mazzola and Rheims 2021). Several studies have suggested that, in addition to severe seizures, brain stem respiratory dysfunction, autonomic dysfunction, and cardiac arrhythmias may contribute to the terminal event (Li, O'Brien et al. 2019, Pensel, Nass et al. 2020, Petrucci, Joyal et al. 2020, Akyuz, Uner et al. 2021, Costagliola, Orsini et al. 2021, Fialho, Wolf et al. 2021, Mazzola and Rheims 2021). Diagnostic overlap between epilepsy and cardiac conduction disease can confound understanding of causative links between the two phenotypes (Massey, Sowers et al. 2014). Cardiac conduction abnormalities may be poorly recognized in patients with epilepsy and seizures may be mistaken as syncope in cardiac patients (Zaidi, Clough et al. 2000, Ravindran, Powell et al. 2016). In addition to DEE, *SCN1B* variants are linked to inherited cardiac arrhythmia disorders that lack a seizure component but that also predispose patients to sudden death (Watanabe, Koopmann et al. 2008, Watanabe, Darbar et al. 2009, Holst, Saber et al. 2012, Hu, Barajas-Martínez et al. 2012, Liu, Tester et al. 2014, Riuró, Campuzano et al. 2014,

Neubauer, Rougier et al. 2018, El-Battrawy, Muller et al. 2019) (Table 1.2). There may be overlap between these diagnoses. A retrospective electrocardiography study revealed that abnormal ventricular conduction and abnormal cardiac autonomic response were more common in SUDEP cases than in epileptic controls (Chyou, Friedman et al. 2016, Szurhaj, Leclancher et al. 2021).

For over a decade, our lab has amassed a body of work supporting the hypothesis that DEEs with high SUDEP risk exhibit pro-arrhythmogenic changes that compromise the heart to electrical and structural abnormalities and that cardiac arrhythmias contribute to the mechanism of SUDEP (Lopez-Santiago, Meadows et al. 2007, Auerbach, Jones et al. 2013, Bao, Willis et al. 2016, Frasier, Wagnon et al. 2016, Frasier, Zhang et al. 2018). In one study using patient-derived induced pluripotent stem cell (iPSC) cardiac myocytes, we were able to predict cardiac arrhythmia in a Dravet Syndrome (DS) patient prior to their clinical diagnosis (Frasier, Zhang et al. 2018). In spite of this evidence, patients with DEE are not routinely evaluated by cardiologists and thus are not usually under cardiac surveillance. Clearly, we need better insight into genotype-to-phenotype correlations of *SCN1B*-linked and other channelopathies to determine whether *SCN1B* DEE patients should be candidates for cardiovascular evaluation.

iPSC: phenotyping human cells in a dish

The remarkable field of iPSC research has opened critical new frontiers for basic and translational biomedical research, personalized medicine, and regenerative medicine (Shi, Inoue et al. 2017, Liu, David et al. 2020, Yamanaka 2020). This method of reprogramming somatic cells into a pluripotent state, using a cocktail of transcription factors, has relieved scientists of the ethical controversies involved with using embryonic stem cells. Although this technology is rapidly improving, there are several unresolved problems that currently limit the clinical and therapeutic potential of iPSC derived cells (Ahmed, Anzai et al. 2020, Karbassi, Fenix et al. 2020). Despite those limitations, iPS derived cells present a novel way for researchers to investigate human cells in a rigorous, ethically sourced, and reproducible manner.

In 2006, the Shinya Yamanaka group showed that mouse fibroblasts could be reprogramed to pluripotent stem cells by introducing a cocktail of four transcription factors (Oct3/4, Sox2, Klf4, and cMyc) under embryonic cell culture conditions (Takahashi and Yamanaka 2006). The transcription factors were involved in maintenance of pluripotency. One year later, two separate research groups, the Yamanaka and Thomson group demonstrated the ability to derive pluripotent stem cells from human somatic cells using either the original four transcription factors (Takahashi, Tanabe et al. 2007) or (OCT4, SOX2, NANOG, and LIN28) (Yu, Vodyanik et al. 2007). In 2012, Shinya Yamanaka was co-awarded the Nobel Prize in Physiology or Medicine for the discovery of converting adult mammalian cells into pluripotent cells. Amazingly today, the process to convert somatic cells to iPSCs can be performed from skin fibroblast, cells from the umbilical cord and placenta, mononuclear cells from peripheral

blood, and urine-derived cells (Smith, Macadangdang et al. 2017). The beauty of this technology is that, once the cells are in a pluripotent state, they theoretically can be differentiated into any cells in the body, including cardiomyocytes, while retaining the unique genetic characteristics of the donor.

Without additional interventions, differentiated iPSC cardiomyocytes (iPSC-CMs) normally exhibit immature structural and functional properties (Sinnecker, Laugwitz et al. 2014, Yang, Al-Aama et al. 2015, Goversen, van der Heyden et al. 2018, Koivumaki, Naumenko et al. 2018, Tu, Chao et al. 2018). In humans, CMs take up to decade to acquire adult phenotypes in structure and ploidy (Peters, Severs et al. 1994, Vreeker, van Stuijvenberg et al. 2014). The developing CM adjoins with adjacent CMs to assemble into an electromechanical syncytium connected by mechanical and electrical junctions. Standard differentiation of iPSC-CMs lacks these dynamic physical and environmental cues needed to produce fully mature CMs. Standard iPSC-CM cell culture protocols result in rounded mononucleated cells that exhibit poorly developed sarcoplasmic reticulum and t-tubules. Structural differences between immature iPSC-CM and mature human CMs also have electro-mechanical implications. In excitation–contraction coupling, propagation of depolarization along the sarcolemma and t-tubules induces the opening of L-type calcium channels. There is then an influx of extracellular calcium into the cell, resulting in calcium-induced calcium release from the sarcoplasmic reticulum via ryanodine receptors. The lack of t-tubules in immature iPSC-CMs delays calcium-induced calcium release because of the uncoupling of L-type calcium channels and ryanodine receptors (Kane, Couch et al. 2015). The resting membrane potential is more depolarized in immature iPSC-CMs than in mature human ventricular or atrial CMs (Liu, Laksman et al. 2016). Although immature iPSC-

CMs generate important cardiac currents such as I_{Na}, I_{Ca}, and deficient for I_{K1} that is essential for stabilization of the resting potential (Miller, Ganat et al. 2013, Vaidyanathan, Markandeya et al. 2016, Goversen, van der Heyden et al. 2018, Koivumaki, Naumenko et al. 2018, Tu, Chao et al. 2018). In addition to expression of the fetal isoform of $Na_v1.5$, which leads to slower kinetics of channel activation and inactivation, the more depolarized membrane results in fewer Na_vs available to be activated (Karbassi, Fenix et al. 2020). Therefore, the upstroke velocity (phase 0) is slower in immature iPSC-CMs compared to mature CMs. Immature iPSC-CM APs lack the plateau phase (phase 2), and repolarization commences more rapidly than in mature CMs (Karbassi, Fenix et al. 2020). Consequently, to be able to fully utilize iPSC-CMs, specialized differentiation techniques must be used to confer an adult-like maturation state.

Several methods have been developed to increase maturity of iPSC-CMs in 2D culture (Ahmed, Anzai et al. 2020). An important discovery involved prolonging the culture time. As it takes years for human CMs to mature *in vivo*, that same logic is applied to iPSC-CM culturing. With prolonged cultures up to 360 days, iPSC-CMs display a more mature phenotype in size, structure, and physiology (Kamakura, Makiyama et al. 2013, Lundy, Zhu et al. 2013, Lewandowski, Rozwadowska et al. 2018). However, using this singular method for maturation is inefficient and costly. Other methods, such as the addition of triiodothyronine (T3) or replacement of glucose in the culture media with galactose and fatty acids, have been shown to enhance maturation of iPSC-CMs in a more timely manner (Yang, Rodriguez et al. 2014, Parikh, Blackwell et al. 2017). Since CMs can interact with each other through various mechanical cues, groups have explored adding extracellular matrix components (e.g. collagens, fibronectin) to enhance structural and function maturation of iPSC-CMs (Chun, Balikov et al. 2015, Herron,

Rocha et al. 2016, Ogasawara, Okano et al. 2017, Yoshida, Miyagawa et al. 2018, Abecasis, Gomes-Alves et al. 2019). Additionally, plastic cell culture dishes are much stiffer than native heart tissue. Thus, growing iPSC-CMs on softer matrices can improve the maturation of iPSC-CMs. Softer surfaces created by polydimethylsiloxane (PDMS), hydrogels, or polyacrylamide can also regulate the topology and cell morphology resulting in better maturation (McCain, Yuan et al. 2014, Ribeiro, Ang et al. 2015, Vuorenpaa, Penttinen et al. 2017). Generally, the more mature the iPSC-CM, the more reliable the electrophysiological and structural properties in terms of modeling native cells.

When studying early life diseases such as a DEE, iPSC-CM are proving to be instrumental in determining at-risk populations. Recently, our group identified a potential SUDEP risk biomarker for patients with the DEE DS (Frasier, Zhang et al. 2018). Skin biopsies were collected from *SCN1A*-linked DS patients and differentiated into iPSC-CMs. DS patient iPSC-CMs exhibited increased I_{Na} compared to healthy patient iPSC-CMs (Frasier, Zhang et al. 2018), similar to observations in a *Scn1a* DS mouse model (Auerbach, Jones et al. 2013). iPSC-CMs from one of the DS patients had I_{Na} so large that it was not possibly to accurately control the voltage clamp. This observation led to a recommendation to the attending physician that the pediatric patient receive cardiac evaluation. It was determined that this patient had cardiac abnormalities and autonomic abnormalities and the patient was given additional precautionary care. This study underscores the potential of iPSC technology to uncover patients with higher risk for SUDEP and provides a valuable tool to make genotype-to-phenotype predictions in patient populations.

To date we have extensively studied Na_v-β1 subunit function in heterologous expression systems and animal models. Heterologous cell lines offer investigators the ability to understand Na_v-β1 specific function in ioslation, however, these overexpression systems cannot fully recapitulate Na_v-β1 expression, location, interactions, and signaling in native cells *in vivo*. In contrast, animal models circumvent that issue, by offering a native tissue environment that more closely resembles human cells. However, small mammals, such mice, cannot replicate human cardiac AP waveforms, and thus their usefulness in cardiac research is limited. Mice are comparably inexpensive, easier to handle and genetically manipulate, and have faster breeding and development compared to large mammals that would better represent human cardiac physiology (Camacho, Fan et al. 2016). While murine CMs express the same Na_v genes as humans and thus have similar I_{Na}, they either do not express the same K_vs and Ca_vs compared to humans or the ionic conductances of K_vs and Ca_vs are considerably smaller. For example, in murine ventricular CMs, repolarization is ~four times faster than human CMs because of smaller I_{to} and L-type Ca_v conductance and lack of I_{Kr} expression (Nerbonne and Kass 2005). Although limited, heterologous expression systems and animal models have been pivotal to our understanding of Na_v-β1 role in physiology. Moving forward, we require models that are better representative of human physiology. Importantly, an ideal *SCN1B* cardiac model would incorporate a patient's genetic background, as low penetrance and variable expressivity of ion channel variants, which may stem from epigenetic factors, age, gender, or genetic modifiers, add complexity in understanding pathogenesis. Chapter 3 asks whether *SCN1B* DEE patient iPSC-CMs exhibit pro-arrhythmogenic changes (Figure 1.5). We show that *SCN1B* patient iPSC-CMs exhibit increased transient and persistent I_{Na} and AP prolongation, similar to the *Scn1b* null mouse model. Over the past decade, patient derived iPSC-CMs have been used to understand and predict human

pathophysiology, and even with limitations, this technology will be important to identify the mechanisms underlying SUDEP and to develop individualized therapies.

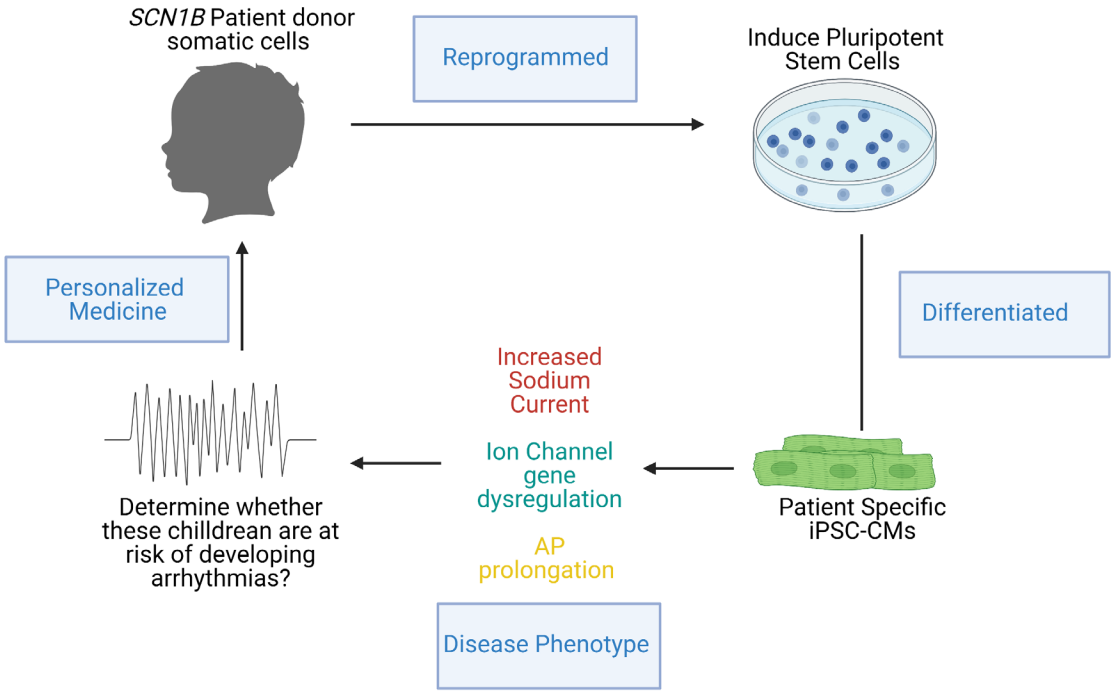

Figure 1.5. Induced Pluripotent Stem Cell Cardiomyocyte model.

We created induced Pluripotent Stem Cell from *SCN1B* patients to determine whether they were at risk of cardiac arrhythmias.

Conclusion

CM excitability relies on the orchestration of multiple ion channels in concert. When an AP is generated, there is a massive influx of sodium ions through Na_vs into the cell, causing rapid depolarization. The cell then repolarizes, a process mediated by L-type calcium channels and families of potassium channels. We propose that Na_v-β1 subunits serve as a central communication hub between Na_v, K_v, and Ca_v families to coordinate depolarization, repolarization, and calcium signaling in CMs. In addition, Na_v-β1 subunits are critical for cell-cell communication via their cell adhesive function and regulate gene expression via RIP. Importantly, we know that *Scn1b* deletion contributes to neurological and cardiac disease mechanisms in mice, via altered ion channel modulation, aberrant transcriptional regulation, and diminished cell adhesion signaling. Here, using a variety of novel techniques, I explore how defects in *SCN1B* signaling contribute to cardiac disease.

Chapter 2. Atrial Arrhythmia and Fibrosis in a Neonatal Mouse Model of Scn1b-Linked Developmental and Epileptic Encephalopathy

Nnamdi Edokobi*, Roberto Ramos-Mondragon*, Samantha Hodges, Alexandra A. Bouza, Chandrika Canugovi, Lena Juratli, William Abel, Caroline Scheuing, Sami Noujaim, Nageswara Madamanchi, Marschall S. Runge, Luis F. Lopez-Santiago, Lori L. Isom

*These authors contributed equally to this work.

Introduction

Loss-of-function (LOF) variants in *SCN1B* (19q13.11), encoding the voltage-gated sodium channel (Na_V) β1/β1B subunits, are linked to human diseases that predispose patients to sudden death, including developmental and epileptic encephalopathy type 52 (DEE52, OMIM 617350), Generalized Epilepsy with Febrile Seizures plus (OMIM 617350), Brugada Syndrome 5 (OMIM 612838), cardiac conduction defects (OMIM 612838) and Atrial Fibrillation (AF) Familial 13 (OMIM 615377) (O'Malley and Isom 2015, Edokobi and Isom 2018). *Scn1b* null mice phenocopy DEE52, which is associated with biallelic inheritance of *SCN1B* variants (Patino, Claes et al. 2009, Ramadan, Patel et al. 2017, Aeby, Sculier et al. 2019), with severe seizures developing after postnatal day (P) 10 and 100% mortality in the third week of life (Chen, Westenbroek et al. 2004). Consistent with evidence linking *SCN1B* variants to human cardiac disease, *Scn1b* null mice also have cardiac arrhythmias that include bradycardia and prolonged QT intervals (Lopez-Santiago, Meadows et al. 2007). Acutely isolated neonatal *Scn1b* null ventricular cardiomyocytes have increased transient and late sodium current ($I_{Na,T}$ and $I_{Na,L}$)

densities, reduced calcium current (I_{Ca}) density, an altered potassium current (I_K) profile, and altered calcium handling, resulting in the generation of arrhythmogenic substrates (Lopez-Santiago, Meadows et al. 2007, Lin, O'Malley et al. 2015, Bouza, Edokobi et al. 2021). These results, together with our work in other models of sodium channelopathies (Auerbach, Jones et al. 2013, Frasier, Wagnon et al. 2016), led us to propose that cardiac arrhythmias contribute to Sudden Unexpected Death in Epilepsy (SUDEP) in DEE patients with Na_vs gene variants.

Na_v-β subunits are multi-functional, non-pore-forming subunits of Na_vs (Catterall 2012). They are transmembrane proteins with type 1 topology consisting of an extracellular N-terminus containing an immunoglobulin (Ig) domain, a single transmembrane segment, and an intracellular C-terminal domain (ICD) (Calhoun and Isom 2014). *SCN1B* encodes Na_v-β1 as well as the splice variant β1B, which includes a retained intron (Kazen-Gillespie, Ragsdale et al. 2000, Patino, Brackenbury et al. 2011). Na_v-β1 subunits associate with multiple Na_v-α subunits to regulate their cell-surface expression and modulate I_{Na} (Calhoun and Isom 2014). β1B subunits appear to be more selective; they associate with and regulate Na_v1.3- and Na_v1.5-generated I_{Na} in heterologous systems (Watanabe, Koopmann et al. 2008, Patino, Brackenbury et al. 2011). β1 subunits also associate with potassium channels to regulate I_K (Deschenes and Tomaselli 2002, Nguyen, Miyazaki et al. 2012, Bouza, Edokobi et al. 2021). While Na_v-β1 association with calcium channels has not been investigated, *Scn1b* null ventricular myocytes have reduced I_{Ca} (Bouza, Edokobi et al. 2021). Na_v-β1 subunits also play non-conducting roles as Ig superfamily cell adhesion molecules, participating in cell-cell and cell-matrix adhesion to regulate cardiac intercalated disk formation as well as neuronal pathfinding and fasciculation in brain (Brackenbury and Isom 2011, Veeraraghavan, Hoeker et al. 2018). Na_v-β1B functions as a

secreted cell adhesion molecule ligand that has developmentally regulated expression patterns (Patino, Brackenbury et al. 2011). Finally, Na_v-β1 subunits undergo regulated intramembrane proteolysis (RIP) through sequential cleavage by the β-site Amyloid Precursor Protein (APP) cleaving enzyme-1 (BACE1) and γ-secretase (Wong, Sakurai et al. 2005, Bouza, Edokobi et al. 2021). These cleavage events release the β1 extracellular Ig domain, which functions as a ligand for cell adhesion (Davis, Chen et al. 2004, Patino, Brackenbury et al. 2011), as well as a soluble intracellular domain (ICD) that translocates to the nucleus to participate in transcriptional regulation of a group of genes, including those encoding ion channels, in the cardiac ventricle (Bouza, Edokobi et al. 2021).

Our previous work focused on the role of *Scn1b* in neurons and cardiac ventricles. Here, we explored whether *Scn1b* also regulates cardiac atrial excitability to understand its potential role in AF, the most common type of cardiac arrhythmia and a significant contributor to mortality (Colilla, Crow et al. 2013, Chugh, Havmoeller et al. 2014). Our results suggest that *Scn1b* null neonatal atria have altered excitability, with changes in $I_{Na,L}$, fibrosis, and cardiac neuronal pathfinding, all contributing to the early development of AF. Our work introduces a new role for *SCN1B* in the regulation of atrial rhythmicity and adds to the growing body of literature suggesting that LOF variants in *SCN1B* predispose patients to a compromised cardiovascular system, in addition to epilepsy, and sudden death.

Results

Genetic analysis of *Scn1b* null atria

In previous work, we showed that Na_v-β1 subunits are sequentially cleaved by BACE1 and γ-secretase, and that the cleaved β1 intracellular domain translocates to the nucleus to contribute to transcriptional regulation of multiple gene families, including ion channels, in the mouse cardiac ventricle (Bouza, Edokobi et al. 2021). Here, we used paired-end RNA-Seq to determine the differential gene expression profiles of *Scn1b* null vs. WT mouse atrial tissue (Figure 2.1A). We performed these experiments at P16, as *Scn1b* null mice die before the end of the third postnatal week. The data were normalized, and differential expression analysis was performed with DESeq2 as fee-for-service by the University of Michigan Advanced Genomics Core. 724 genes were found to be differentially expressed between null and WT atrial tissues (Figure 2.1B). Gene Ontology (GO) analysis revealed groups of genes with altered expression in response to *Scn1b* deletion (Figure 2.1C). The sets of genes most differentially expressed between genotypes included those involved in calcium ion binding, actin binding, and cytoskeletal structure (Figure 2.1C). Importantly, a number of these genes have been previously implicated in cardiac disease (Figure 2.1D). We confirmed the expression of a subset genes using RT-qPCR (Figure 2.2 and Figure 2.3). In contrast to ventricular tissue (Bouza, Edokobi et al. 2021), we did not find changes in Na_v-α subunit gene expression, however we found significant differences in the expression of genes encoding select potassium (*Kcnu1,* p=0.006*; Kcnd2,* p=0.039*; Kcnt1,* p=0.001*; and Kcnv1,* p=0.045) and calcium channel (*Cacng1,* $p=1x10^{-6}$) subunits (Figure 2.3,

panels A-F). Taken together, these data suggested that neonatal *Scn1b* null atria may have structural abnormalities that generate substrates for arrhythmia.

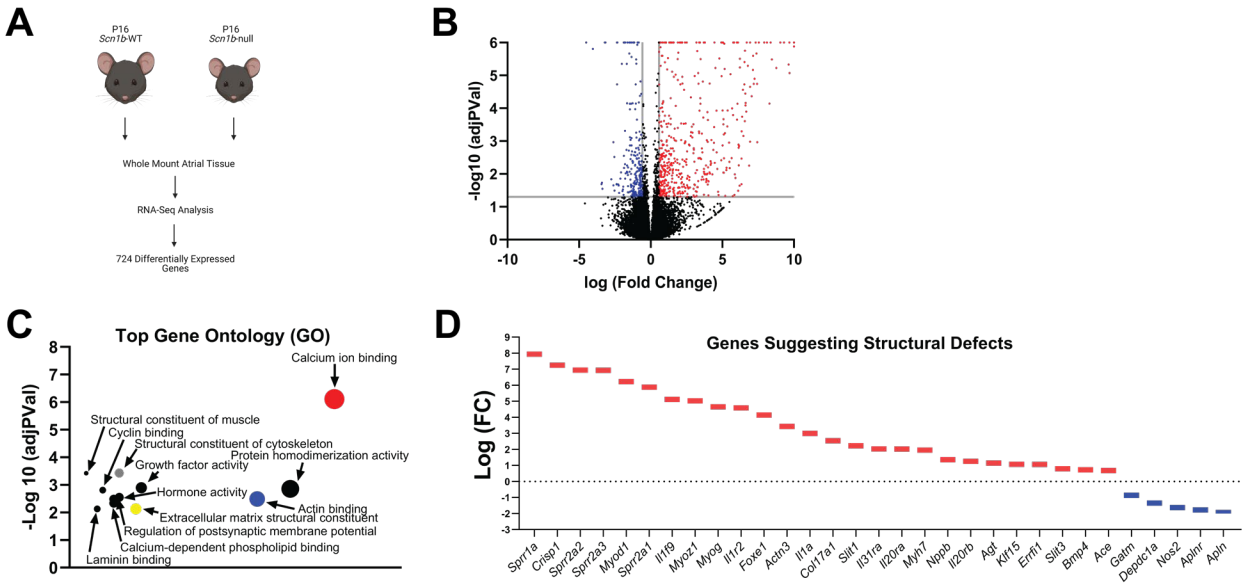

Figure 2.1. Differential gene expression in P16 *Scn1b* null vs WT atria.

(A) Schematic diagram of RNA-Seq analysis in Scn1b-WT and Scn1b-null mice. n = 4 mice per genotype. (B) A volcano plot depicting the whole transcriptomic analysis, genes are represented in terms of their measured expression change (x-axis) and the significance of the change (y-axis). The significance is represented in terms of the negative log (base 10) of the p-value, so that more significant genes are plotted higher on the y-axis. The gray lines represent the thresholds used to select the 724 significantly differentially expressed genes: 0.5849625 for expression change and 0.05 for significance. The up-regulated genes (positive log fold change) are shown in red, while the down-regulated genes are blue. (C) The top gene ontology (GO) terms with a minimum of 5 genes. The Elim pruning method was used to iteratively reduce redundancy. (D) Some differential expressed genes that have been implicated in cardiac disease.

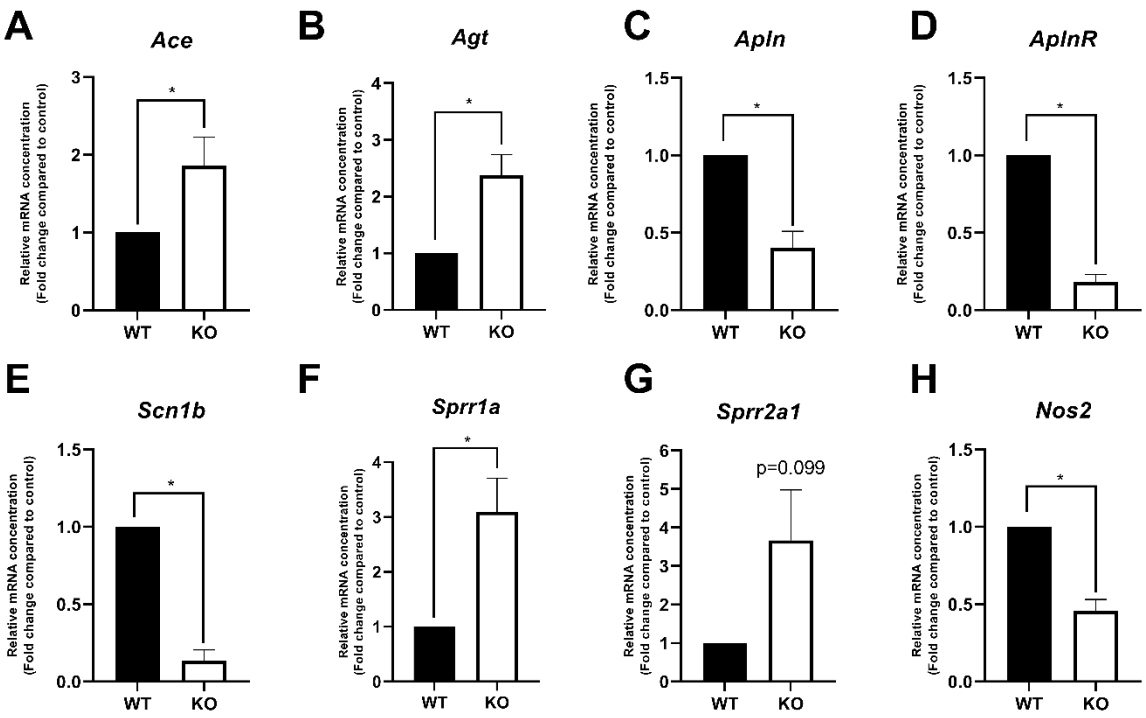

Figure 2.2. Confirmation of RNA-Seq data via RT-qPCR using 10 representative genes from P16 WT and *Scn1b* null atria.

Statistical significance was determined using Student's T-test (p-value < 0.05). (A) Relative expression of *Ace*. (B) Relative expression of *Agt*. (B) Relative expression of *Apln*. (D) Relative expression of *AplnR*. (E) Relative expression of *Scn1b* (confirmation of *Scn1b* deletion). (F) Relative expression of *Sprr1a*. (G) Relative expression of *Sprr2a1*. (H) Relative expression of *Nos2*. Data are represented as the mean ± SEM.

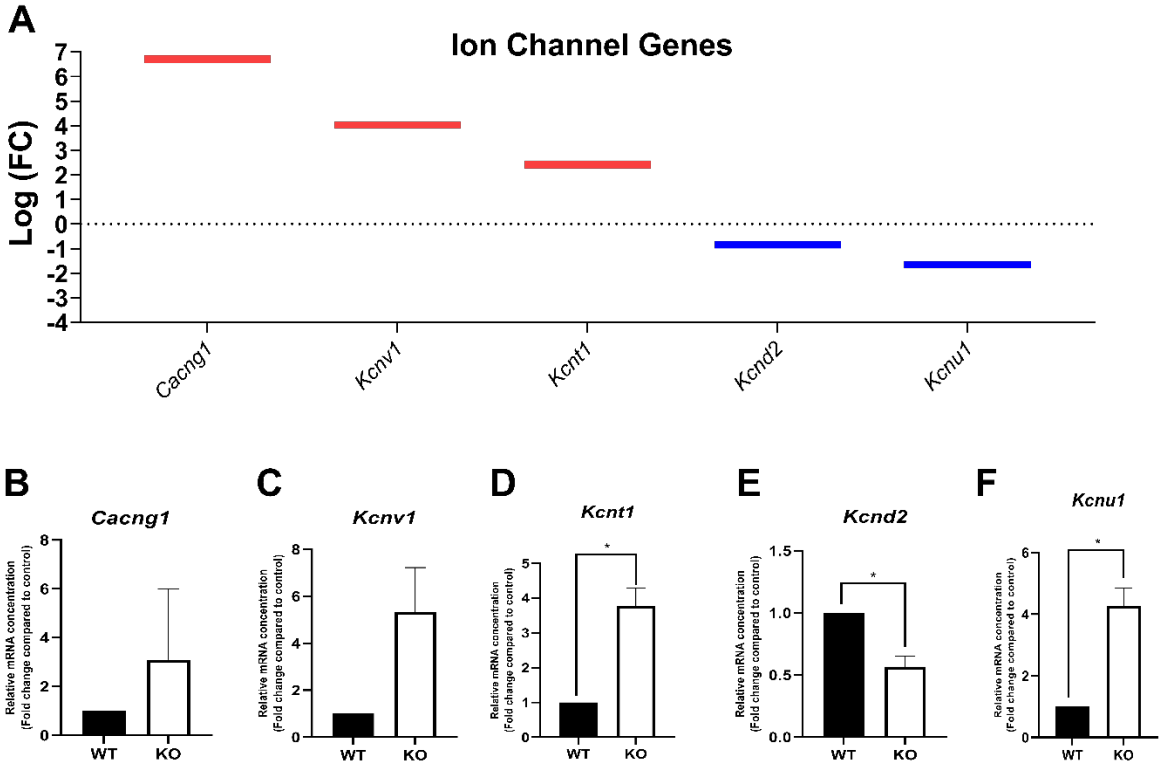

Figure 2.3. Altered Ion Channel Genes

(A) RNA-Seq differential expressed ion channel genes. (B-F) RT-qPCR from P16 WT and *Scn1b* null atria. Statistical significance was determined using Student's T-test (p-value < 0.05). (B) Relative expression of *Cagna1*. (C) Relative expression of *Kcnv1*. (D) Relative expression of *Kcnt1*. (E) Relative expression of *Kcnd2*. (F) Relative expression of *Kcnu1*. Data are represented as the mean ± SEM

Fibrosis in *Scn1b* null atria

We assessed atrial size and then probed for evidence of atrial fibrosis in *Scn1b* null and WT atria using echocardiography and picrosirius red staining, respectively. Histological examination revealed significant collagen deposition in the null atria compared to WT, consistent with fibrosis (Figure 2.4A and B). Echocardiography showed that atrial dimensions, as well as systolic and diastolic function, were similar between genotypes (Figure 2.5 A-F).

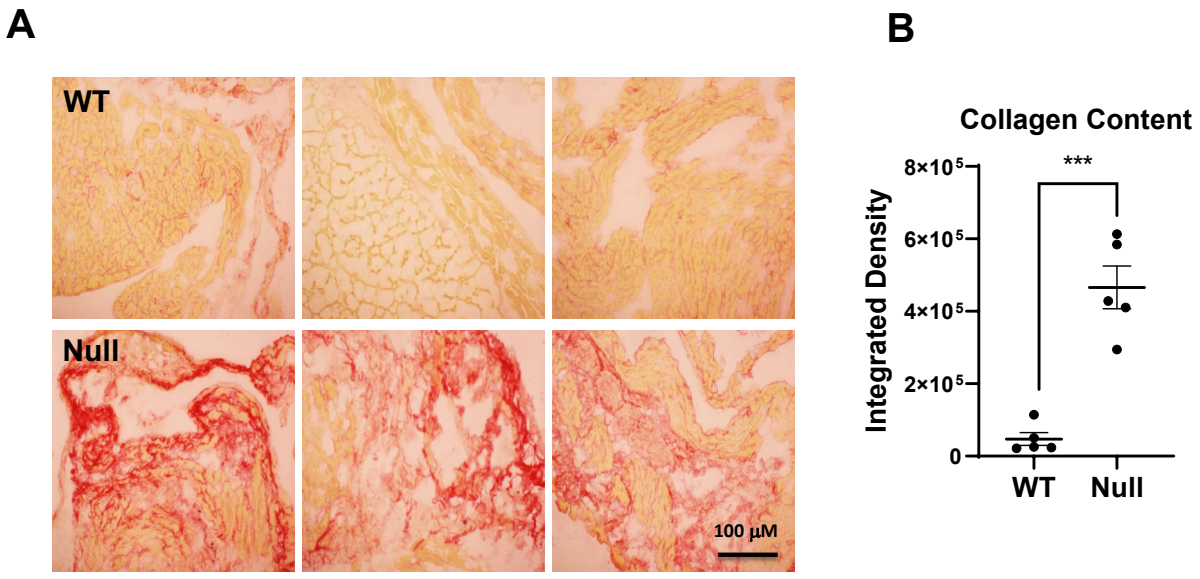

Figure 2.4. Evidence of fibrosis in P16-17 *Scn1b* null atria

(A) Representative picrosirius stained longitudinal sections of atrial tissue from WT and null mice. (B) Quantification of the collagen content in WT and null atria, presented as integrated density. Data are presented as mean ± SEM. ***$p<0.0001$ using Students t-test. Atrial sections were generated from 5 mice per genotype. Each dot in the plot represents data from a single sample. Scale bar is 100 µM

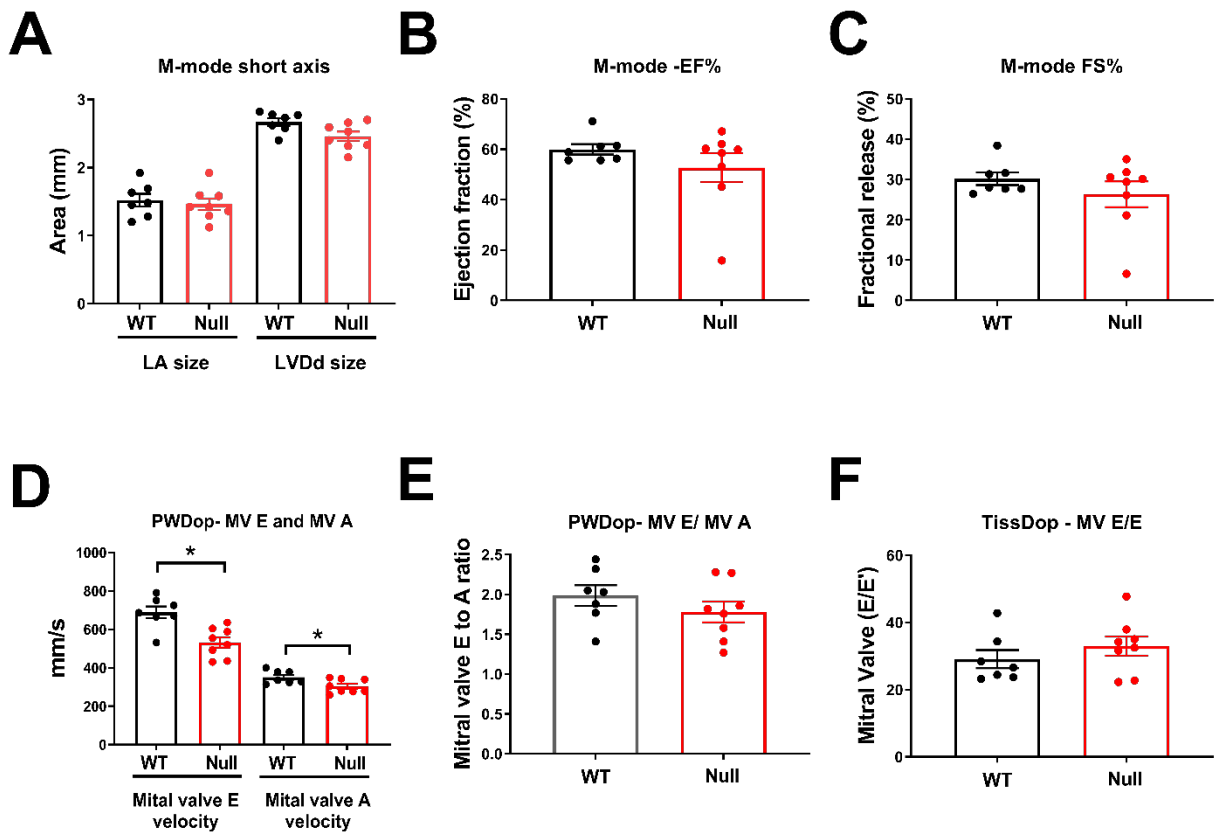

Figure 2.5. Echocardiography studies in *Scn1b* null mice.

(A) Left atria (LA) size and left ventricular size at diastolic phase (LVDd). Systolic parameters including percentage of (B) ejection fraction (EF) and (C) fractional release (FS) mode were determined by M-mode echocardiograms in WT and null mice. Diastolic parameters including (D) Mitral valve E and Mitral valve A velocity and (E) Mitral valve E to A ratio were obtained by PV Doppler. (F) Mitral Valve E/E' ratio. Date are presented as mean ± SEM. Statistical analysis was conducted using Student's t-test. Each dot represents one animal.

Scn1b null mice have increased susceptibility to pacing-induced AF

We performed intracardiac recordings in anesthetized mice to test the hypothesis that fibrosis in P16 null atria may provide an anatomical substrate for AF. We compared the incidence of AF between genotypes using atrial burst pacing (50 Hz for 2 s) before and after the i.p. administration of carbachol. The efficacy of carbachol was assessed by the observation of decreased heart rate following drug administration. AF was defined as rapid atrial activity and high RR interval variability observed in the ECG (Figure 2.6A, top panels) and atrial electrogram (Figure 2.6A, lower panels). AF episodes lasting more than 1 second were counted as AF and an animal was considered to be susceptible to AF if at least two AF episodes were elicited during the experiment. Under basal conditions, we observed a significantly higher incidence of AF in the null mice (6 of 9) compared to WT (0 of 5) (Figure 2.6B). Following the administration of carbachol, AF was inducible in 100 % of the null mice (9 of 9) compared to WT (0 of 5), with prolongation of the AF episodes in null hearts (Figure 2.6C). In a separate experiment, we administered atropine (1 mg/kg) to null mice in which AF was observed to be induced under basal conditions. Atropine administration prevented the subsequent pacing-induced AF episodes in 5 of 6 null mice, with 1 null mouse still showing AF episodes (Figure 2.6D). These data suggest that, in addition to fibrosis, vagal tone may contribute to the high incidence of atrial arrhythmia in *Scn1b* null animals.

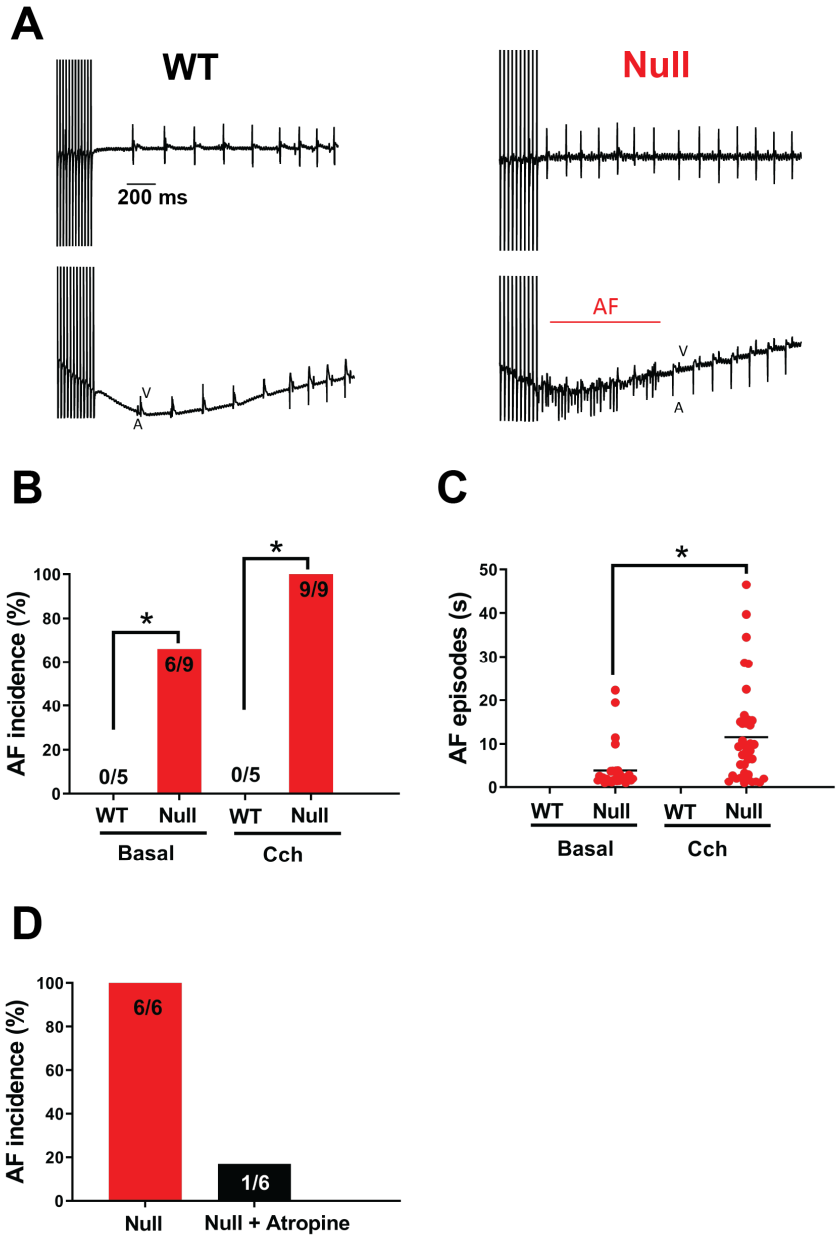

Figure 2.6. Neonatal *Scn1b* null mice have increased susceptibility to AF in vivo.

(A) Representative recordings of surface ECG and atrial electrograms from P16 WT or Scn1b null mice. Atrial burst pacing was delivered at 50 Hz for 2 sec. (B) AF incidence with pacing before and after i.p. administration of carbachol (Cch) (0.025 mg/kg). (C) Duration of induced AF episodes. Each dot represents a single AF episode. (D) Incidence of AF before and after i.p. administration of atropine (1mg/kg). Numbers of animals tested are showed in the bar graphs. *p<0.05 using Fisher exact test.

Scn1b null mice exhibit sinoatrial node dysfunction

We reported previously that *Scn1b* null mice have reduced heart rate (HR) (Lopez-Santiago, Meadows et al. 2007), suggesting altered SAN function. Here, ECG analysis confirmed that P16 null mice have reduced HR (443.0 ± 18.0 WT vs. 367 ± 16 bpm null; $p<0.05$; Figure 2.7A). We also observed sinus node pauses in one null mouse (example shown in the Figure 2.7B). These data suggest SAN dysfunction. We conducted intracardiac recording to assess sinus function by measuring sinus node recovery time (SNRT). As shown in the representative recording (Figure 2.7C), resumption of sinus rhythm after electrical pacing was prolonged in the *Scn1b* null mice. This prolongation was significant at the 80 ms pacing cycle length (160.0 ± 10 WT vs. 244.0 ± 33.0 ms null; Figure 2.7D). Evaluation of ECG properties in animals at increasing postnatal developmental timepoints demonstrated that decreased HR and increased RR interval, along with confirmation of the previously reported QTc prolongation (Lopez-Santiago, Meadows et al. 2007), become evident by P14 in the null mice (Figure 2.8), suggesting that the level of SAN dysfunction increases with development in *Scn1b* null mice.

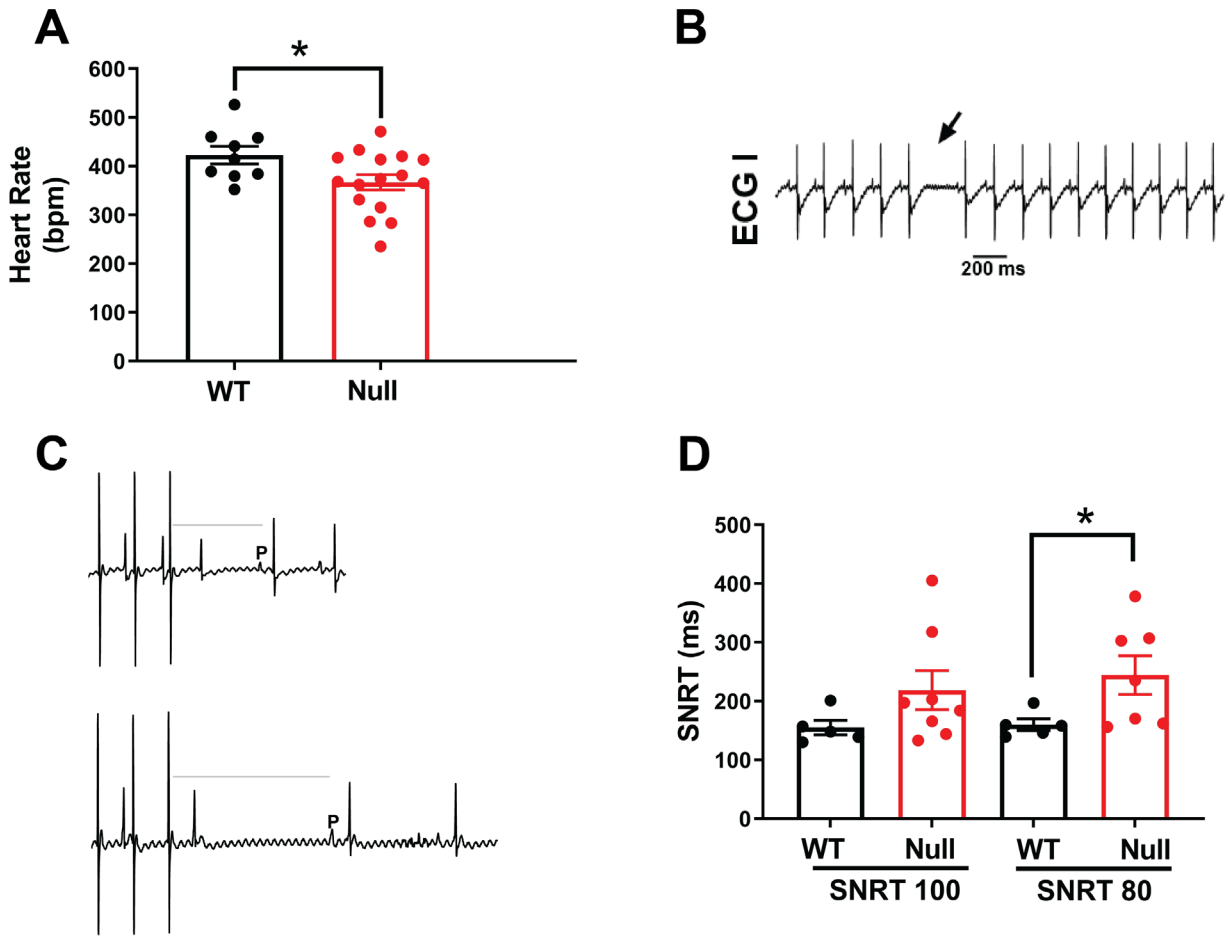

Figure 2.7. Neonatal *Scn1b* null mice exhibit SAN dysregulation.

(A) Heart rates of P16 WT and null mice. (B) Example of a sinus pause in a null mouse during the monitoring of surface ECG. (C) Representative ECG recording showing the time required to resume sinus rhythm following electrical stimulation, or sinus node recovery time (SNRT). (D) Comparisons of SNRT between genotypes assessed at cycle lengths of 100 or 80 ms. Each dot represents the value from one animal. Data are presented as mean ± SEM. *p< 0.05 using Students t-test.

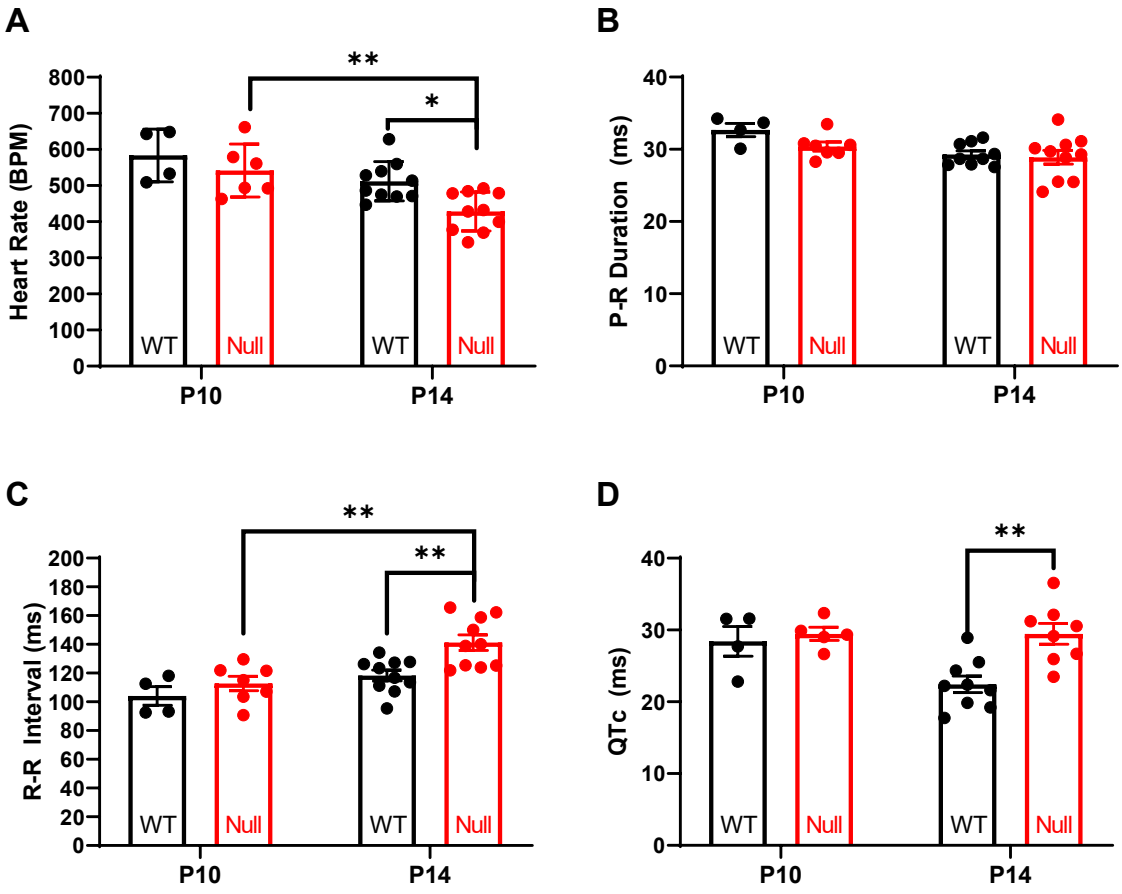

Figure 2.8. Development of bradyarrhythmia in *Scn1b* null mice

Surface ECG recordings from anesthetized P10 or P14 WT or *Scn1b* null mice. (A) Heart rate, measured as beats per minute (BPM), decreases between P10 and P14 in the null mice. Heart rate was significantly different between genotypes at P14. (B) P-R duration, measured in milliseconds (ms) was unchanged over time or between genotypes. (C) R-R interval was prolonged in null mice at P14 but not at P10. (D) QTc prolongation was observed in the null mice compared to WT at P14 but not at P10. Each dot represents one animal. Data are presented as mean ± SEM. *p<0.05, *p<0.01 using two-way ANOVA with Tukey's post-hoc comparison test.

Scn1b deletion results in altered cardiac neuroanatomy

Intrinsic cardiac nerves modulate the function of the cardiac conduction system, and autonomic nervous system dysfunction has been linked to several cardiac disorders (Chen, Chen et al. 2014, Buckley, Shivkumar et al. 2015, Fukuda, Kanazawa et al. 2015, Ripplinger, Noujaim et al. 2016, Bassil, Chang et al. 2018). To investigate possible neuroanatomical differences in *Scn1b* null atria compared to WT, we performed immunofluorescence confocal microscopy of whole-mount preparations of P15-17 atria stained with antibodies to the sympathetic marker, tyrosine hydroxylase (TH), as well as the parasympathetic marker, choline acetyltransferase (ChAT) (Figure 2.9A and 2.10A). In agreement with previous work (Rysevaite, Saburkina et al. 2011), we found cardiac neuronal soma to be either ChAT-positive (ChAT+), bi-phenotypic (ChAT+ and TH+), or TH+. Figure 2.9 and 2.10, panels B-D show high magnification images of the right ganglionic cluster (RGC), which is outlined in yellow in Figure 2.9A and 2.10A. ChAT staining is shown in gray (Figure 2.9B and 2.10B) and TH staining is shown in red (Figure 2.9C and 2.10C). A merged image is shown in 2.9D and 2.10D. The total number of neurons (ChAT+ plus TH+ staining) in the left and right ganglionic clusters combined (LGC + RGC) was comparable between genotypes (Table 2.1). However, we found genotypic differences in the number of ChAT+ neurons located in the LGC vs. RGC, respectively. We observed a significant increase in the number of ChAT+ neurons located in the WT LGC compared to null (Table 2.1). In contrast, we observed a significant increase in the number of ChAT+ neurons located in the null RGC compared to WT (Table 2.1). We found no differences between genotypes in the number of neurons that were TH+ alone (Table 2.2). The SAN is predominantly innervated by the RGC

(Figure 2.11) (Pauza, Saburkina et al. 2013, Pauza, Rysevaite et al. 2014), while the LGC predominantly innervates the atrial ventricular nodal (AVN) region (Pauza, Saburkina et al. 2013). In Figure 2.9A, 2.10A, and 2.11, white arrowheads point to the intrinsic cardiac nerves from the RGC that extend toward the SAN. Taken together, our results suggest that increased numbers of ChAT+ neurons in the null RGC alter SAN function and influence heart rate.

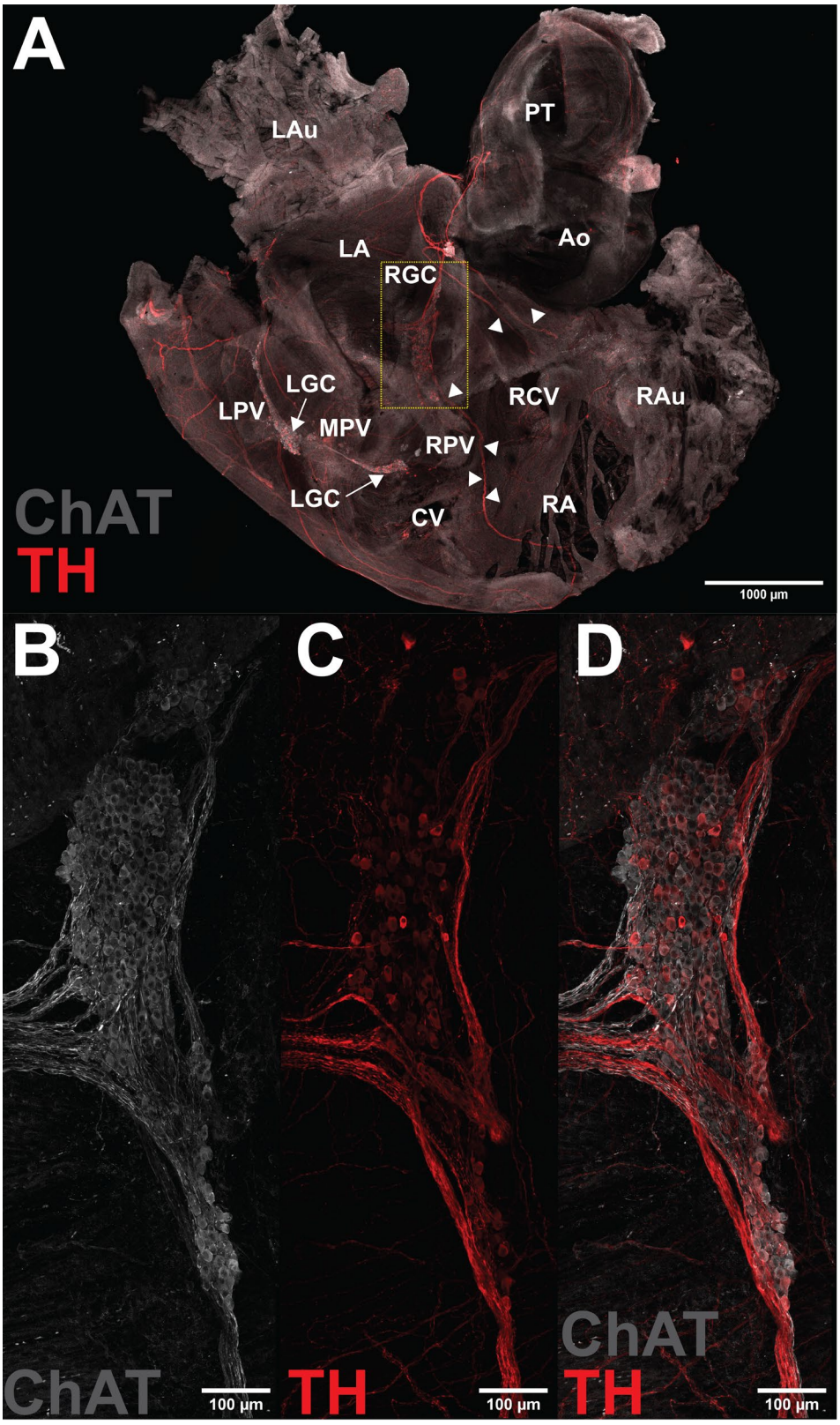

Figure 2.9. Whole-mount atrial preparation from a P16 *Scn1b* null heart.

Immunofluorescence of murine atrial intrinsic ganglia. ChAT+ neurons are labeled in gray, TH+ neurons are labeled in red. Arrows point to intrinsic ganglia; arrowheads point to nerves from the RGC that innervate the SAN. Scale bar = 1000 μm. Box shows the area that was examined at higher magnification (scale bar = 100 μm) for (B) ChAT+ ganglionic cells or (C) TH+ ganglionic cells. (D) Merged image of B and C. Ao – ascending aorta; CV – caudal vein; LA – left atrium; Lau – left auricle; LCV – left cranial cava vein; LGC – left ganglion cluster; LPV – left pulmonary vein; MPV – middle pulmonary vein; PT – pulmonary trunk; RA – Right atrium; Rau – right auricle; RCV -right cranial cava vein; RGC – right ganglion cluster; RPV – right pulmonary vein. Scale bar is 100 μM.

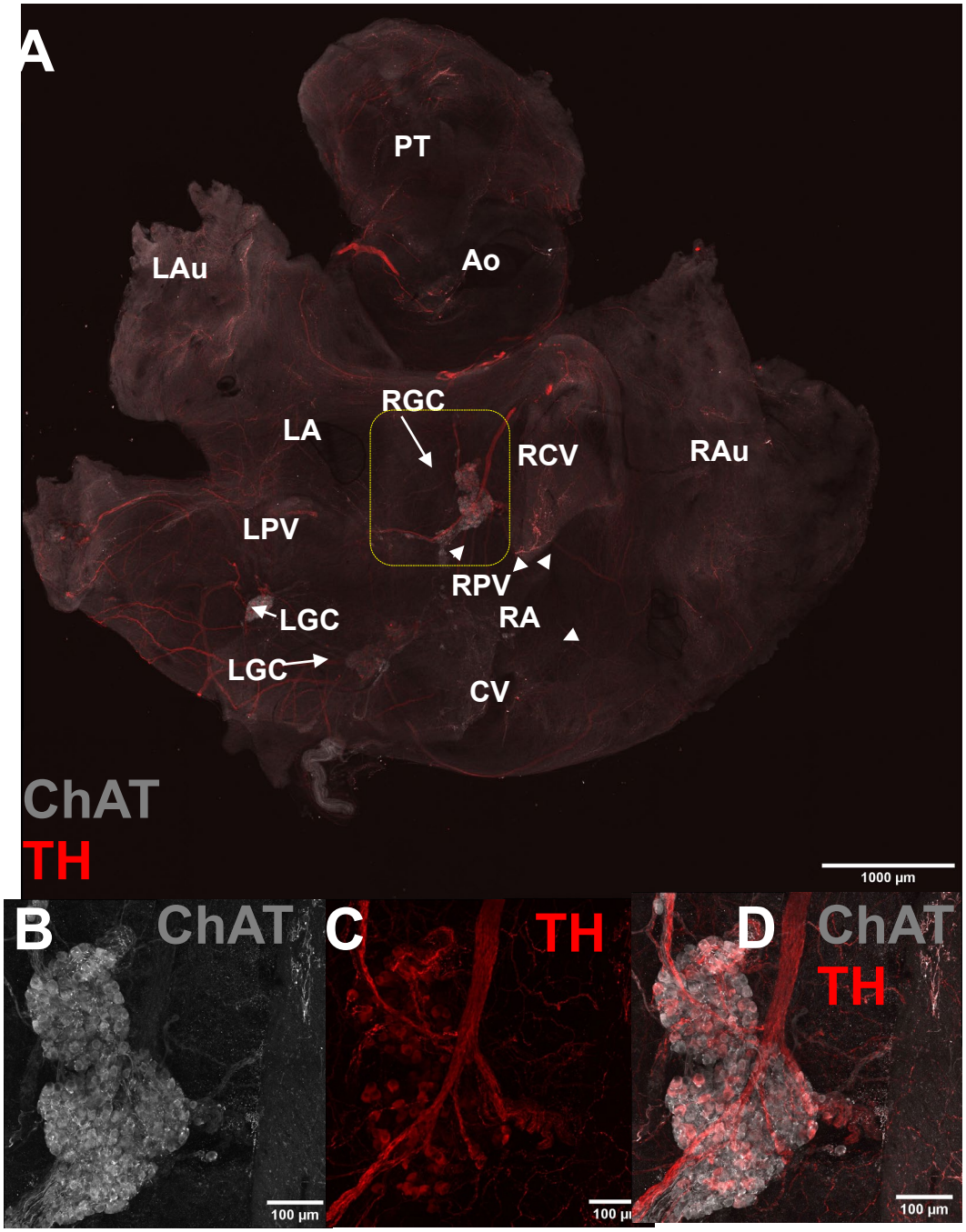

Figure 2.10. Whole-mount atrial preparation from a P16 *Scn1b* WT heart.

Immunofluorescence of murine atrial intrinsic ganglia. ChAT+ neurons are labeled in gray, TH+ neurons are labeled in red. Arrows point to intrinsic ganglia; arrowheads point to nerves from the RGC that innervate the SAN. Scale bar = 1000 µm. Box shows the area that was examined at higher magnification (scale bar = 100 µm) for (B) ChAT+ ganglionic cells or (C) TH+ ganglionic cells. (D) Merged image of B and C. Ao – ascending aorta; CV – caudal vein; LA – left atrium; Lau – left auricle; LCV – left cranial cava vein; LGC – left ganglion cluster; LPV – left pulmonary vein; PT – pulmonary trunk; RA – Right

atrium; Rau – right auricle; RCV -right cranial cava vein; RGC – right ganglion cluster; RPV – right pulmonary vein. Scale bar is 100 µM.

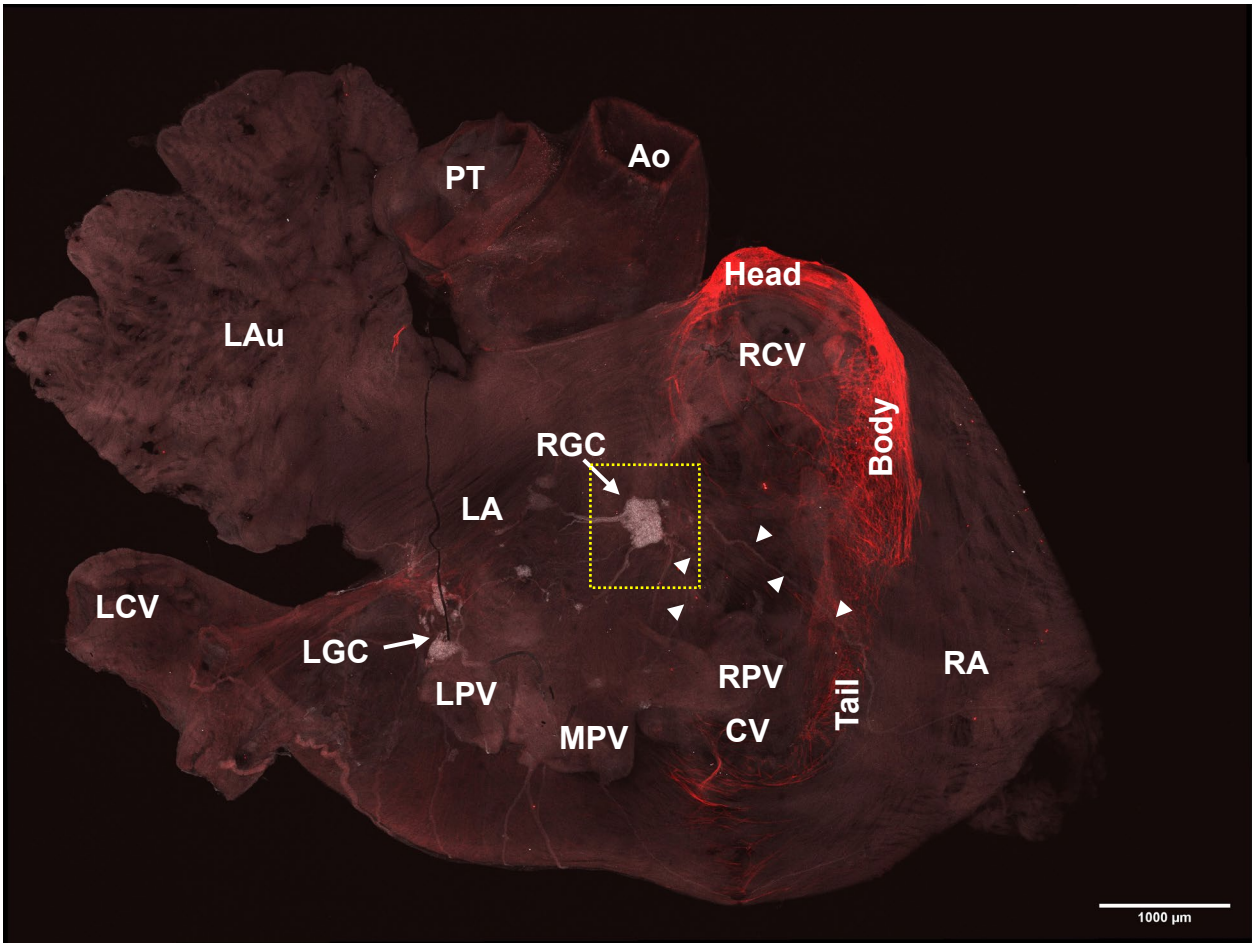

Figure 2.11 Whole-mount preparation demonstrates the distribution of HCN4 immunoreactive (IR) myocytes.

Immunofluorescence of murine atrial intrinsic ganglia. ChAT+ neurons are labeled in gray, Sino Atrial Nodal cells (HCN4 IR) myocytes are labeled in red. The head, body, and tail in the upper panel mean the portions of the mouse SAN region. Arrows point to intrinsic ganglia; arrowheads point to nerves from the RGC that innervate the SAN. Scale bar = 1000 µm. Box shows the Ao – ascending aorta; CV – caudal vein; LA – left atrium; Lau – left auricle; LCV – left cranial cava vein; LGC – left ganglion cluster; LPV – left pulmonary vein; MPV – middle pulmonary vein; PT – pulmonary trunk; RA – Right atrium; RCV -right cranial cava vein; RGC – right ganglion cluster; RPV – right pulmonary vein. Scale bar is 100 µM.

ChAT+ Cells	WT			Null		
	Mean ± SD	Range	n	Mean ± SD	Range	n
LGC+RGC	606.4 ± 184.6	384.0 – 883.0	5	551.0 ± 129.2	434.0 – 689.0	4
RGC	183.8 ± 154.7	46.00 – 499.3	9	331.9 ± 121.8*	128.0 – 508.0	9
LGC	456.4 ± 96.59	337.0 – 566.0	5	264.0 ± 69.58*	173.0 – 329.0	4

Table 2.1. Quantification of ChAT+ neurons

The mean and range of ChAT+ and biphenotypic intrinsic cardiac neurons are presented for all ganglia (LGC + RGC) vs. the right (RGC) or left (LGC) ganglionic clusters from *Scn1b* WT and null mouse whole mount atrial preparations. *Indicates significant difference between null and WT of $p<0.05$.

TH+ Cells	WT			Null		
	Mean ± SD	Range	n	Mean ± SD	Range	n
LGC+RGC	80.60 ± 40.46	47.00 – 127.0	5	50.00 ± 32.59	27.00 – 98.00	4
RGC	21.00 ± 17.87	0.00 – 50.00	9	28.00 ± 19.81	0.00 – 52.00	9
LGC	55.40 ± 21.52	26.00 – 79.00	5	35.26 ± 21.08	13.00 – 57.00	4

Table 2.2. Quantification of TH+ neurons

The mean number and range of TH+ (TH only, with no ChAT staining) intrinsic cardiac neurons overall (LGC + RGC combined), in the RGC, or in the LGC from *Scn1b* WT or null mouse heart preparations. No significant differences were found between genotypes.

Scn1b null atrial myocytes show prolonged APD and increased $I_{Na,L}$

We investigated the electrical properties of acutely isolated P16 null and WT mouse atrial myocytes. APs were elicited at 1 Hz in current clamp mode. No differences in the resting membrane potential or AP amplitude were observed between genotypes (Figure 2.12B), however, the maximal velocity of the AP upstroke was significantly reduced in null myocytes compared to WT (141.5±14.4 WT vs. 93.8 ± 11.0 null) (Figure 2.12C). Moreover, null myocytes showed significantly prolonged APD at 30%, 50% and 90% of the membrane repolarization (APD30: 3.6 ± 0.4 WT vs. 13.0 ± 3.2 ms null; APD 50: 7.8 ± 1.0 WT vs. 23.8 ± 5.0 ms null; APD90: 35.5 ± 6.4 ms WT vs. 68.4 ± 13.0 ms null) (Figure 2.12, panels A and D). No early afterdepolarization (EAD) waveforms were observed in either genotype. Voltage clamp experiments revealed reduced membrane capacitance (Cm) of the null myocytes (Table 2.3), similar to what we observed previously in ventricular myocytes (Lopez-Santiago, Meadows et al. 2007). Finally, while peak $I_{Na,T}$ density was not statistically different between genotypes (-104.8 ± 7.7WT pA/pF vs. -131.00 ± 13.00 null pA/pF; Figure 2.12E), $I_{Na,L}$ density was significantly increased in the *Scn1b* null myocytes (-0.38 ± 0.06 WT pA/pF vs. -0.75 ± 0.13 pA/pF null; Figure 2.12F).

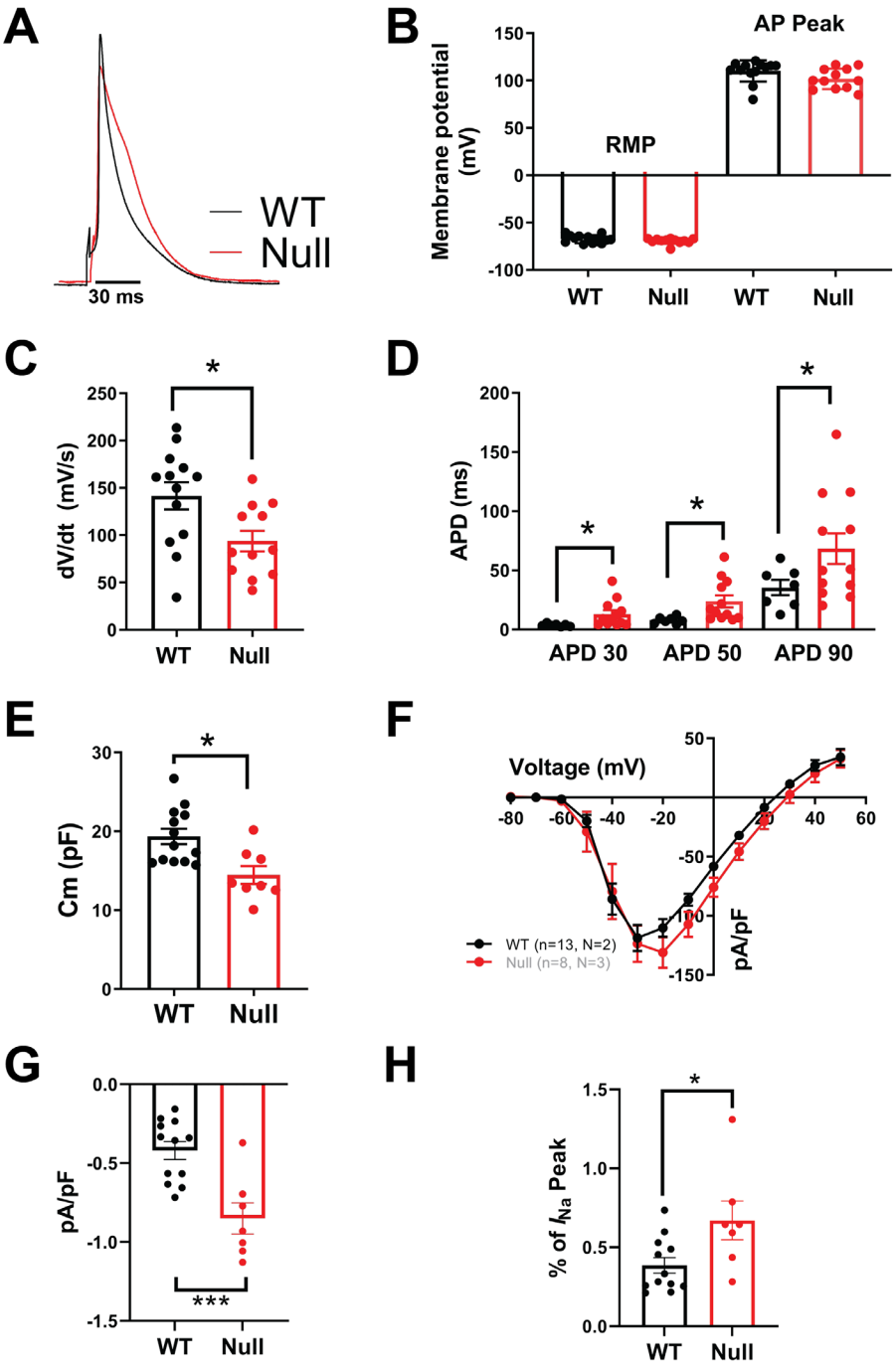

Figure 2.12. *Scn1b* deletion alters atrial cellular electrophysiology.

(A) Representative recordings of APs from acutely isolated P16 WT or *Scn1b* null atria myocytes. (B) Resting membrane potential (RMP) and AP peak. (C) AP upstroke velocity. (D) AP duration at 30, 50 and 90 % of membrane repolarization. (E) *Scn1b* null atrial myocytes are significantly smaller than WT. (F) I-V relationships for transient I_{Na}. (G) I_{Na}L shown as current density (H) Percentage of the peak

current. Each dot represents the value from one cell. Date are presented as mean ± SEM. AP recordings and I_{Na} recordings were obtained from the same cell isolation. Animals: N = 2-3 mice from each genotype. *p<0.01 vs WT using Student's T-test

	***Scn1b* WT**	***Scn1b* null**
Membrane capacitance (pF):	19.4 ± 1.0	14.5 ± 1.1*
Activation parameters		
G_{max} (pS)	50.6 ± 5.0	44.4 ± 6.0
k	4.30 ± 0.2	4.538 ± 0.3
$V_{½}$ (mV)	-38.8 ± 1.6	-37.1 ± 2.7
Inactivation parameters		
k	-7.5 ± 0.4	-8.0 ± 0.51
$V_{½}$ (mV)	-78.4 ± 1.76	-75.6 ± 1.7
n=	13	8
*p<0.05 vs WT		

Table 2.3. Voltage dependent properties of atrial I_{Na}

Discussion

SCN1B is expressed in both brain and heart. LOF variants in *SCN1B* are linked to epilepsy and cardiac arrhythmia. *Scn1b* null mice, which model DEE52, have severe seizures and early death plus a cardiac phenotype that includes bradycardia, QTc prolongation, increased $I_{Na,T}$ and $I_{Na,L}$ densities, altered I_K, reduced I_{Ca}, and altered calcium handling in isolated ventricular myocytes (Chen, Westenbroek et al. 2004, Lopez-Santiago, Meadows et al. 2007, Lin, O'Malley et al. 2015, Bouza, Edokobi et al. 2021). Importantly, cardiac specific *Scn1b* null mice have a similar cardiac phenotype as the global null animals (Lin, O'Malley et al. 2015), demonstrating that arrhythmias are not secondary to seizures but instead that there are intrinsic differences in cardiac muscle resulting from *Scn1b* deletion. Taken together, this body of work has contributed to the hypothesis that both seizures and cardiac arrhythmias may contribute to sudden death in DEE52 patients. The present study reports the first investigation of the effects of *Scn1b* deletion on cardiac atrial structure, function, and electrophysiology, modeling the effects of *SCN1B* LOF variants in the atrium. *Scn1b* deletion results in the differential expression of several genes that are associated with atrial dysfunction, leading to the prediction that *Scn1b* mice have abnormally formed atrial substrates that are conducive to arrhythmogenesis. We tested this hypothesis and found that *Scn1b* null neonatal hearts have a significant accumulation of atrial collagen, indicating fibrosis, and suggesting increased susceptibility to pacing induced AF. We found that *Scn1b* null neonates have SAN dysfunction and increased cholinergic innervation to the SAN compared to WT. Consistent with these findings, atropine administration prevented the re-induction of AF in null animals. In agreement with previous work in atrial myocytes isolated

from human AF patients or from diabetic mice with AF (Poulet, Wettwer et al. 2015, Jin, Jiang et al. 2019), we found increased $I_{Na,L}$ density, with no change in $I_{Na,T}$ density, in neonatal *Scn1b* null atrial myocytes, contributing to the mechanism of atrial APD prolongation in these cells. These important new results show that *Scn1b* plays critical roles in atrial as well as ventricular physiology early in life and suggest that *SCN1B* LOF variants can have devastating implications for the pediatric heart in addition to the developing brain (Graphical Abstract).

Alterations in I_{NaT} and I_{NaL} components of the sodium channels contribute to the pathophysiology of AF. We observed increased $I_{Na,L}$ in acutely isolated neonatal *Scn1b* null atrial myocytes compared to WT with no changes in the expression of genes encoding Na_v-α subunits. While parallel translational studies have not been reported in pediatric patients, alterations in $I_{Na,T}$, $I_{Na,L}$, and Na_v-α subunit expression have been reported in right atrial appendage myocytes isolated from adult patients with permanent AF (Sossalla, Kallmeyer et al. 2010). This work showed a 16% decrease in $I_{Na,T}$, which was reflected in decreased expression of $Na_v1.5$ protein. In addition, they observed a 26% increase in $I_{Na,L}$, with a concomitant increase in $Na_v1.1$ protein. It is not known whether changes in Na_vs expression and function in adult AF patients are causative or adaptive in response to high atrial excitability. However, our work suggests that increased $I_{Na,L}$, with no changes in Na_v-α subunit gene expression, may contribute to the mechanism of AF, at least for *SCN1B* LOF patients. AF is the most common cardiac arrhythmia seen in clinical practice(Colilla, Crow et al. 2013, Chugh, Havmoeller et al. 2014). While AF occurs predominantly in the adult population, familial AF sporadically occurs in younger patients. There are reports of AF in patients with *SCN1B* variants, some of whom were diagnosed with AF

before the age of 40 (Watanabe, Darbar et al. 2009, Olesen, Holst et al. 2012, Hayashi, Konno et al. 2015). A case report showed familial AF in a patient with double heterozygous variants in *SCN5A* and *KCNQ1*, respectively, at age 13 (Kanai, Toyohara et al. 2021). Importantly, however, DEE52 is a pediatric disease that begins in the first year of life (Aeby, Sculier et al. 2019). Estimating that one human year is approximately equivalent to 9 mouse days (Dutta and Sengupta 2016), the P16-17 mice used in this study may be equivalent to 21 month old children. Thus, this work is clinically relevant because it predicts that children with DEE52 may be at risk for developing AF and should be checked periodically by a pediatric cardiologist. Our previous work using induced pluripotent stem cell cardiac myocytes derived from Dravet syndrome patients with variants in the *SCN1A*, predicted cardiac arrhythmia prior to clinical diagnosis (Frasier, Wagnon et al. 2016). Taken together, our work supports the hypothesis that SUDEP in DEEs linked to Na_Vs genes is an arrhythmia of heart and brain (Goldman, Glasscock et al. 2009).

We were not able to induce AF in WT neonates, even with the administration of carbachol. Remarkably, neonatal *Scn1b* null mice had a high incidence of pacing-induced AF, even in the absence of carbachol, and we were able to induce AF in all null mice tested following carbachol treatment. Atropine administration prevented pacing-induced AF episodes in 5 of 6 null mice. Parasympathetic over-stimulation and/or bradycardia are known AF triggers (Goldberger and Pavelec 1986, Wang, Page et al. 1992, Allessie, Boyden et al. 2001, Chen, Chen et al. 2014). The intrinsic cardiac ganglia play important roles in triggering AF (Haissaguerre, Jais et al. 1998), and studies have shown that surgical ablation of these ganglia can terminate atrial arrhythmias (Lemola, Chartier et al. 2008, Lu, Scherlag et al. 2009, Stavrakis, Nakagawa et al. 2015). *Scn1b*

null mice have bradycardia that becomes evident by P14. Cardiac parasympathetic ganglia, glial cells, and nerve fibers in mice develop through the third postnatal week, the time point at which *Scn1b* null mice die. Innervation of the AVN occurs earlier than the SAN, suggesting a critical role for early initiation of AVN conduction in the developing heart (Fregoso and Hoover 2012). Consistent with these results, P16 WT mice had increased numbers of ChAT+ neuronal cell bodies in the LGC, which predominantly innervates the AVN (Pauza, Saburkina et al. 2013), compared to the RGC. We found the situation to be reversed in *Scn1b* null atria, in which we observed a significant increase in the number of ChAT+ neurons located in the RGC, which predominantly innervates the SAN (Pauza, Saburkina et al. 2013, Pauza, Rysevaite et al. 2014), vs. the LGC. We propose that neuronal migration and pathfinding may be impaired in the *Scn1b* null atrium. Our previous work using mouse cerebellar granule neurons showed that β1-β1 *trans* homophilic cell adhesion promotes neurite extension (Davis, Chen et al. 2004). *Scn1b* null mice, which lack this signaling mechanism, have aberrant neuronal migration, pathfinding, and fasciculation in the cerebellum as well as in the corticospinal tract and hippocampus (Brackenbury, Davis et al. 2008, Brackenbury, Yuan et al. 2013). Thus, we suggest that differences in cardiac neuronal development, increased $I_{Na,L}$, altered gene expression, and the development of fibrosis may synergistically contribute to AF susceptibility in *Scn1b* null animals.

Our body of work shows that *Scn1b* and *Scn2b* are necessary for normal atrial rhythm, however, there are important differences in the null mouse phenotypes. Adult *Scn2b* null mice have atrial remodeling and increased susceptibility to AF (Bao, Willis et al. 2016). ECG measurements

showed that adult *Scn2b* null mice had normal heart rates compared to WT. In contrast, our present results show bradycardia in neonatal *Scn1b* null mice. While AF induction in adult *Scn2b* null mice required carbachol administration, we observed a high incidence of pacing-induced AF in neonatal *Scn1b* null mice prior to the injection of carbachol. Similar to our observations in adult *Scn2b* null mice, we found that the APD was significantly prolonged in neonatal *Scn1b* null atrial myocytes with no effects on resting membrane potential or AP amplitude. We found that $I_{Na,L}$ was increased in *Scn1b* null atrial myocytes, providing a possible mechanism for APD prolongation. In contrast, we found no differences in I_{Na} density in *Scn2b* null atrial myocytes compared to WT. Instead, downregulation of the non-inactivating steady-state potassium currents, I_K and I_{KSS}, was implicated in the delayed AP repolarization observed in this model. Finally, both *Scn1b* and *Scn2b* deletion appear to be linked to atrial fibrosis, suggesting that the ICDs of both β1 and β2 may regulate transcription in fibroblasts, although at different developmental timepoints.

In conclusion, we propose that *SCN1B* LOF variants may increase susceptibility to atrial arrhythmias via a neuro-cardiac mechanism that includes aberrant cardiac innervation, SAN dysfunction, altered $I_{Na,L}$ leading to APD prolongation, and altered atrial modeling through fibrosis (Figure 2.13). Combined loss of the multi-functional roles of Na_v-β1 and -β1B subunits in channel modulation, cell-cell and cell-matrix adhesion, and transcriptional regulation may explain this complex mechanism. Further studies are necessary to explore whether targeting Na_v-β1 regulation will open new therapeutic avenues for AF and cardiac fibrosis.

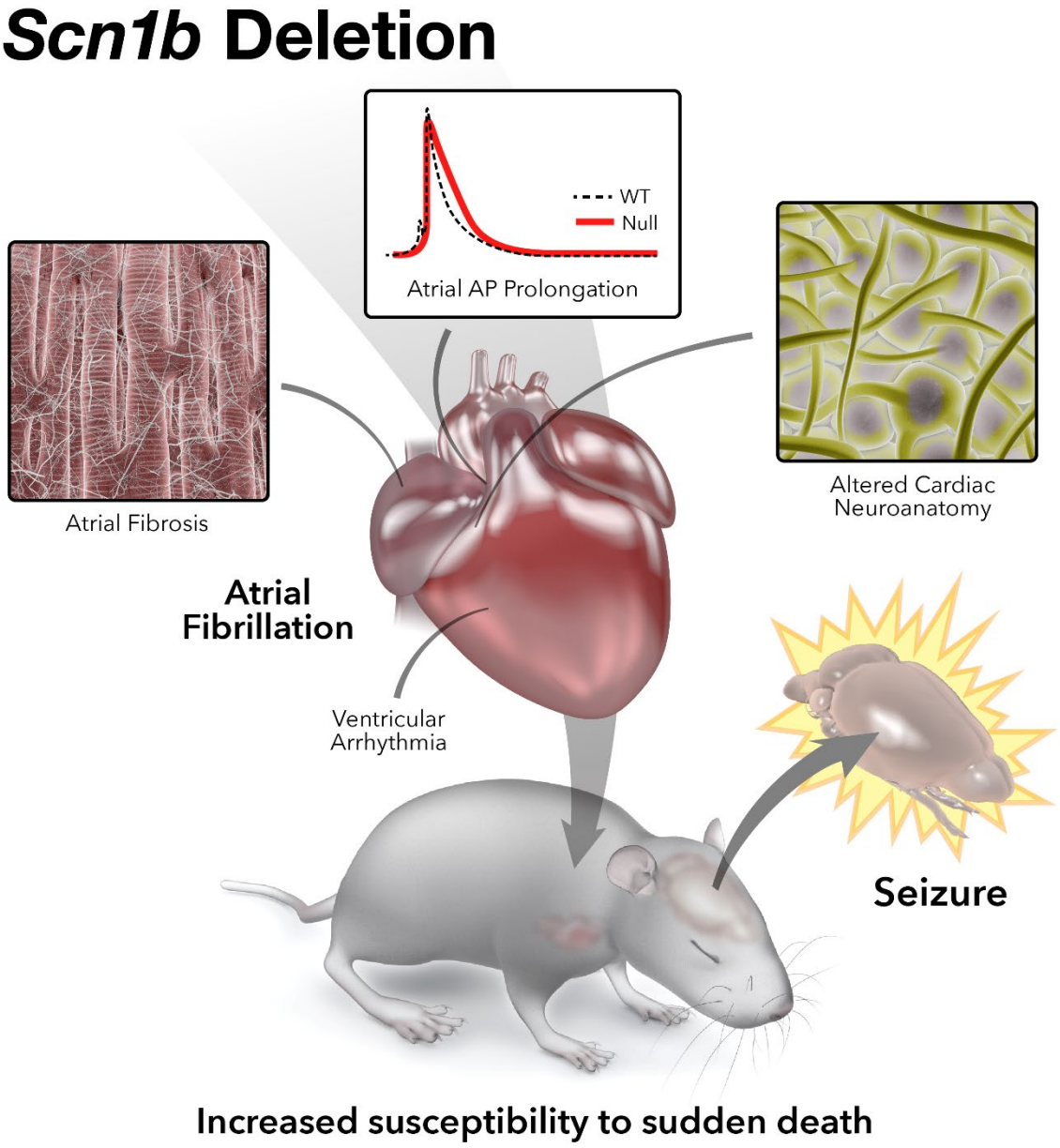

Figure 2.13. Cartoon detailing main findings

Scn1b deletion increases susceptibility to atrial fibrillation in neonatal mice via a neuro-cardiac mechanism that includes impaired atrial modeling through altered gene expression and fibrosis, increased atrial myocyte late sodium current resulting in action potential (AP) prolongation, and aberrant cardiac innervation

Methods

Animals

Scn1b null and WT littermate mice were generated from *Scn1b*$^{+/-}$ mice that were congenic on the C57BL/6J background for over 25 N generations(Chen, Westenbroek et al. 2004). Animals were housed in the Unit for Laboratory Animal Medicine at the University of Michigan Medical School. All procedures were performed in accordance with NIH guidelines and approved by the University of Michigan Institutional Animal Care and Use Committee (IACUC). Investigators were blinded to genotype for all experiments. Male and female mice were used in all experiments.

RNA-Seq

RNA was isolated from the atria of four P16 *Scn1b* WT and four P16 *Scn1b* null mice using the Qiagen RNeasy Plus kit according to the manufacturer's instructions. Sequencing was performed by the University of Michigan Advanced Genomics Core, with libraries constructed and subsequently subjected to 151 bp paired-end cycles on the NovaSeq-6000 platform (Illumina). Data quality was assessed using FastQC (version v0.11.8). Reads were mapped to the reference genome GRCm38 (ENSEMBL), using STAR (v2.7.3a) and assigned count estimates to genes with RSEM (v1.3.2). The University of Michigan Bioinformatics Core pre-filtered the data to remove genes with 0 counts in all samples. Differential gene expression analysis was performed using DESeq2. Genes and transcripts were considered differentially expressed if they met the following three criteria: test status = "OK", false discovery rate ≤0.05, and a log fold change of

expression with absolute value of at least 0.5849625. GO-term enrichments were performed using iPathway Guide (Advaita).

qRT-PCR

Atrial tissue from P16 *Scn1b* null (n = 4-6) and WT (n = 5) mice were individually homogenized, and total RNA was isolated from samples using the Qiagen RNeasy Fibrous Tissue Mini Kit according to the manufacturer's instructions. Atrial tissue was homogenized with a Tissue-Tearor (BioSpec Products, Inc.) followed by lysis through a sterile, 18 gage hypodermic needle, and sonication. RNA samples were run on a NanoDrop One Spectrophotometer (ThermoFisher Scientific) to ensure adequate concentration and purity and then stored at -80°C. cDNA was generated from 1 mg of RNA using Reverse Transcriptase SuperScript III (RT SS III), random primers (Invitrogen), and dNTPs (Invitrogen). RNA, random primers, and dNTPs were incubated at 65°C for 5 min. Salt buffers, 0.1M DTT, RNase Out, and RT SS III were added and reactions were incubated at 25°C for 5 min, 50°C for 60 min, and at 70°C for 15 min. cDNA was diluted 1:3 in RNase-free water. Quantitative PCR was performed using SYBR Green (Applied Biosystems) and gene-specific primers (Integrated DNA Technologies) on a QuantStudio 7 Flex Real-Time PCR System (Applied Biosystems). Gene-specific measurements of each cDNA sample were run in triplicate, along with the endogenous control gene (*Gapdh*) used for normalization, and then compared to WT expression levels. The relative expression level of each gene was quantified using the comparative threshold ($2^{-\Delta\Delta Ct}$) method of quantification. Data are presented as the fold change in gene expression ± SEM. Statistical significance ($p < 0.05$) between genotypes was determined using a Student's *t*-test.

Picrosirius Red Staining

Hearts from P16-17 WT (n=10) or null (n=10) animals, were perfused with PBS (in mM; 137 NaCl, 2.7 KCl, 8 Na_2HPO_4, and 2 KH_2PO_4) before extraction. Whole hearts were frozen separately in Tissue Plus OCT compound and were sliced with a microtome to obtain 10 micrometer thick transverse cross sections. Sections consisting of atrial and ventricular regions were fixed in 3.7% paraformaldehyde followed by cold methanol for 15 min each, followed by washing with PBS twice for 5 min at room temperature (RT). Tissue sections were stained with picrosirius red (Abcam) for 10 min at RT. Excess stain was washed twice with acetic acid. The slides were then dehydrated with ethanol for 90 s. Stained tissue sections were air-dried and mounted in Vectashield H100 mounting medium without DAPI. Images were acquired with a Nikon Microphot-FXA fluorescence microscope under brightfield at equal exposure time for all images. The red color intensity per area was measured using NIH Image J software. Data are presented as average integrated density per area ± SEM.

Echocardiography

Echocardiography on P16 mice was performed as fee-for-service by the University of Michigan Small Animal Phenotyping Core with IACUC approved protocols. Induction of anesthesia was performed in an enclosed container filled with 5% isoflurane. After induction, the mouse was placed on a warming pad to maintain body temperature. 0.5 – 1.5% isoflurane was supplied via a nose cone to maintain a surgical plane of anesthesia. The hair was removed from the upper abdominal and thoracic areas with depilatory cream. Eye lubricant was applied to prevent

corneal damage during prolonged anesthesia. Electrocardiogram (ECG) and respiration were monitored via non-invasive resting electrodes. Transthoracic echocardiography was performed in the supine or left lateral position. Two-dimensional, M-mode, Doppler, and tissue Doppler echocardiographic images were recorded using a Visual Sonics Vevo 2100 high resolution *in vivo* micro-imaging system with a MS 550D transducer with a center frequency of 40 MHz and a bandwidth of 22-55 MHz. We measured LV ejection fraction from the two-dimensional long axis view. In addition, we measured systolic and diastolic dimensions and wall thickness by M-mode in the parasternal short axis view at the level of the papillary muscles. Fractional shortening and ejection fraction were calculated from the M-mode parasternal short axis view. Diastolic function was assessed by conventional pulsed-wave spectral Doppler analysis of mitral valve inflow patterns (early [E] and late [A] filling waves). Doppler tissue imaging (DTI) was used to measure the early (Ea) diastolic tissue velocities of the septal and lateral annuluses of the mitral valve in the apical 4-chamber view. Left atrial volumes were calculated by applying a prolate ellipse method, using apical 4-chamber and parasternal long axis views.

Atrial myocyte isolation

Each experimental mouse was euthanized at P16, the heart was removed, and the blood was cleared using gentle perfusion with cold Hank's balanced salt solution (Gibco) supplemented with 10 mM HEPES and 1 $MgCl_2$. The heart was cannulated through the aorta and retrograde perfused on a Langendorff apparatus for 5 min at 37 °C. HBSS buffer containing 50 μg/mL Liberase^{TM} (Roche, Indianapolis, IN) was perfused into the heart for 10 to 12 min at 37 °C. Right and left atria were removed from the heart and placed in a 3 cm petri dish containing fresh

enzyme. Digestion of the tissue was continued by gentle stirring with a stir bar at 37 °C for 5 min. Digested tissue was passed through a plastic pipette to fully disperse the myocytes. Atrial myocytes were transferred into Hank's Balanced Salt Solution (Thermofisher) containing 10% fetal bovine serum (stopping solution) and centrifuged at 250 x g for 2 min. Cells were suspended in fresh stopping solution and subjected to calcium re-introduction until reaching a final concentration of 1.2 mM $CaCl_2$.

ECG and programmed electrical stimulation.

Scn1b null mice have a failure-to-thrive phenotype and do not exceed ~5 g during their lifetime (Yuan, O'Malley et al. 2019). Thus, they are too small to perform telemetry experiments. Instead, *in vivo* studies were performed in anesthetized P16 mice (induction period 5.0 vol. %, maintenance 2.0 % vol. isofluorane in 0.5L/min 100% O_2.) After the disappearance of reflexes, mice were placed onto a temperature-regulated operating table. Platinum electrodes were inserted subcutaneously in the limbs and connected to a custom-ECG amplifier for standard leads I and II. Standard ECG parameters, including HR, P wave duration and RR, QRS, PR-I, QTc intervals, were analyzed under stable baseline conditions. A 1.1 Fr Octapolar stimulation-recording catheter (EP catheter, Science) was inserted through the jugular vein and advanced into the right atrium and ventricle. A S1S1 protocol at 2x the threshold of capture was applied to determine the basal sinus node recovery time (SNRT) at 100 ms and 80 ms cycle lengths ($SNRT_{100}$ and $SNRT_{80}$). Atrial arrhythmia was assessed by atrial burst pacing for 2 s at 30, 40, or 50 Hz before and after the intraperitoneal (i.p.) application of carbachol (0.025 mg/kg) or atropine (1 mg/kg). AF was defined as the occurrence of rapid and fragmented atrial

electrograms (lack of regular P waves), with irregular AV-nodal conduction and ventricular rhythm, lasting at least 1 s.

Whole Cell Patch Clamp Analysis

I_{Na} recording in acutely isolated P16 atrial myoctes: Membrane capacitance was estimated by applying a 100 ms pulse from -100 to -120 mV before and after the rupture of the patch. Integration of the difference between these values was proportional to membrane capacitance (Cm). After establishing the whole cell configuration, membrane capacitive components were eliminated using the features of the amplifier to avoid amplifier saturation. Electronic compensation was used to reduce the series resistance. Residual linear components were eliminated with a *P/4* online subtraction protocol. I_{Na} was elicited by applied repetitive squared 200 ms pulses ranging from -70 to 60 mV from a holding potential of -120 mV at RT. The pipette solution contained (in mM): 120 CsCl-Asp, 1 NaCl, 10 EGTA, 1 $MgCl_2$, 1 Na_2ATP, 10 TEA-Cl and 10 HEPES (pH 7.2 with CsOH). The bath solution contained (in mM): 10 NaCl, 50 CsCl, 20 TEA-Cl, 1.2 $CaCl_2$, 60 Choline-Cl 1.0 $MgCl_2$, 1 4-aminopyridine, 0.05 $CdCl_2$ and 10 HEPES (pH 7.4 with CsOH). Nifedipine at a final concentration of 10 μM was added to the bath to block L-type calcium currents**.**

AP recordings in acutely isolated P16 atrial myocytes: The threshold for AP initiation was determined by the application of 2 ms incremental current pulses from 100 to 800 pA. Steady AP capture was obtained by applying current pulses at 1.5x the threshold. APs were recorded at 1.0

Hz at RT. The pipette solution contained (in mM): 120 K-aspartate, 20 KCl, 1 $MgCl_2$, 5 Na_2ATP, 10 EGTA and 10 HEPES (pH 7.4 with NaOH). The bath solution consisted of HBSS 1x solution containing (in mM) 10 HEPES, 1 $MgCl_2$ and 1.2 mM $CaCl_2$ (pH 7.4 with NaOH). Only myocytes with resting membrane potentials of at least -65 mV were included in the analysis.

Patch pipettes with resistance between 2.5-3.0 MΩ were used for all patch clamping experiments.

Whole-Mount Atrial Preparations

Cardiac dissections were performed in euthanized P15-17 mice as described previously (Rysevaite, Saburkina et al. 2011, Rysevaite, Saburkina et al. 2011, Pauza, Saburkina et al. 2013). In brief, the heart was perfused with cold PBS to ensure clearance of blood. The heart was then excised and placed in a Sylguard-coated dish containing cold PBS. The greater ascending vessels were separated from the atria. Then the atria were separated from the ventricles. The atria were gently dissected open, flattened, and fixed for 30 min in methanol at RT, and then rinsed 3×10 min in cold PBS and prepared for immmunohistochemistry.

Immunohistochemistry

Mouse tissues were permeabilized for 1 h in 0.5% Triton-X in PBS and blocked in 5% normal donkey serum in PBS for 2 h at RT. The preparations were incubated in a mixture of primary antibodies (goat anti–choline acetyltransferase [anti-ChAT; 1:100; millipore], rabbit anti–

tyrosine hydroxylase [anti-TH; 1:750; abcam], or rabbit anti-HCN4 [anti-HCN4; 1:200; Chemicon]) for 24-48 h at 4°C. After washing, tissues were incubated in a mixture of secondary antibodies for 4 h at RT. Tissues were then mounted on glass slides using Prolong Gold Mounting Medium (Invitrogen), coverslipped, and sealed with clear nail polish.

Confocal microscopy and image analysis

Fluorescent images were acquired using a Nikon A1R inverted confocal microscope (Nikon Instruments) located in the University of Michigan Microscopy Core. Image analysis was performed using Fiji software. The number of cells and identification of ChAT positive (+) or TH + signals were determined by manually counting cell bodies. Investigators were blinded to mouse genotype for each image. The cell labeling of each cardiac ganglion was counted independently at least twice and the results averaged.

Data availability

RNA-Seq data reported in this paper have been deposited in the Gene Expression Omnibus (GEO) database, https://www.ncbi.nlm.nih.gov/geo (accession no. GSE152617).

Research materials availability

Scn1b$^{+/-}$ mice are available from the University of Michigan under Materials Transfer Agreement.

Chapter 3. *Scn1b*-Linked DEE52 Patient-Derived Cardiac Myocytes Show Substrates for Arrhythmia

Nnamdi Edokobi, Tracy Qiao, Samantha L. Hodges, Alexandra A. Bouza, Caroline Scheuing, Louis T. Dang, Yao-Chang Tsan, PhD, Adam S. Helms, MD, MS, Sarah Weckhuysen[3], Jack M. Parent, Lori L. Isom

Introduction

Sudden Unexpected Death in Epilepsy (SUDEP) is the leading cause of death in people with uncontrolled seizures. While all patients with epilepsy are at risk for SUDEP, patients with developmental and epileptic encephalopathy (DEE) syndromes have the highest risk. In spite of this knowledge, no biomarkers exist to predict the extent of SUDEP risk in individual patients other than the presence of variants in specific genes. To gain insight into the mechanism of SUDEP, we are focusing on DEE syndromes with the highest SUDEP incidence. DEEs are a group of disorders characterized by pharmacoresistant seizures, cognitive impairment, and premature mortality (Jain, Sharma et al. 2013). Patients with DEE52 have inherited, biallelic variants in *SCN1B*, the gene encoding voltage-gated sodium channel (Na_v) β1 and β1B subunits. DEE52 patients have clinical presentations comparable to Dravet Syndrome (DS) or to the more severe early infantile developmental and epileptic encephalopathy (EIDEE), for which there is a

SUDEP risk of up to 25% (Patino, Claes et al. 2009, Ogiwara, Nakayama et al. 2012, Ramadan, Patel et al. 2017, Aeby, Sculier et al. 2019). Inherited monoallelic *SCN1B* variants are linked to Generalized Epilepsy with Febrile Seizures plus (GEFS+) (Wallace, Wang et al. 1998, Wallace, Scheffer et al. 2002, Audenaert, Claes et al. 2003) and cardiac conduction disorders such as Brugada syndrome and Long-QT syndrome, that are also associated with sudden death (Edokobi and Isom 2018). Although the mechanism of SUDEP remains unclear, it is hypothesized that, in addition to generalized seizures, SUDEP involves cardiac arrythmias (Bagnall, Crompton et al. 2017). We proposed previously, using DS patient-derived induced pluripotent stem cell cardiomyocytes (iPSC-CMs), that increased sodium current (I_{Na}) density may be a biomarker for SUDEP risk by providing a substrate for cardiac arrhythmia (Frasier, Zhang et al. 2018). Testing this hypothesis requires the investigation of iPSC-CMs from additional DEE patient cohorts. In this study, we assessed changes in the excitability of DEE52 patient-derived iPSC-CMs.

Na_v-α subunits are critical for the generation and propagation of cardiac action potentials (APs). Membrane depolarization results in rapid Na_v activation and inactivation to allow the controlled influx of sodium into CMs (Nerbonne and Kass 2005). The resulting I_{Na} is responsible for the upstroke (phase 0) of non-pacemaker cardiac cell APs (Nerbonne and Kass 2005). Na_vs are heterotrimers composed of a single pore-forming α subunit and two non-pore-forming β subunits that modulate the α subunit in a cell type specific manner (O'Malley and Isom 2015). In addition to modulating channel expression and gating, the Na_v-β subunits are all members of the immunoglobulin superfamily of cell adhesion molecules (Ig-CAMs) (Malhotra, Kazen-Gillespie et al. 2000, Brackenbury, Davis et al. 2008, Yereddi, Cusdin et al. 2013). More recent work by our group has shown that Na_v-β1 subunits also function as transcriptional

regulators of genes critical to excitation-contraction coupling in CMs (Bouza, Edokobi et al. 2021). *Scn1b* deletion in mice results in severe seizures and death by the third week of life (Chen, Westenbroek et al. 2004). Importantly, *Scn1b* deletion is also arrhythmogenic; *Scn1b* null mice have an increased susceptibility to ventricular arrhythmias (Lopez-Santiago, Meadows et al. 2007, Lin, O'Malley et al. 2015). Taken together, this work suggests that cardiac dysregulation, in addition to severe seizures, may play a role in the mechanism of SUDEP in DEE52.

Here, we study the mechanism of a DEE52 Is patient variant, *SCN1B*-c.265c>T, predicting p.R89C, that was reported previously in a patient family (Darras, Ha et al. 2019). In contrast to the previous report, the patient studied here has a more severe disease presentation, suggesting that *SCN1B*-c.265c>T may result in a spectrum disorder. We used patient-derived iPSC-CMs and heterologous cell expression to investigate the mechanism of this *SCN1B* variant in terms of the known effects of Na_v-β1 subunits to promote Na_v cell surface expression, modulate I_{Na} density, and regulate I_{Na} kinetics. We found that β1-p.R89C is expressed at the plasma membrane and undergoes regulated intramembrane proteolysis (RIP), similar to WT, in heterologous cells. Co-expression of $Na_v1.5$, $Na_v1.1$, or $Na_v1.6$ with mutant β1 subunits in heterologous cells showed that β1-p.R89C increases $Na_v1.6$-generated $I_{Na.}$but not I_{Na} generated by $Na_v1.1$ or $Na_v1.5$, suggesting differential modulation of α subunit subtypes. We generated ventricular iPSC-CMs from three non-epileptic controls and two biallelic c.265c>T DEE52 patients, including a patient from the previously reported family as well as the new patient. Both patient iPSC-CM lines had increased transient and late I_{Na} compared to healthy controls, similar

to our previously reported results in acutely isolated *Scn1b* null mouse ventricular myocytes. Interestingly, we observed AP prolongation in the more severe patient iPSC-CMs (Patient 1) but not in the patient reported previously (Patient 2), suggesting a higher risk of cardiac complications and potentially higher SUDEP risk.

Results

Clinical Presentation

Patient 1 (male) was born after a normal pregnancy to healthy unrelated parents. Postnatal adaptation was normal. At 6 months of age the patient presented with a clonic seizure after a febrile infection, and at 7 months seizures evolved into status epilepticus. Until 3 years of age seizures always occurred at the beginning of illness. Two of these prolonged seizures required sedation at the intensive care unit. The patient began to experience afebrile seizures during the third year of life. Antiepileptic therapy failed to control seizures for the long term despite testing various combinations of phenobarbital, valproic acid, topiramate, clonazepam, stiripentol, and primidone. Neurological examination showed microcephaly, ataxia, central hypotonia, and severe intellectual disability. The clinical presentation of Patient 2 (female) was previously reported (Darras, Ha et al. 2019). Patient 2 exhibited a less severe neurological phenotype compared to Patient 1.

β1-p.R89C protein localizes to the plasma membrane in heterologous cells.

We used stably transfected Chinese Hamster Lung (CHL) fibroblasts to determine whether β1-p.R89C showed normal cell surface expression. CHL cells are an ideal cell line for this experiment because they do not express endogenous Na_v-β1 subunit mRNA or protein (Isom, Scheuer et al. 1995). We generated a bicistronic, full-length β1 subunit cDNA expression vector containing a C-terminal V5 epitope tag, a cleaving 2A sequence, and enhanced Green Fluorescent Protein (eGFP) to establish stable cells lines overexpressing β1-V5-2AeGFP-CHL, β1-p.R89C-V5-2AeGFP, or eGFP alone. We performed cell surface biotinylation assays to compare the presence of β1-p.R89C-V5 vs. β1-WT-V5 in the plasma membrane fraction. Total protein and neutravidin-selected cell surface proteins were analyzed by western blot with anti-V5 antibody. An antibody directed against HSP90 was used as an intracellular control to ensure only cell-surface proteins were biotinylated. We found β1-p.R89C-V5 in the plasma membrane fraction similar to WT, although at lower levels (Figure 3.1C, D). Quantification of the western blot results was performed by dividing the immunoreactive signal of the plasma membrane fraction by the total fraction of each construct (Figure 3.1D). We next used immunofluorescence confocal microscopy as an alternative method to assess cell surface expression. β1-WT-V5 or β1-p.R89C-V5 localization was examined in the stably transfected cell lines using anti-V5 antibody. Cells were co-stained with the fluorescently conjugated plasma membrane marker, wheat germ agglutinin (WGA). Colocalization of the anti-V5 and WGA signals confirmed the localization of β1-p.R89C at the plasma membrane (Figure 3.1E). The anti-V5 signal is also represented in an orthogonal confocal view (Figure 3.1F).

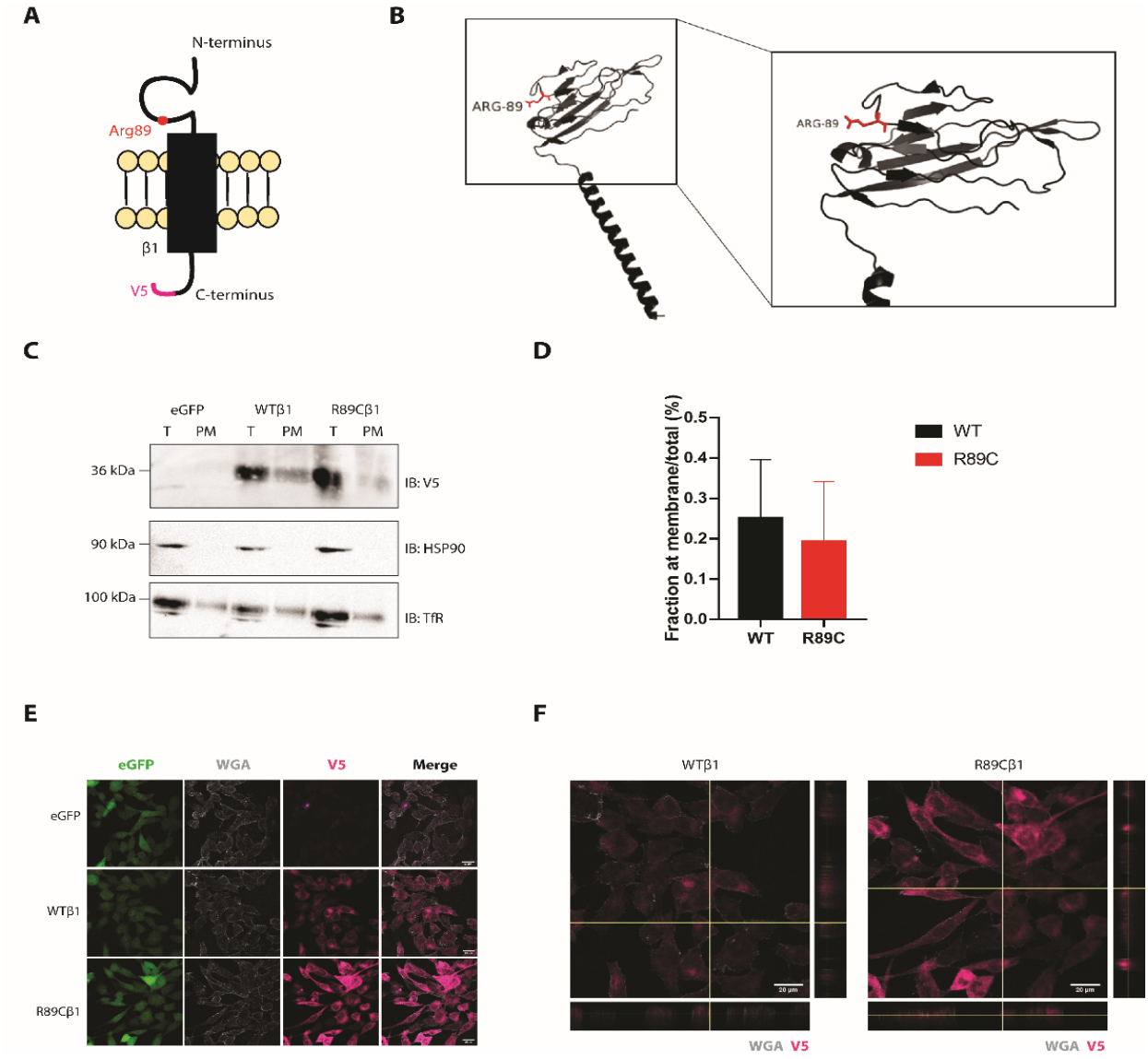

Figure 3.1. β1-p.R89C localizes to the plasma membrane.

(A) Cartoon diagram of p.R85C. (B) Crystal structure of WTβ1 (PDB: 6AGF). The residue, Arg89, is shown in red. Right: 20 angstrom area showing detail of the Ig domain. (C) Cell surface biotinylation shows that p.R89C can localize to the plasma membrane, similar to WT, N=3 (D) Quantification of biotinylation experiment. (E) β1-WT and β1-p.R85C colocalize with the plasma membrane marker, WGA N=2. (F) Orthogonal views of a single z-stack (YZ plane to right, XZ plane below) from immunofluorescence microscopy indicating colocalization between V5 and WGA signals. Key: Wheat germ agglutinin (WGA), to identify the plasma membrane, and V5 antibody, to label WT or mutant β1 subunits

β1-p.R89C undergoes RIP *in vitro*

Na_v-β1 subunits are cleaved sequentially by BACE1 and γ-secretase, resulting in release of the soluble β1 extracellular Ig domain that becomes a ligand for cell adhesion, as well as a soluble intracellular domain (β1 ICD) that can translocate to the nucleus (Wong, Sakurai et al. 2005, Bouza, Edokobi et al. 2021). We demonstrated previously that initial BACE1 cleavage of β1 results in a ~20 kDa immunoreactive band, representing the β1 C-terminal fragment (CTF) that remains in the membrane (Bouza, Edokobi et al. 2021). Pharmacological inhibition of the normally subsequent γ-secretase cleavage event results in increased levels of β1 CTF, which can be detected by western blot. Permitting γ-secretase activity generates the β1 ICD, which translocates to the nucleus where it is involved in the regulation of gene expression. We used a similar assay to determine whether β1-p.R89C undergoes RIP. β1-V5-2AeGFP-CHL or β1-p.R89C-V5-2AeGFP-CHL cells were treated with vehicle (0.1% DMSO) or 10 μM of either of two γ-secretase inhibitors, L-685,458 or Avagacestat. In both cell lines, γ-secretase inhibitor treatment resulted in β1-CTF accumulation compared to DMSO treatment (Figure 3.2), demonstrating that the β1-p.R89C variant does not prevent RIP.

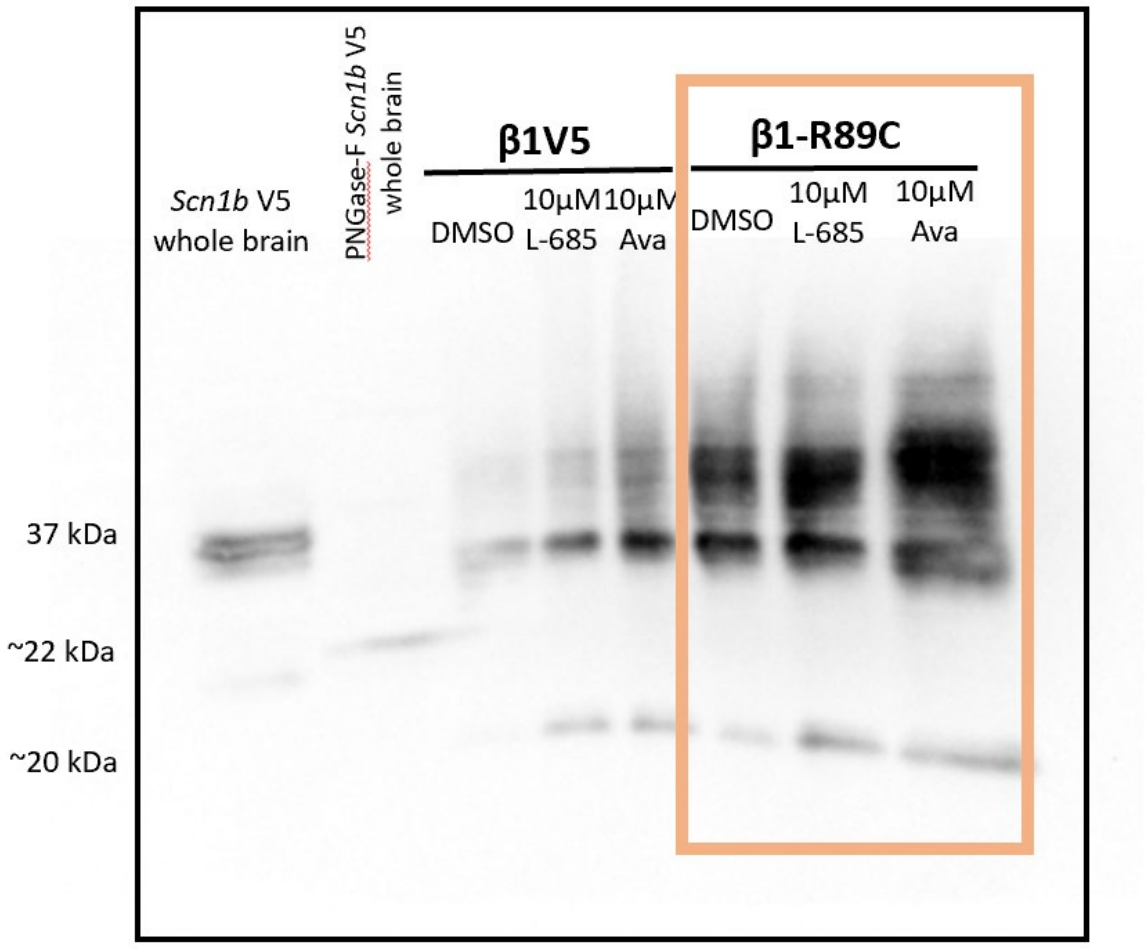

Figure 3.2. β1-p.R89C remains a substrates for BACE1 and γ-secretase intramembrane cleavage

Treatment with γ-secretase inhibitor, L-685,458 or Avagacestat, leads to an accumulation of β1-p.R89C-CTF.

Electrophysiological characterization of β1-p.R89C regulation of I_{Na}

Previously analyzed *SCN1B*-linked channelopathy variants have shown abnormalities in modulation of I_{Na} density and voltage dependent properties when expressed in heterologous systems (Watanabe, Koopmann et al. 2008, Patino, Claes et al. 2009, Watanabe, Darbar et al. 2009, Yuan, Koivumaki et al. 2014, Martinez-Moreno, Selga et al. 2020, Scala, Efthymiou et al. 2021). We and others have shown previously that Na_v-α subunit-generated I_{Na} is increased by co-expression of β1 subunits via their chaperone function of α to the plasma membrane (Isom, De Jongh et al. 1992). Here, we assessed the effects of β1-p.R89C subunit co-expression on I_{Na} expressed by the TTX-resistant channel $Na_v1.5$ or the TTX-sensitive channels $Na_v1.1$ or $Na_v1.6$ expressed in stable cell lines. We co-transfected eGFP (control), β1-WT, or β1-p.R89C into HEK cells stably expressing human $Na_v1.5$ (Figure 3.3), human $Na_v1.1$ (Figure 3.4), or human $Na_v1.6$ (Figure 3.5). As expected, β1-WT co-expression with all three channels significantly increased transient I_{Na} density ($p<0.001$) compared to α alone (eGFP) (Figure 3.3B, 3.4B, and 3.5B). In contrast, β1-p.R89C co-expression with $Na_v1.5$ or $Na_v1.1$ had no effect on transient I_{Na} density (Figure 3.3B and 3.4B). In contrast, β1-p.R89C co-expression with $Na_v1.6$ resulted in increased transient I_{Na} density ($p<0.001$) compared to α alone (eGFP) (Figure 3.5B). Neither WT-β1 nor β1-p.R89C significantly modulated the voltage dependence or kinetic properties of $Na_v1.5$-, $Na_v1.1$-, or $Na_v1.6$-generated I_{Na} (Figure 3.3D and E, 3.4D and E, and 3.5D and E and Table 3.1, 3.2, and 3.3). These results suggest that β1-p.R89C interacts differentially with Na_v-α subunits and may specially affect the plasma membrane localization of $Na_v1.6$.

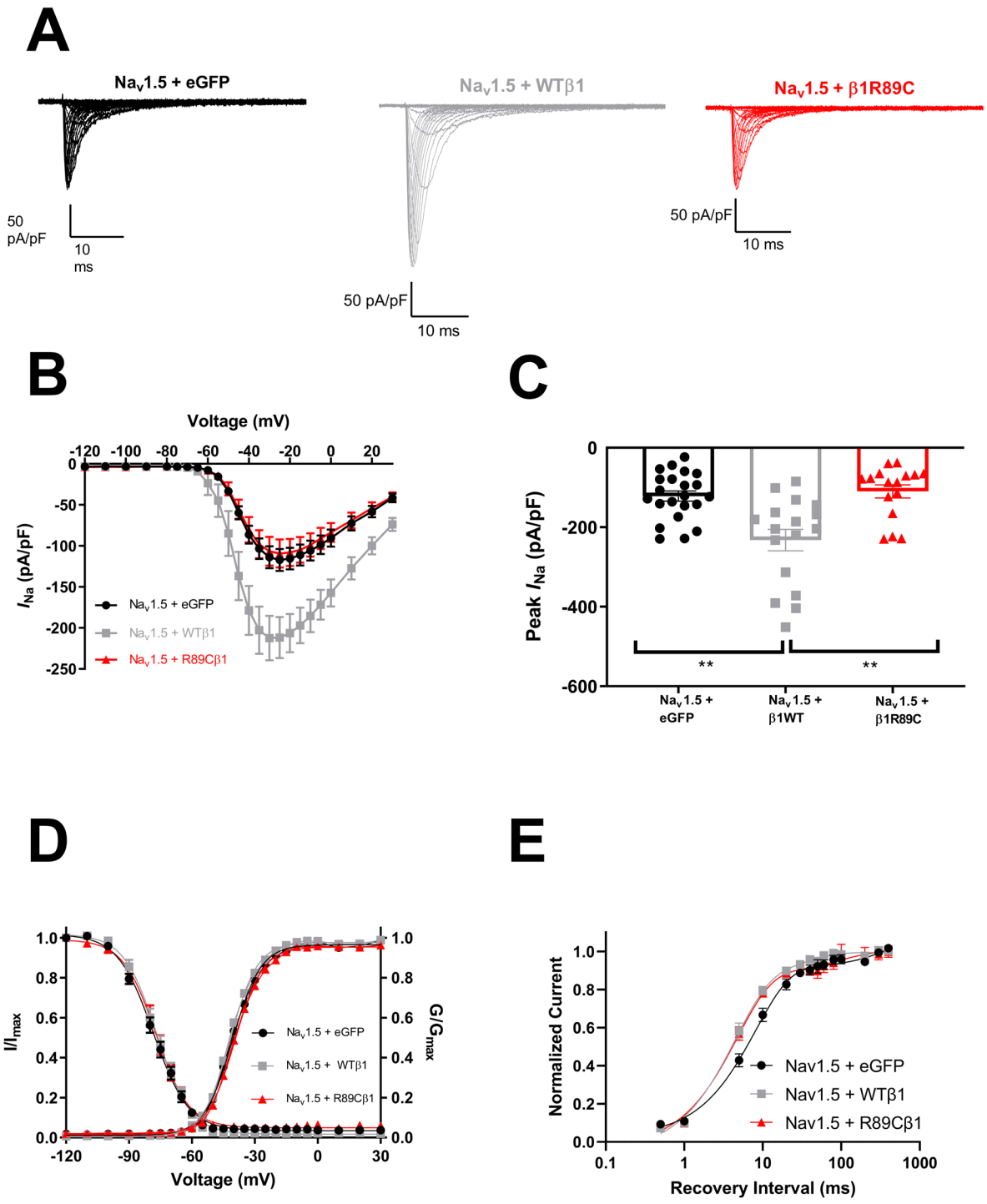

Figure 3.3 β1-p.R89C does not modulate Na$_v$1.5 I_{Na} density.

Cells stably expressing human $Na_v1.5$ in a HEK-293 background were transiently co-transfected with either β1-WT (grey squares) or β1-p.R89C (red triangles). Cells transfected only with eGFP (black circles) were used as negative controls. (A) Representative I_{Na} density traces. I_{Na} was recorded in response to a series of voltage steps between -120 and +30mV in 5 mV increments, from a holding potential of -120 mV for 200 msec. (B) $Na_v1.5$ I_{Na} current-voltage (I-V) relationship. (C) Sodium current density is increased with co-expression of WTβ1 and is unchanged in the presence of p.R89C. (D) No differences in the mean voltage-dependent activation and inactivation curves. Data were obtained by fitting individual activation or inactivation curves to a Boltzmann equation. (E) A standard two pulse protocol was used to investigate the recovery from inactivation. Recovery from inactivation is expressed as the fraction of current produced by a second pulse over time following an identical pre-pulse. The data are fit to a double exponential function. Data in (B), (C), (D), and (E) are presented as means ± SEM. **p < 0.01 by a one-way ANOVA with Tukey's post-hoc comparison test. Dots represent an individual cell.

Nav1.5	**+ eGFP**	**+ β1WT**	**+ β1R89C**
Voltage dependence of activation			
$V_{1/2}$ (mV)	-40.61 ± 0.24	-41.78 ± 0.39	-39.50 ± 0.24
k (mV)	6.77 ± 0.21	6.53 ± 0.34	6.65 ± 0.21
n	18	16	14
Voltage dependence of inactivation			
$V_{1/2}$ (mV)	-78.45 ± 0.48	-76.71 ± 0.43	-77.20 ± 0.56
h (mV)	-8.45 ± 0.40	-7.90 ± 0.37	-7.83 ± 0.48
n	18	16	14
Recovery from Inactivation			
τ_{fast} (ms)	7.55 ± 0.78	4.845 ± 0.60*	4.932 ± 0.51*
n	9	6	7

Table 3.1 Biophysical properties of I_{Na} expressed by $Na_v1.5$

Data are presented as means ± SEM. *p < 0.05 versus + eGFP using a one-way ANOVA with Tukey's post-hoc comparison test.

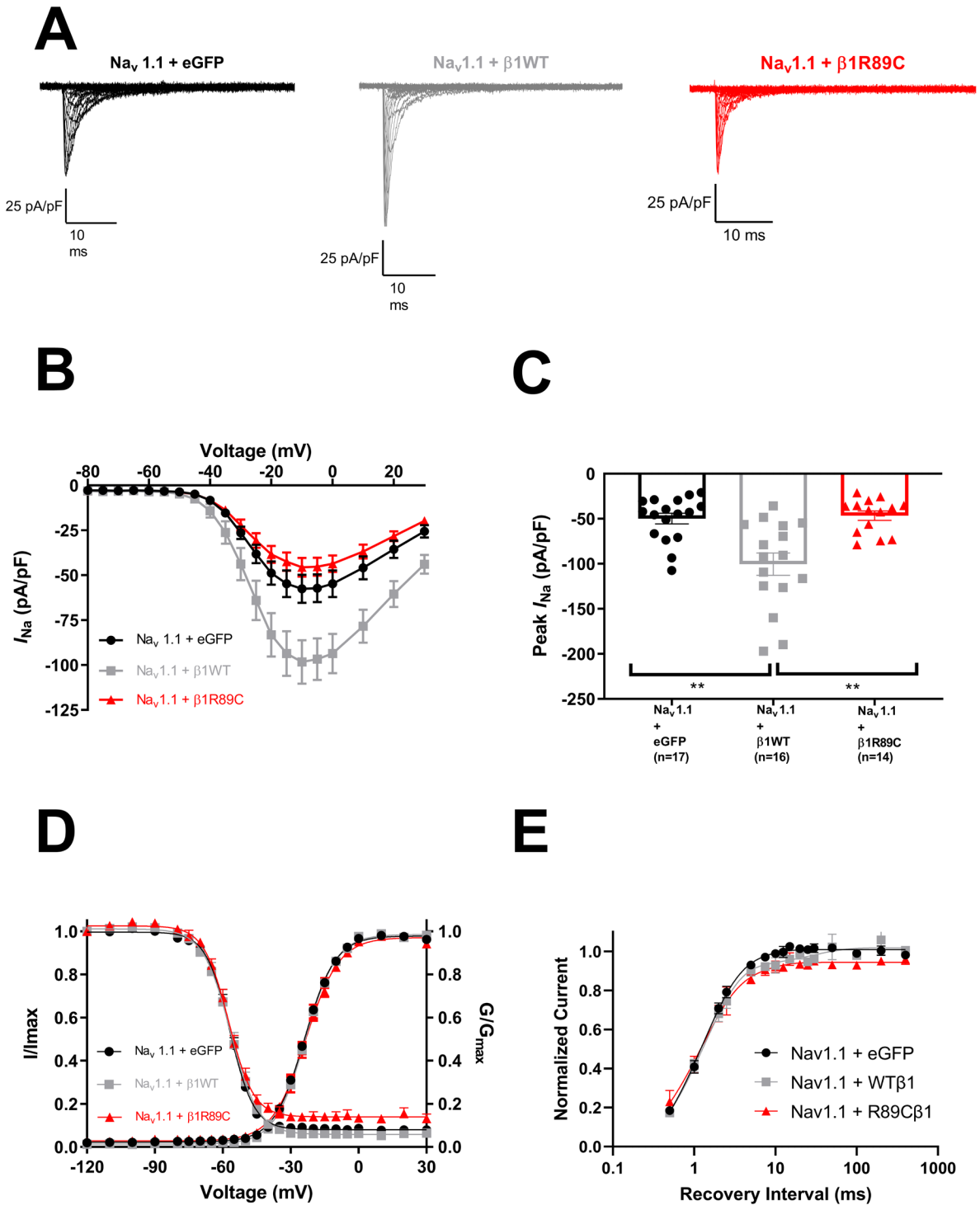

Figure 3.4. β1-p.R89C does not modulate $Na_v1.1$ I_{Na} density

Cells stably expressing human $Na_v1.1$ in a HEK-293 background were transiently co-transfected with either β1-WT (grey squares) or β1-p.R89C (red triangles). Cells transfected only with eGFP (black circles) were used as negative controls. (A) Representative I_{Na} density traces. (B) $Na_v1.1$ I_{Na} current-voltage (I-V) relationship. (C) Sodium current density is increased with co-expression of WTβ1 and is unchanged in the presence of p.R89C. (D) No differences in the mean voltage-dependent activation and inactivation curves. (E) Recovery from inactivation is expressed as the fraction of current produced by a second pulse over time following an identical pre-pulse. The data are fit to a double exponential function. Data in (B), (C), (D), and (E) are presented as means ± SEM. **p < 0.01 by a one-way ANOVA with Tukey's post-hoc comparison test. Dots represent an individual cell.

Nav1.1	**+ eGFP**	**+ β1WT**	**+ β1R89C**
Voltage dependence of activation			
$V_{1/2}$ (mV)	-23.90 ± 0.18	-23.51 ± 0.28	-23.34 ± 0.26
k (mV)	6.81 ± 0.15	6.78 ± 0.24	7.40 ± 0.22
n	17	16	14
Voltage dependence of inactivation			
$V_{1/2}$ (mV)	-56.86 ± 0.25	-56.61 ± 0.40	-57.40 ± 0.40
h (mV)	-5.32 ± 0.22	-6.07 ± 0.35	-5.52 ± 0.35
n	17	16	14
Recovery from Inactivation			
τ_{fast} (ms)	1.17 ± 0.14	1.01 ± 0.25	1.05 ± 0.18
n	8	6	6

Table 3.2 Biophysical properties of I_{Na} expressed by $Na_v1.1$

Data are presented as means ± SEM.

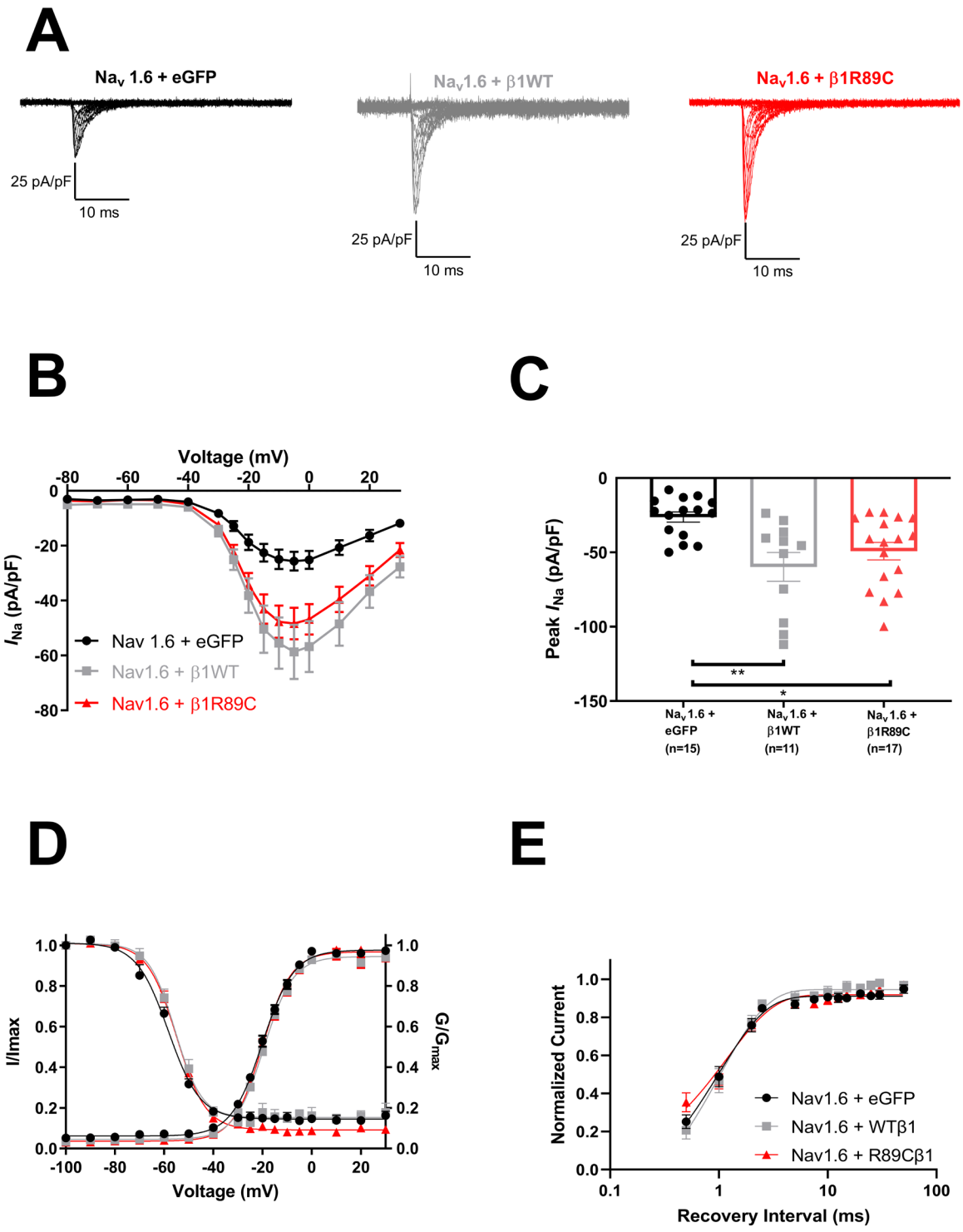

Figure 3.5. β1-p.R89C does modulate $Na_v1.6$ I_{Na} density

Cells stably expressing human $Na_v1.6$ in a HEK-293 background were transiently co-transfected with either β1-WT (grey squares) or β1-p.R89C (red triangles). Cells transfected only with eGFP (black circles) were used as negative controls. (A) Representative I_{Na} density traces. (B) $Na_v1.6$ I_{Na} current-voltage (I-V) relationship. (C) Sodium current density is increased with co-expression of WTβ1 and in the presence of p.R89C. (D) No differences in the mean voltage-dependent activation and inactivation curves. (E) Recovery from inactivation is expressed as the fraction of current produced by a second pulse over time following an identical pre-pulse. The data are fit to a double exponential function. Data in (B), (C), (D), and (E) are presented as means ± SEM. **p < 0.01, *p < 0.05 by a one-way ANOVA with Tukey's post-hoc comparison test. Dots represent an individual cell.

Nav1.6	**+ eGFP**	**+ β1WT**	**+ β1R89C**
Voltage dependence of activation			
$V_{1/2}$ (mV)	-20.06 ± 0.29	-19.49 ± 0.32	-20.12 ± 0.21
k (mV)	6.36 ± 0.26	6.00 ± 0.26	5.91 ± 0.26
n	15	11	17
Voltage dependence of inactivation			
$V_{1/2}$ (mV)	-58.29 ± 0.64	-55.55 ± 0.78	-54.93 ± 0.41
h (mV)	-6.46 ± 0.56	-5.41 ± 0.66	-5.95 ± 0.35
n	15	11	17
Recovery from Inactivation			
τ_{fast} (ms)	1.42 ± 0.56	0.93 ± 0.24	2.28 ± 0.49
n	8	8	10

Table 3.3 Biophysical properties of I_{Na} expressed by $Na_v1.1$

Data are presented as means ± SEM.

β1-p.R89C has no detectable dominate negative effects on WT-β1

DEE52 patients express biallelic *SCN1B* variants that are inherited from parents with expression of one WT and one mutant *SCN1B* allele. A subset of patients with monoallelic *SCN1B* variants have been diagnosed with GEFS+ or cardiac conduction disorders (Audenaert, Claes et al. 2003, Scheffer, Harkin et al. 2006, Watanabe, Koopmann et al. 2008, Orrico, Galli et al. 2009, Watanabe, Darbar et al. 2009, Fendri-Kriaa, Kammoun et al. 2011, Holst, Saber et al. 2012, Hu, Barajas-Martínez et al. 2012, Liu, Tester et al. 2014, Riuró, Campuzano et al. 2014, Neubauer, Rougier et al. 2018). Thus, it is possible that some *SCN1B* variants may have dominant-negative effects on the co-expressed WT allele. We explored whether this was the case for β1-p.R89C. Using methods similar to the previous experiment, we co-transfected eGFP (control) or β1-p.R89C into HEK cells stably expressing human $Na_v1.5$ plus β1-WT. We found no significant differences in peak I_{Na} or voltage dependent properties between groups (Figure 3.6 and Table 3.4). Therefore, we concluded that β1-p.R89C is not a dominant negative mutation in terms of I_{Na} regulation.

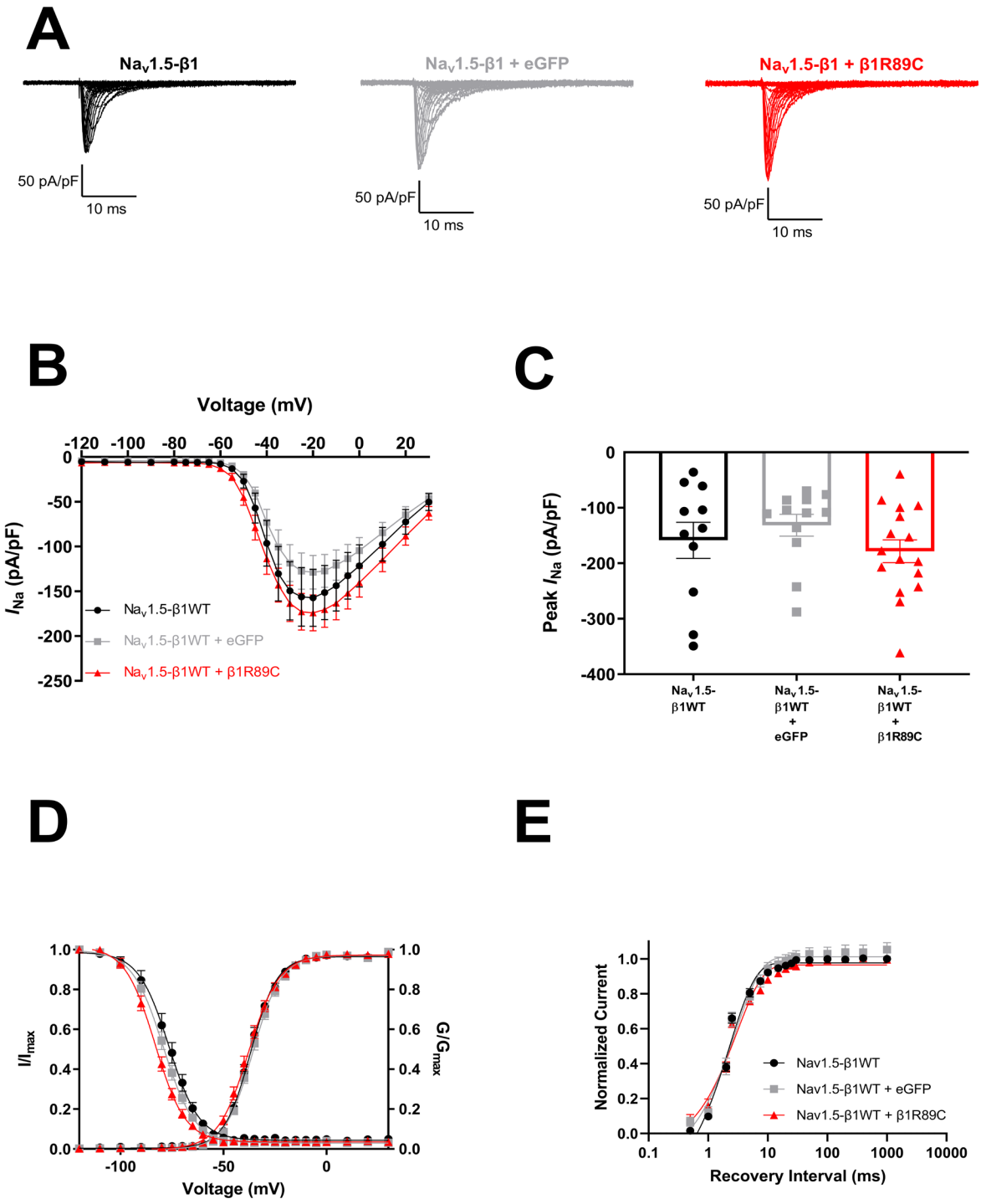

Figure 3.6. β1-p.R89C does not display a dominant-negative effect.

Cells stably expressing human $Na_v1.5$ and β1WT in a HEK-293 background were transiently co-transfected with either eGFP (grey squares) or β1-p.R89C (red triangles) (A) Representative I_{Na} density traces. (B) $Na_v1.6$ I_{Na} current-voltage (I-V) relationship. (C) Sodium current density is unchanged with co-expression of eGFP or β1-p.R89C. (D) No differences in the mean voltage-dependent activation and inactivation curves. (E) Recovery from inactivation is expressed as the fraction of current produced by a second pulse over time following an identical pre-pulse. The data are fit to a double exponential function, and the parameters (k, τ, and t½ for both the fast and slow components) are reported in Table. Data in (B), (C), (D), and (E) are presented as means ± SEM. Dots represent an individual cell.

Nav1.5-β1	**No plasmid**	**+ eGFP**	**+ β1R89C**
Voltage dependence of activation			
$V_{1/2}$ (mV)	-36.77 ± 1.02	-35.64 ± 0.86	-37.70 ± 1.13
k (mV)	6.08 ± 0.17	6.59 ± 0.26	6.996 ± 0.27
n	11	12	16
Voltage dependence of inactivation			
$V_{1/2}$ (mV)	-77.23 ± 2.27	-79.45 ± 1.43	-83.29 ± 1.26
h (mV)	-6.48 ± 0.19	-7.08 ± 0.22	-6.79 ± 0.21
n	11	12	16
Recovery from Inactivation			
τ_{fast} (ms)	1.59 ± 0.17	1.92 ± 0.19	2.04 ± 0.22
n	10	12	15

Table 3.4 Biophysical properties of I_{Na} expressed by $Na_v1.5$-β1

Data are presented as means ± SEM

SCN1B patient-derived iPSC-CMs

We generated iPSCs from *SCN1B* c.265>T DEE52 Patients 1 and 2 (Table 3.5) as well as one non-epileptic Control and the mother of Patient 2, who is non-epileptic and monoallelic for the variant (Table 3.6). Two separate lines were generated for Patient 1. Patient 1 and the two non-epileptic control lines were generated from skin fibroblasts. Lines from Patient 2 and mother of Patient 2 lines were derived from peripheral blood mononuclear cells by commercially available methods (Stem Cell Genetics). All iPSC lines were differentiated to CMs using the small molecular regulation method based on Wnt signaling pathway modulation (Lian, Hsiao et al. 2012).

	Patient 1-Clone 1	**Patient 1-Clone 2**	**Patient 2**
SCN1B	R89C	R89C	R89C
Sex	M	M	F
Sample type	Fibroblasts	Fibroblasts	Peripheral blood mononuclear cells
Note	Pt1-1	Pt1-2	

Table 3.5. Information on iPSC-CM patient lines

	Control 1	**Control 2**	**Het Control**
SCN1B	Normal	Normal	R89C heterozygous
Sex	F	M	F
Sample type	Fibroblasts	Fibroblasts	Peripheral blood mononuclear cells
Note			Mother of patient 2

Table 3.6. Information on iPSC-CM control lines

DEE52 patient iPSC-CMs have increased I_{Na}

We performed whole-cell voltage-clamp recordings to investigate whether iPSC-CMs from the biallelic DEE52 patients had altered transient or persistent I_{Na}. Initially, for the voltage clamp experiments we used an external solution containing 120 mM NaCl. We found that I_{Na} from Patient 1 CMs to be so large that proper voltage control could not be consistently maintained, and voltage-dependent properties could not be accurately measured (Figure 3.7). Therefore, we switched to an external solution containing 60 mM NaCl for all subsequent iPSC-CM voltage clamp experiments. Using the lower Na^+ external solution, we found the transient I_{Na} to be significantly increased in Patient 1 and Patient 2 iPSC-CMs (-130.40 ± 9.60 pA/pF and -116.20 ± 10.58 pA/pF, respectively) compared to the Het Control (-42.18 ± 4.78 pA/pF) and healthy Control iPSC-CMs (-52.44 ± 7.22 pA/pF) (Figures 3.8B and 3.8C). In addition, we found a significant increase in the mean persistent I_{Na} density at -50mV in Patient 1 (-1.68 ± 0.24 pA/pF) and Patient 2 (-1.82 ± 0.33 pA/pF) iPSC-CMs over pooled controls (-0.77 ± 0.16) pA/pF iPSC-CMs (Figure 3.8E), with no change in the ratio of persistent to peak transient I_{Na} densities (Figure 3.8F). There were no differences in cell capacitance, slope factor, or $V_{½}$ values for the voltage dependence of activation or steady-state inactivation (Table 3.7). Peak conductance (G_{max}) was significantly increased ($p<0.0001$) in Patient 1 and Patient 2 iPSC-CMs compared to control and Het control cells, suggesting increased cell surface Na_V expression in both Patient CM lines (Table 3.7).

Figure 3.9 shows separate vs. pooled data from control and Patient 1 iPSC-CMs clones. Because functional properties of iPSC-CM clones generated from the same patient can vary, we evaluated each clone separately (Figure 3.9A-D). We observed no significant differences between Control 1 (-58.41 ± 10.58 pA/pF) and Control 2 (-45.12 ± 10.10 pA/pF) transient peak I_{Na} density values (Figure 3.9C). There also was no significant difference in transient peak I_{Na} density between the Patient 1 clones: Pt1-1, -138.6 ± 13.19 pA/pF and Pt1-2, -123.2 ± 14.10 pA/pF (Figure 3.9C). Taken together, these results allowed us to confidently pool results from the Patient 1 and Control 1 and 2 iPSC-CM clones.

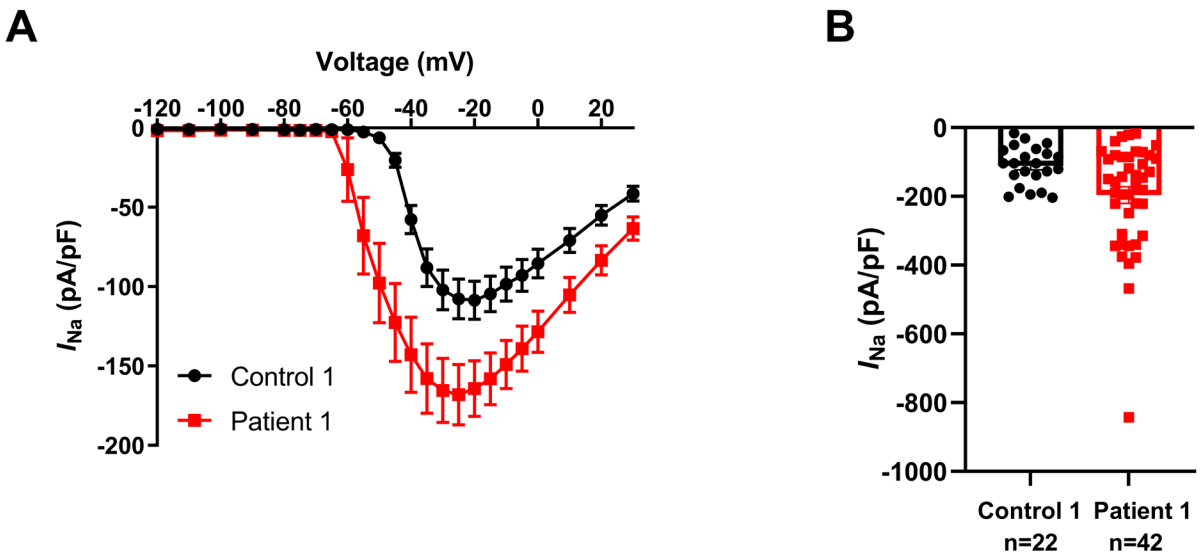

Figure 3.7 Large transient I_{Na} in Patient 1 iPSC-CMs

(A) I_{Na} current-voltage (I-V) relationship for Control 1 and Patient 1 iPSC-CM lines using an external Na^+ recording external solution containing 120mM NaCl. (B) Transient peak I_{Na} is increased in Patient 1 vs Control iPSC-CMs, however, consistent voltage control could not be maintained in Patient 1 iPSC-CMs.

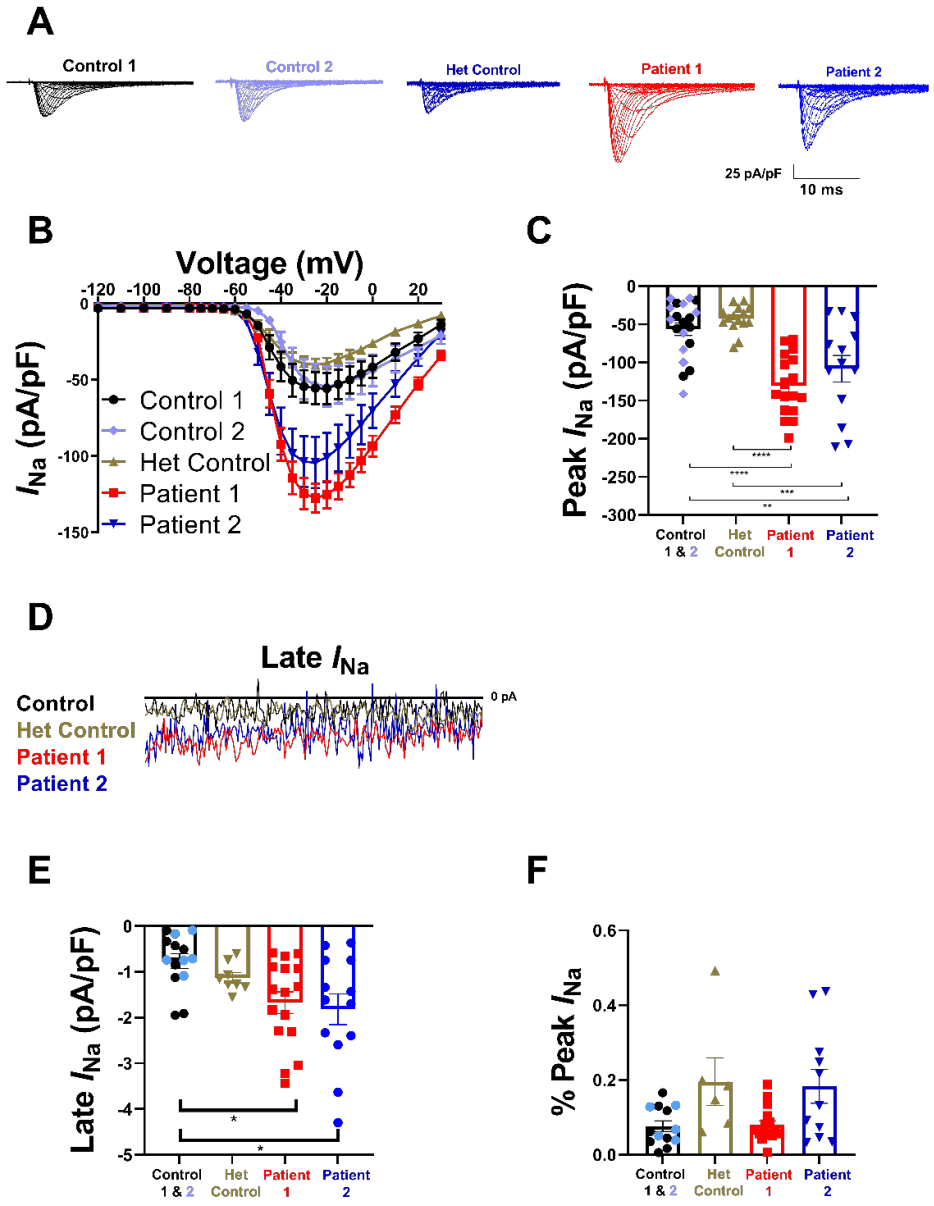

Figure 3.8. Transient and persistent I_{Na} are increased in both patient iPSC-CMs.

(A) Representative I_{Na} density traces. I_{Na} was recorded in response to a series of voltage steps between -120 and +30mV in 5 mV increments, from a holding potential of -120 mV for 200 msec. (B) I_{Na} current-voltage (I-V) relationship for control and patient iPSC-CM lines. (C) Transient peak I_{Na} is increased 2-fold in patient 1 and patient 2 vs control iPSC-CMs. (D) Zoomed traces of Late I_{Na}. Showing the current from 50-60 ms following the depolarizing pulse. (E) The mean Late I_{Na} is significantly increased in the patient iPSC-CMs. (F) Late I_{Na} normalized to the peak current. Data in (C), (E), and (F) are presented as means ± SEM. *$p < 0.05$; **$p < 0.005$; ***$p < 0.0005$; ****$p < 0.0001$ using a One-Way Anova with Tukey's post-hoc comparison test. Dots represent an individual cell.

	Control 1 & 2	Het control	Patient 1	Patient 2
Voltage dependence of activation				
$V_{1/2}$ (mV)	-36.59 ± 0.43	-38.66 ± 0.41	-39.92 ± 0.29	-41.57 ± 0.37
k (mV)	6.87 ± 0.38	6.33 ± 0.6	5.90 ± 0.25	6.28 ± 0.33
G_{max} (pS)	19.04 ± 0.96	14.50 ± 0.65	34.19 ± 0.96$^{*,\#}$	32.41 ± 1.47$^{*,\#}$
n	19	13	17	16
Voltage dependence of inactivation				
$V_{1/2}$ (mV)	-72.83 ± 0.66	-70.89 ± 0.61	-73.64 ± 0.41	-69.64 ± 0.32
h (mV)	-8.78 ± 0.58	-8.10 ± 0.54	-8.81 ± 0.36	-7.65 ± 0.28
n	19	13	17	16
Capacitance (pF)	18.54 ± 2.58	19.70 ± 1.67	23.77 ± 2.90	21.89 ± 2.25

Table 3.7 Biophysical properties of I_{Na} from iPSC-CMs

Data are presented as means ± SEM. *p < 0.001 versus Control; $^{\#}$p < 0.001 versus Het control using a one-way ANOVA with Tukey's post-hoc comparison test.

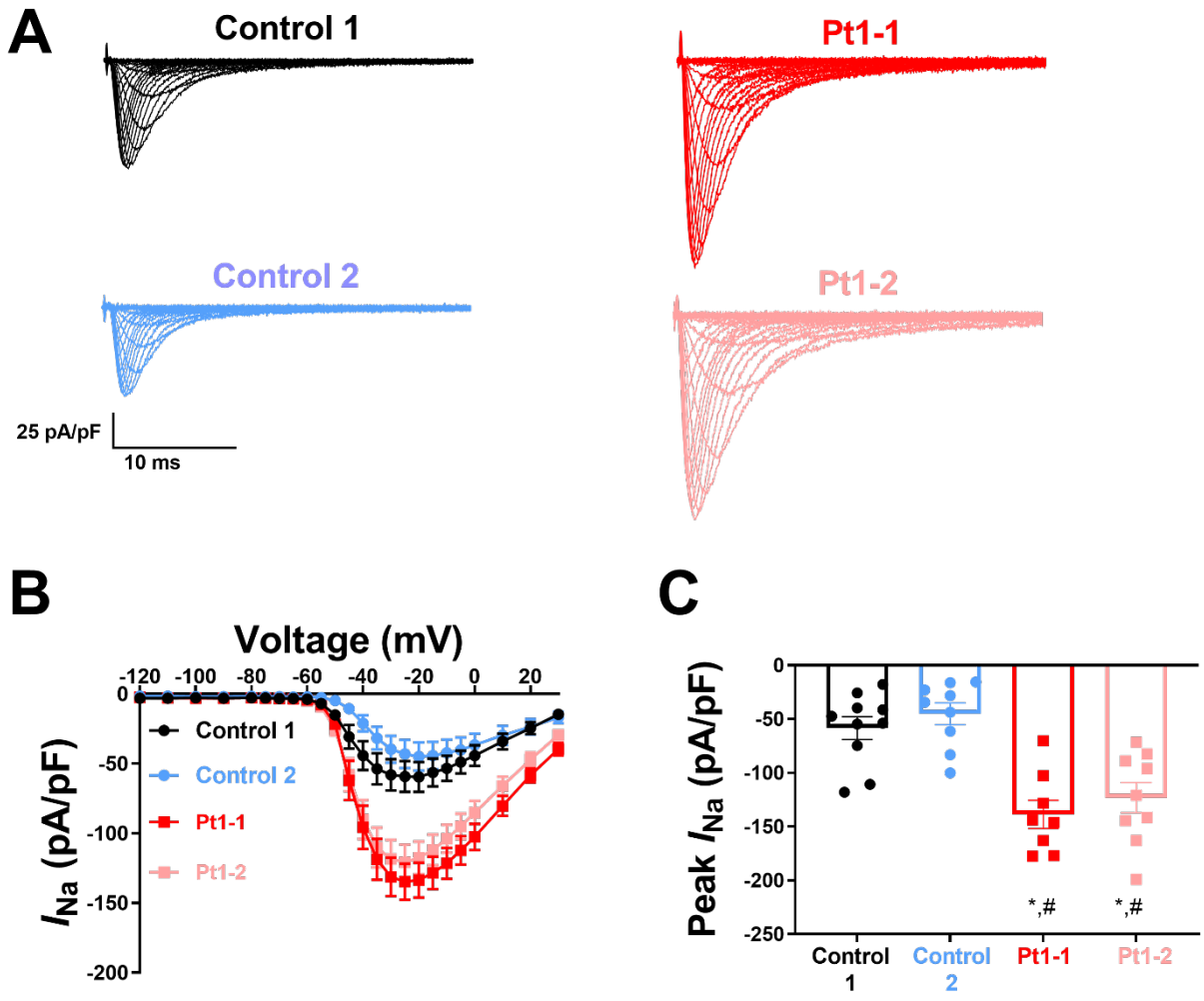

Figure 3.9. Independent representation of pooled Data.

(A) Representative I_{Na} density traces. (B) I_{Na} current-voltage (I-V) relationship for control 1, control 2, and patient 1 clones iPSC-CM lines. (C) Transient peak I_{Na} is increased 2-fold in patient 1 clones vs control iPSC-CM. Data in (C) are presented as means ± SEM. *$p < 0.001$ versus control 1; $^{\#}p < 0.001$ versus control 2 using a one-way ANOVA with Tukey's post-hoc comparison test. Dots represent an individual cell.

AP Prolongation in *SCN1B* patient iPSC-CMs

We generated iPSC cardiac tissue using the micron-scale two-dimensional cardiac tissue method. This method has been shown to control for cell shape and enabled reproducible characterization of cellular excitability using a polydimethylsiloxane (PDMS) micropatterned surface (Tsan, Zhao et al. 2021). Figure 3.10A presents representative traces of pooled Control and individual Patient APs elicited at 1 Hz in current clamp mode. The resting membrane potentials between pooled Control, Het Control, Patient 1, and Patient 2 iPSC-CMs were not significantly different (Figure 3.10B). Additionally, the peak amplitude and upstroke velocity (dV/dT) of the APs were not significantly different between Patient and pooled Control iPSC-CMs (Figure 3.10B and C). Notably, Patient 1, but not Patient 2, iPSC-CMs showed significantly prolonged APDs at 30%, 50% and 90% of the membrane repolarization (Figure 3.10D). This result suggests pro-arrhythmic properties in Patient 1, but not Patient 2, iPSC-CMs, consistent with the more severe phenotype of this patient.

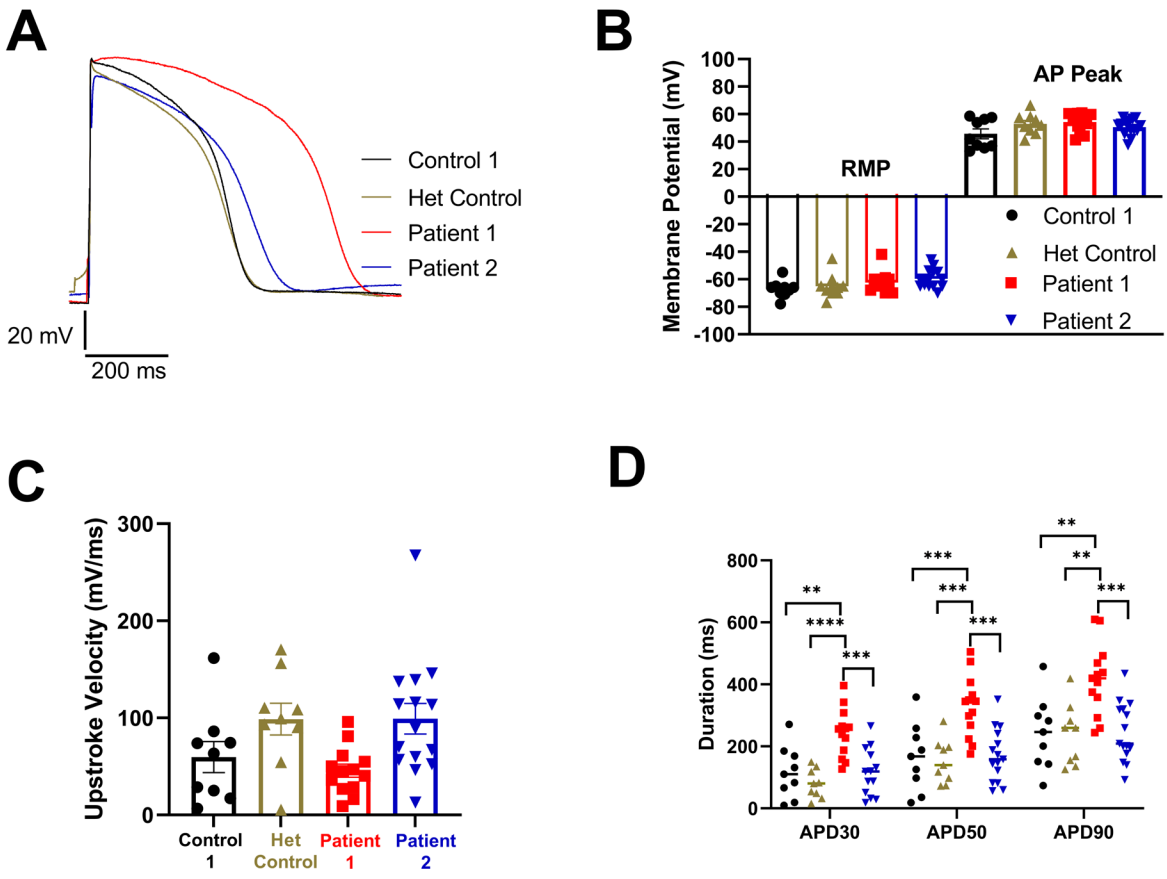

Figure 3.10. Action potential properties in iPSC-CMs.

Action potentials (AP) were evoked by pulses of 1.5 times the stimulus threshold at 1 Hz in current clamp mode. All the parameters of APs were compared between cells from control and the patient. (A) Representative traces of APs. (B) Mean values of resting membrane potentials (RMP) and action potential peak amplitude. (C) Maximal depolarization velocity of action potentials. (D) Patient 1 iPSC-CMs were exhibited significant differences in AP prolongation at 30% (APD30), 50% (APD50), 70% (APD70), and 90% repolarization (APD90). **p < 0.01; ***p < 0.001 using a one-way ANOVA with Tukey's post-hoc comparison test. Dots represent an individual cell

Discussion

This work presents the first characterization of DEE52 patient derived iPSC-CMs as well as the first demonstration of heterologous expression of the *SCN1B*-p.R89C variant. We demonstrate that β1-p.R89C polypeptides expressed in CHL are transported to the cell surface and are sequentially cleaved by BACE1 and γ-secretase. β1-R89C does not increase I_{Na} when co-expressed with Nav1.5 or Nav1.1. In contrast, we show that β1-R89C can increase I_{Na} in cells expressing Nav1.6. Electrophysiological analysis of patient derived iPSC-CMs revealed increased I_{Na} in cells derived from Patient 1 and Patient 2, but AP prolongation only in Patient 1 cells. These results support the hypothesis that *SCN1B*-linked DEE variants result in cardiac dysfunction, in addition to epilepsy, and suggest that these DEE52 patients, especially Patient 1, may be candidates for cardiac evaluation.

Nearly a dozen *SCN1B* variants have been characterized in *vitro*, although only some, p.R85C (Xu, Thomas et al. 2007), p.R85H (Xu, Thomas et al. 2007), p. R125C (Patino, Claes et al. 2009), p.C121W (Kruger, O'Malley et al. 2016), and now p.R89C, have been analyzed for defects in cell surface expression. Surface biotinylation analysis confirmed that a fraction of p.R85C (Aeby, Sculier et al. 2019), p.C121W (Kruger, O'Malley et al. 2016), and p.R89C polypeptides are expressed at the cell surface in transfected heterologous cell systems or cultured neurons. In contrast, p.R125C (Patino, Claes et al. 2009) is retained inside the cell at 37C (Patino, Claes et al. 2009). When cells were maintained at non-physiological temperature of 27C, normal cell surface localization of p.R125C was observed. These results suggest that at least a fraction of these β1 mutant proteins can localize to the cell surface, however, it is not known

whether this fraction is sufficient for complete regulation of cellular excitability. Using confocal imaging, another group showed that p.R85C and p.R85H have low levels of cell surface expression compared to β1-WT (Xu, Thomas et al. 2007). Our study of β1-p.C121W homozygous mice showed a lower level of cell surface expression of mutant proteins along with incomplete glycosylation compared to WT (Kruger, O'Malley et al. 2016). While a fraction of β1-p.C121W polypeptides is expressed at the cell surface in isolated cultured cortical neurons, association with $Na_v1.1$, $Na_v1.2$, or $Na_v1.3$ could not be detected. β1-p.C121W subcellular localization was shown to be restricted to neuronal cell bodies and not detected at axon initial segments in the cortex or cerebellum or at optic nerve nodes of Ranvier (Kruger, O'Malley et al. 2016). Thus, while p.R85C (Aeby, Sculier et al. 2019), p.C121W (Kruger, O'Malley et al. 2016), and p.R89C can be detected at the cell surface using biochemical methods, the subcellular distribution of these mutant proteins in native cells *in vivo* may be abnormal. In mouse CMs, β1 subunits are normally localized to subcellular domains that are critical for intracellular signaling or excitation contraction coupling (Edokobi and Isom 2018). Therefore, in native CMs β1-p.R89C protein may be expressed, but improperly localized, resulting in aberrant cellular and/or molecular function. Consequently, therapeutic strategies aimed at increasing plasma membrane trafficking of these mutant protein may not be sufficient if improper subcellular localization cannot also be corrected. Future investigations will require using a CRISPR-generated homozygous β1-p.R89C animal model, now in progress in our lab, to determine channel association and localization properties in native cells.

To date, with the exception of β1-p.C121W, which has been shown to lack trans homophilic CAM function (Meadows, Malhotra et al. 2002), *SCN1B* variant functionality has been limited to assessment of I_{Na} regulation. Several studies have shown that these variants are loss-of-function based on electrophysiological criteria (Wallace, Wang et al. 1998, Xu, Thomas et al. 2007, Watanabe, Koopmann et al. 2008, Patino, Claes et al. 2009, Watanabe, Darbar et al. 2009, Hu, Barajas-Martínez et al. 2012, Yuan, Koivumaki et al. 2014, Aeby, Sculier et al. 2019, Martinez-Moreno, Selga et al. 2020, Scala, Efthymiou et al. 2021). In this study, we showed that co-expression of β1-p.R89C with $Na_v1.5$ or $Na_v1.1$ results in no changes to I_{Na} density compared to α subunit expression alone. However, we also observed that co-expression of β1-p.R89C with $Na_v1.6$ results in increased $I_{Na,}$ density, similar to the effects of β1-WT. Thus, the β1-p.R89C mutation does not completely abolish interaction with or modulation of Na_v α subunits. In neurons, β1 and $Na_v1.6$ have a reciprocal relationship. β1 is required for $Na_v1.6$-dependent high-frequency firing, while $Na_v1.6$ is required for β1-mediated neurite outgrowth (Brackenbury, Calhoun et al. 2010). Our *in vitro* electrophysiological analysis suggests that β1-p.R89C may regulate the excitability of $Na_v1.6$ *in vivo*, however, the CAM function of this variant is unknown. We postulate that *SCN1B* variants that change amino acids within the Ig domain can weaken or prevent their cell adhesive functionality. In support of this hypothesis, β1-p.C121W polypeptides localize to the plasma membrane yet do not participate in trans homophilic cell-cell adhesion (Meadows, Malhotra et al. 2002). Thus, in CMs, we predict that β1-p.R89C may be LOF for both α subunit plasma membrane trafficking and cell-cell adhesion, thus increasing arrhythmia risk through multiple mechanisms.

While biallelic *SCN1B* variants are linked to DEE52, monoallelic *SCN1B* variants are linked to cardiac channelopathies and GEFS+ (Table 1.2), suggesting that they may have dominant-negative effects. Using patch clamp analysis, we asked whether β1-p.R89C displayed a dominant-negative effect when co-expressed in HEK stably expressing $Na_v1.5$ and β1-WT. We found no differences in I_{Na} between the groups, confirming that β1-p.R89C is not a dominant negative mutation on currents expressed by $Na_v1.5$. Future studies will be needed to determine whether this is Nav-α subunit subtype dependent.

In this study, we used patient derived iPSC-CMs to investigate how biallelic expression of *SCN1B*-p.R89C alters cardiac cellular electrophysiology. While heterologous expression systems are informative, they cannot replicate the native cellular environment. In contrast, human iPSC-CMs provide a native cardiac cell environment that is more amenable to understanding disease mechanisms. We determined that iPSC-CMs derived from two unrelated *SCN1B*-p.R89C patients had significantly increased transient and late I_{Na} compared to healthy controls and a Het control. Maximal conductance, g_{max}, was also significantly increased in patient iPSC-CMs compared to controls. Because there were no changes to voltage-dependent properties, we interpret the g_{max} increase as increased expression of Na_v α subunits at the plasma membrane in patient iPSC-CMs. Acutely isolated ventricular CMs from *Scn1b* null mice have a similar phenotype, with increased transient and late I_{Na} mediated by mRNA and protein upregulation of $Na_v1.3$ and $Na_v1.5$ (Lopez-Santiago, Meadows et al. 2007, Lin, O'Malley et al. 2015, Bouza, Edokobi et al. 2021). *In* vivo, the β1-ICD regulates the expression of a complex group of genes encoding proteins important in modulating ion channels (Bouza, Edokobi et al. 2021). Here, we

present data showing that β1-R89C can produce the CTF, and we can subsequentially block the production of the ICD with γ-secrreatase inhibitors. Thus, we propose that the β1-R89C-ICD may cause similar changes in ion channel gene expression as observed for β1-WT, resulting in aberrant Na_v α subunit expression and increased I_{Na} (Bouza, Edokobi et al. 2021).

Acutely isolated ventricular CMs from *Scn1b* null mice have AP prolongation. Here, we asked whether *SCN1B* patient derived iPSC-CMs have abnormal APs properties. Immaturity is a major hurdle of iPSC-CMs technology, as they may not express critical ion channels needed to fully recapitulate native human CMs. To overcome these technical and physiological limitations, several groups have explored the use of differing growth surfaces to promote mature iPSC-CM differentiation. Here, we collaborated with Dr. Adam Helms to generate micropatterned elastic polydimethylsiloxane (PDMS) substrates to anchor thin, purified, and mature cardiac tissue strips in 2D arrays. This micropatterning technique allows us to control for the geometry, maturation, and uniformity of cell morphology and physiological properties in a highly controlled biomechanical environment (Helms, Tang et al. 2020, Tsan, Zhao et al. 2021, Ufford, Friedline et al. 2021). We found several AP properties to be similar between control and patient iPSC-CMs. Importantly, however, Patient 1 but not Patient 2 iPSC-CMs exhibited AP prolongation. Clinically, Patient 1 has a more severe disease phenotype compared to Patient 2 (Darras, Ha et al. 2019). DEE52 patients present with disease phenotypes that are closely related to *SCN1A*-linked DS and *SCN8A*-linked DEE13. Similar to *Scn1b* null mice, *Scn1a* DS and *Scn8a* DEE13 mice exhibit both neurological and cardiac dysfunction (Auerbach, Jones et al. 2013, Frasier, Wagnon et al. 2016). Bradycardia, autonomic dysfunction, altered AP

repolarization, and ultimately SUDEP are shared between the three mouse models (Lopez-Santiago, Meadows et al. 2007, Auerbach, Jones et al. 2013, Frasier, Wagnon et al. 2016) It will be interesting to analyze the cardiac phenotype of our recently generated *Scn1b*-p.R89C mouse model. Clinical and genetic analyses of additional DEE52 patients are also needed to understand the factors accounting for the differences between the patient phenotypes.

In summary, this study presents the first biochemical and electrophysiological characterization of the *SCN1B*-p.R89C DEE52 patient variant as well as the first demonstration of any DEE52 variant in human patient iPSCs. This study highlights the complexities of understanding the multifunctionality of *SCN1B*. Future analysis of the cell adhesive and transcriptional regulatory properties will be needed to fully understand this variant. Furthermore, these results support our hypothesis that increased I_{Na} in iPSC-CMs may be a biomarker for SUDEP risk.

Methods

Human iPSCs:

iPSCs were reprogrammed by the episomal plasmid method with Neon Transfection system (Life Technolgies). Dr. Andrew Tidball generated the control 1 (Ctrl1) and *SCN1B* patient 1 (Pt1-8 and Pt1-10) iPSC lines. Dr. Louis Dang generated the heterozygous control (Het) and patient 2 (Pt2) iPSC lines. Control 2 (Ctrl2-2) were obtained from the Human Stem Cell and Gene Editing Core at the University of Michigan. iPSCs were maintained in feeder-free conditions on 0.5% Matrigel coated plates (Corning) in mTeSR1 medium (Stem Cell Technologies), passaged every 4–5 days with 0.1μM EDTA as described(Frasier, Zhang et al. 2018). Medium was changed daily. Genomic alteration of iPSCs were checked by SNP-CHIP at cell passage 10-20. The cells were cultured in 37°C with 5% CO_2.

iPSC-CM Differentiation:

iPSCs were differentiated to CMs using a small molecular regulation method, based on the Wnt signaling pathway modulation (Lian, Hsiao et al. 2012). Briefly, iPSCs were dissociated by Accutase (STEMCELL Technologies) and plated at 1-1.5x10^6 cells/well in mTeSR-1 on 6-well plates coated with 1% Matrigel. When the cells reached >90% confluence, differentiation was initiated. The cells were cultured in a basal medium [RPMI/B27 without insulin (Fisher Scientific)] for approximately 10 days. During the first 24 hours of differentiation the basal medium contained glycogen synthase kinase-3β inhibitor 6uM CHIR99021 (Cayman Chemical). On day 3-5 of differentiation, the basal medium included the 5 μM Wnt inhibitor IWP4

(Stemgent). On day 10-14, the basal media was changed, and the cells were cultivated in maintenance medium (RPMI/B27 with insulin). Between days 8-14 of differentiation, the cells began to spontaneously contract. On day 14 of differentiation, the cells were maintained in a media containing; lactate enrichment medium [RPMI no glucose with HEPES (Fisher Scientific), bovine albumin (Fisher Scientific), lactate (Fisher Scientific), and L-asorbic acid (Fisher Scientific)](Tohyama, Hattori et al. 2013) for 4-8 days. The cells were then changed to the maintenance medium, which was changed every 2-3 day until day 40. The cells were dissociated by TrypLE and 0.5-1.2x10^4 cells were plated on Matrigel coated 12mm^2 glass coverslips in maintenance medium for electrophysiological analyses, immunostainings, and image analyses.

Whole-cell patch clamp analysis of iPSC-CMs:

Na^+ current (I_{Na}): iPSC-CMs were plated at a low density onto 12 mm glass coverslips coated with 0.1% matrigel. After ~ 7 days, I_{Na} recordings were made using an Axopatch 700B (Molecular Devices, Sunnyvale, CA, USA) and pClamp (version 11, Axon Instruments, Foster City, CA). Voltage-clamp measurements were obtained using an extracellular solution containing (in mM): 60 NaCl, 110 CsCl, 1 $BaCl_2$, 2 $MgCl_2$, 0.2 $CdCl_2$, 1 $CaCl_2$, 10 HEPES, 20 TEA-Cl, and 10 glucose (pH = 7.35 with CsOH, osmolarity = 300–305 mosm). Fire polished pipettes with resistance of 1.5-3 mΩ were filled with internal solution containing (in mM): 1 NaCl, 150 N-methyl-d-glucamine, 10 ethyleneglycoltetraacetic acid (EGTA), 2 $MgCl_2$, 40 HEPES, and 25 phosphocreatine-tris, 2 MgATP, 0.02 Na_2GTP, 0.1 leupeptin (pH = 7.2 with H_2SO4). All recordings were performed within 10 to 60 min after the culture medium was replaced by the external recording solution. Whole cell I_{Na} was recorded using established

protocols[24]. Briefly, once access to the cell was gained, series resistance compensation (<50%) was performed and leak currents were subtracted using a P/4 protocol. I_{Na} was recorded in response to a series of voltage steps between -120 and +30 mV in 5 mV increments, from a holding potential of -120 mV for 200 msec. A step back to -20 mV for 200 msec was used to determine the voltage-dependence of inactivation. Current traces were normalized against the whole-cell capacitance (Cm). Na^+ conductance (G_{Na}) at each test voltage, were determined from the equation:

$$G_{Na}=I_{Na}/(V-E_{Na})$$

where I_{Na} is the Na^+ current and E_{Na} is the Na^+ reversal potential. Peak G_{Na} (G_{max}) was plotted as a function of voltage to produce activation curves. I_{Na} was normalized to the maximum elicited current and plotted against the conditioning voltage to yield inactivation curves. Both curves were fitted to the following Boltzmann function:

$$G/G_{max} \text{ or } I/I_{max}=1/(1+\exp((V-V_{½})/k))$$

where G/Gmax is the normalized activation and I/I_{max} is normalized inactivation, $V_{½}$ is the voltage of half-maximal activation or inactivation, k is the slope factor, and V is the test voltage. Recovery from inactivation was determined using a double-pulse P1 and P2 protocol that delivered two identical depolarizing pulses to −20 mV of 50-ms duration. The time interval between P1 and P2 was initially incremented by 1 ms up to 6 ms, followed by 2-ms increments

to 20 ms, then 5-ms increments to 60 ms, followed by 10-ms increments to 120 ms, and finally 20-ms increments to 200 ms to ensure enough time was allowed for full recovery and to allow adequate capture of the fast components. Peak currents from P2 were normalized to those obtained in response to the conditioning P1 step and plotted against the time intervals. These plots were fitted with a double exponential function as follows:

$$y=A_1\exp(-t/\tau_1)-A_2\exp(-t/\tau_2)$$

where t is the time, and τ is the time constant of recovery from inactivation.

Action Potential Recording:

iPSC-CMs were recorded on the micron-scale two-dimensional cardiac tissue (M2DCT) platform. To create the M2DCT platform, individual stamps were cut from polydimethoxysiloxane PDMS as previously reported (Helms, Tang et al. 2020, Tsan, Zhao et al. 2021, Ufford, Friedline et al. 2021). M2DCT substrates consisted of micropatterned 8 kPa PDMS. Soft PDMS was formulated by mixing Sylgard® 527 and Sylgard® 184. Each component was first mixed with its own curing agent (i.e. 50:50 for Sylgard® 527 and 10:1 for Sylgard® 184). Approximately, 135 µl of the PDMS mixture was pipetted into 35 mm culture dishes and allowed to cover the entire surface of the dish. To directly microprint the PDMS surface, a 2-step transfer process with a fibronectin micropatterned polyvinyl alcohol (PVA) film intermediary was used. To create the PVA film, 65 ml of 5% (w/v), 70 µm strainer filtered, PVA solution was poured on to a leveled flat glass panel and left to air dry (2-3 days). Completely

dried PVA films were peeled and trimmed. To print micropatterns, PDMS micropatterning stamps were first cleaned in 70% ethanol sonication bath. Then rinsed with 100% ethanol and left to air dry. 350 µl of 1:20 diluted 0.1% human serum derived fibronectin (Sigma-Aldrich) in cold sterile cell culture was added per stamp and incubated at room temperature for 1 hour, then aspirated. Following air drying, stamps were pressed on pre-cut, individual stamp-size PVA films and incubated for 30 minutes. The PVA films with fibronectin micropatterns were then peeled and inverted onto cured PDMS dishes. Microprinted dishes were stored up to 2 weeks at 4°C prior to use and the PVA films remaining adherent.

The PVA films were dissolved in sterile water at room temperature on an orbital shaker (70 RPM) for 15 minutes to expose the micropattern, and surfaces were sterilized by UV in the culture hood for 10 min. Differentiated iPSC-CMs iPSC-CMs were dissociated with TrypLE and 0.1-0.3x10^6 cells/well were plated on MD2CT culture dishes in maintenance medium. Approximately, seven days post plating the iPSC-CMs were recorded for AP characterization. The threshold for AP initiation was determined by the application of 2 ms incremental current pulses from 100 to 1500 pA. Steady AP capture was obtained by applying current pulses at 1.5x the threshold. APs were recorded at 1.0 Hz at RT. The bath solution contained (in mM): 135 NaCl, 4 KCl, 1.8 CaCl2, 1 MgCl2, 10 Hepes, 1.2 NaH2PO4, 10 glucose, pH 7.35 with NaOH. Patch pipettes were filled with the internal solution containing (in mM): 130 K-aspartate, 10 KCl, 9 NaCl, 0.33 MgCl2, 5 Mg-ATP, 0.1 GTP, 10 Hepes, 10 glucose, pH 7.2 with KOH. The resting membrane potential (RMP) was determined under current clamp at zero current.

Expression Vectors:

Human β1-WT-V5-2AeGFP was generated by gBLOCK from Integrated DNA Technologies. The gBLOCK was inserted into pENTR-SD/D TOPO by Gateway TOPO reaction according to the manufacturer's instructions. β1-p.R89C-V5-2AeGFP was generated by site-directed mutagenesis using the β1-WT-V5-2AeGFP cDNA construct in pENTR-SD/D TOPO as the template. Both β1 constructs contained an in-frame, C-terminal V5-epitope tag followed by a 2A endoproteolytic sequence and eGFP on the 3' end of the construct for detection of equimolar expression of a fluorescence marker protein. The eGFP alone control was generated by PCR from the full-length β1-WT-V5-2AeGFP construct using gene-specific primers followed by gel-purification. The eGFP alone control was inserted into pENTR-SD/D TOPO by Gateway TOPO reaction according to the manufacturer's instructions. All constructs were subsequently moved to the Gateway-compatible destination vector, pcDNAdest40, using a LR clonase reaction according to the manufacturer's instructions.

Cell culture:

Chinese hamster lung (CHL) fibroblasts and stable Human embryonic kidney (HEK) cell lines expressing human $Na_v1.1$, $Na_v1.5$, or $Na_v1.6$ were maintained at 37°C and 5% CO2 in Dulbecco's Modified Eagle Medium (DMEM) supplemented with 5% heat-inactivated fetal bovine serum (Corning) and 100 U/mL penicillin/streptomycin (Gibco). Stably transfected CHL cells and HEK-$Na_v1.5$ cells were supplemented with 600 µg/mL G418 (Gibco). Stable β1-WT-V5-2AeGFP or β1-p.Arg89Cys-V5-2AeGFP CHL cell lines were generated by transfecting 1 µg

of cDNA with 5 μL of Lipofectamine 2000. About 48 h following transfection, cells were passed into media containing 600 μg/mL G418 and incubated until individual, eGFP-positive colonies were visible (approximately 7–10 days). Clonal colonies were isolated, expanded, and verified for β1-WT-V5 or β1-p.Arg89Cys-V5 expression via western blot with anti-V5 antibody. For electrophysiological analyses, HEK-$Na_v1.1$, -$Na_v1.5$, or -$Na_v1.6$ cells were transiently transfected with β1-WT-V5-2AeGFP, β1-p.Arg89Cys-V5-2AeGFP, or eGFP only (1 μg of cDNA with 5 μL of Lipofectamine 2000). After 12-24 hours the cells were split to a lower density onto 35-mm dishes and GFP-positive HEK cells were recorded for voltage-clamp analysis. Transfected cells were identified by eGFP fluorescence by an investigator blind to genotype. Cells used in electrophysiological experiments come from three or more separate transfections.

Cell surface biotinylation and western blot analyses:

Stable cell lines were grown in 100-mm tissue culture plates until 90–100% confluent. Cell surface proteins were biotinylated using the Cell Surface Protein Isolation Kit (Pierce) according to the manufacturer's protocol. Loading buffer containing 1% sodium dodecyl sulfate, 1 mmol/L β-mercaptoethanol, and 0.2% dithiothreitol was added to samples and heated for 10 min at 85°C. Samples were separated on 10% Tris-Glycine polyacrylamide gels, transferred to nitrocellulose membrane (16 h, 55 mA, 4°C), and probed with antibodies as noted in the figure legends. Membranes were probed with three primary antibodies: anti-V5 (1:1000 dilution, Invitrogen), HSP90 (1:1000 dilution, EnzoScientific), and Transferrin Receptor (1:1000, Thermo). Mouse HRP-conjugated secondary antibodies were utilized (1:1000 dilution for Transferrin Receptor;

1:10,000 dilution for V5 and HSP90). Anti-V5 and its secondary antibody incubations were completed using a SnapID with 10-minute incubations. Antibodies were diluted in 0.25% milk and 0.1% BSA in TBST. Anti-HSP90 antibody was incubated overnight at 4°C and secondary antibody was incubated for 1 h at room temperature (RT), both in 2% milk in TBST. HSP90 immunoblot was subsequently stripped for 10 minutes and incubated overnight in Transferrin Receptor antibody (diluted in 5% milk in TBST) at 4°C. Secondary antibody was incubated for 1 h at RT (diluted in 5% milk in TBST). Immunoreactive bands were detected using West Femto chemiluminescent substrate (GE Health Sciences) and imaged on an iBright FL1000 (Invitrogen) within the linear range of the instrument by utilizing the iBright smart exposure feature. Immunoreactive signals were quantified using ImageJ. Plasma membrane fraction signal was normalized to signal from the total fraction of the construct. Statistical significance was determined using Student's t-test (p-value < 0.05).

Immunocytochemical analysis of heterologous cell lines:

Stably-transfected CHL cells overexpressing β1-WT-V5-2AeGFP, β1-p.Arg89Cys-V5-2AeGFP, eGFP alone constructs were incubated for 10 minutes at 4°C with WGA. Cells were subsequently washed 3 times for 5 minutes each with DPBS at 4°C. Immediately following, cells were fixed with 4% paraformaldehyde at room temperature for 15 minutes. Quickly, the cells were washed 3 times with DPBS to remove any remaining paraformaldehyde. Cells were blocked and permeabilized for 1 hour in a dark, humidified chamber with 90% DPBS, 10% goat serum, and 0.3% triton X-100. Cells were incubated in anti-V5 antibody (1:1000, Invitrogen) overnight in a dark, humidified chamber. Cells were washed 3 times for 10 minutes each in

DPBS and incubated in secondary antibody (Alexa Fluor 647) for 2 hours in a dark, humidified chamber. Cells were washed 3 times for 10 minutes each in DPBS and air dried. Stained cells were mounted in Prolong Gold (Invitrogen) and imaged on a Nikon A1 confocal microscope at the University of Michigan Department of Pharmacology.

Whole-cell patch clamp analysis of HEK cells:

HEK-Nav1.5 cells were transiently transfected and I_{Na} was recorded using voltage clamp protocols as described above. Electrophysiological recordings were performed ~12 h following final plating. I_{Na} was recorded from GFP-positive HEK cells in the presence of an external solution containing (in mM): 120 NaCl, 1 $BaCl_2$, 2 $MgCl_2$, 0.2 $CdCl_2$, 1 $CaCl_2$, 10 HEPES, 20 TEA-Cl, and 10 glucose (pH = 7.35 with CsOH, osmolarity = 300–305 mosm). Fire polished pipettes with resistance of 1.5-3 mΩ were filled with an internal solution containing (in mM): 1 NaCl, 150 N-methyl-d-glucamine, 10 ethyleneglycoltetraacetic acid (EGTA), 2 $MgCl_2$, 40 HEPES, and 25 phosphocreatine-tris, 2 MgATP, 0.02 Na_2GTP, 0.1 leupeptin (pH = 7.2 with H_2SO4, osmolarity = 280–285 mosm). All recordings were performed within 10 to 60 min after the culture medium was replaced by the external recording solution and the dish with cells was placed on the recording setup. Holding potential was −80 mV.

Chapter 4. Discussion and Future Directions

Nnamdi Edokobi, Alexandra A. Bouza, PhD, Yilong Yao, Peng Li, PhD, and Lori L. Isom, PhD

Summary and Significance

The heart consists of several specialized cells working together to accomplish one seemingly simple task: to provide blood and nutrients to the body. The duties of the heart are simple in principle, but in practice the hearts' function is intricate and complex. Without the coordination of multiple cellular and molecular systems, the heart cannot contract in synchrony, resulting in the impaired function of other vital organs. Therefore, as investigators we must continue to uncover the process of heart development and to understand the communication process between the different cell types found in the heart. The work presented in this thesis utilized several models to demonstrate that, without proper Na_V-β1 subunit function, the heart is susceptible to arrhythmias.

Our research group is focused on understanding the disease mechanism(s) of *SCN1B* linked channelopathies to determine why DEE52 patients have a high risk of SUDEP. Patients with refractory epilepsy, especially those with DEEs, face the highest risk of SUDEP (Bell and Sander 2001, Tomson, Nashef et al. 2008). Many of these patients exhibit autonomic nervous system and cardiovascular dysfunction in addition to severe seizures (Laxer, Trinka et al. 2014, Donner, Camfield et al. 2017, Beghi 2020). The exact mechanism(s) of SUDEP is unclear, but we postulate that a breakdown of neurological-cardiovascular communication is key. The work

described in this thesis demonstrates that, in addition to our previous work showing ventricular arrhythmias (Lopez-Santiago, Meadows et al. 2007, Lin, O'Malley et al. 2015), *Scn1b* deletion increases susceptibility to atrial fibrillation in neonatal mice via a neuro-cardiac mechanism that includes impaired atrial modeling through altered gene expression and fibrosis, increased atrial myocyte late sodium current resulting in action potential (AP) prolongation, and aberrant cardiac innervation. Additionally, we report the first biochemical and electrophysiological characterization of the DEE52 variant *SCN1B* c.265c>T, predicting β1-p.R89C, using both heterologous cell expression systems and patient-derived iPSC-CMs. We show that in heterologous cells, β1-p.R89C is expressed at the plasma membrane, undergoes regulated intramembrane proteolysis (RIP), and differentially modulates Na_vs-α subunit subtypes. We then generated ventricular iPSC-CMs from two biallelic *SCN1B* c.265c>T DEE52 patients. Both patient iPSC-CM lines had increased transient and late I_{Na} compared to healthy controls. In contrast, we observed AP prolongation in the patient iPSC-CMs with the more severe disease phenotype, suggesting that this patient may be at higher risk for cardiac complications with potentially a higher SUDEP risk compared to the other patient. Importantly, healthcare providers and parents of children with DEE52 variants must consider both neurological and cardiac dysfunction. Our body of work using animal models supports the hypothesis that cardiac dysfunction contributes to the mechanism of SUDEP in patients with DEE. Additional work in patient-derived CMs will be required to produce an accurate genotype-phenotype correlation between *SCN1B*-linked DEE and cardiac arrhythmias.

Our work predicts that patients with *SCN1B*-linked DEE variants have a compromised cardiovascular system. Although this thesis identified several cardiac pathophysiological factors that may contribute to SUDEP risk, it has also raised important new questions. For example, is *Scn1b* involved in the activation and differentiation of cardiac fibroblasts (CFs)? Is *Scn1b* expression critical for excitability and axonal pathfinding in cardiac neurons? What role does *Scn1b* have in sinoatrial (SA) nodal cell excitability? How do *SCN1B*-linked DEE variants alter transcriptional regulation mediated by the β1 ICD? What are non-cardiac related mechanisms of SUDEP in *SCN1B*-linked DEE? The remainder of this chapter is dedicated to proposing approaches and future directions for these important questions.

Future Directions

Potential role of *Scn1b* in cardiac hypertrophy

Chapter 2 of this thesis showed that *Scn1b* deletion resulted in 724 genes that were differentially expressed between the null and WT atrial tissue (Figure 2.1). Importantly, we found several genes that have been implicated in cardiac disease and cardiac hypertrophy, predicting that *Scn1b* null neonatal hearts have structurally abnormal atria. Some of the most upregulated individual genes belonged to the family of small proline-rich proteins (SPRRs), *Sprr1a* and *Sprr2a1-3* (Figure 2.1D and Figure 2.2). SPRR proteins were originally identified as markers for terminal squamous cell differentiation, however subsequent work showed that the biological functioning of SPRR proteins was not restricted to squamous cells (Carregaro,

Stefanini et al. 2013). *Sprr1a* is expressed in cardiomyocytes during biomechanical/ischemic stress, where it functions to protect cells against further damage (Pradervand, Yasukawa et al. 2004). *Sprr2a* can be induced through the inflammatory response to suppress p53-dependent transcriptional activity (Mizuguchi, Specht et al. 2012). Interestingly, *Sprr2b* expression was shown to also contribute to the development of pathological cardiac fibrosis by facilitating degradation of p53 (Burke, Lighthouse et al. 2018). A closer examination of the RNA-Seq data from the *Sprr2b* investigation showed that CFs isolated from mice with either pathological [transverse aortic constriction (TAC)] or physiological (exercise) remodeling had approximately twice the expression of *Scn1b* compared to controls (Burke, Lighthouse et al. 2018). In agreement with this work, another study found that chronic swim-training in mice resulted in ventricular hypertrophy and increased expression of *Scn1b* mRNA along with that of several other Na_vs, Ca_vs, and K_vs ion channels subunit (Yang, Foeger et al. 2010). In a different study, mice were subjected to TAC surgery either at P1 or at P7 and ventricular tissue was isolated at P14 for RNA-Seq analysis (Malek Mohammadi, Abouissa et al. 2019). The goal of this study was to determine the adaption of neonatal mice to pressure overload during the regenerative (P1) phase and non-regenerative phase (P7) of cardiac development. Interestingly, *Scn1b* was upregulated with several other pro-regenerative genes in the regenerative neonatal mice, suggesting that during regenerative cardiac remodeling*, Scn1b* is upregulated with genes that promote cardiomyocyte proliferation, myocardial inflammatory cell recruitment, angiogenesis, and nerve growth (Malek Mohammadi, Abouissa et al. 2019). Finally, another RNA-Seq analysis from a study using TAC surgery to promote pathological hypertrophy showed that *Scn1b* is significantly upregulated compared to WT sham controls (Green, Anthony et al. 2019). Together,

these studies suggest that *Scn1b* expression in either CFs or CMs is increased in ventricular tissue during cardiac hypertrophy. It will be interesting to determine whether *Scn1b* deletion results in a blunted pathological or physiological cardiac hypertrophic response, thus future investigations will be required to support a functional role for *Scn1b* in the progression of cardiac remodeling.

Role of *Scn1b* in cardiac fibroblasts

CFs make up a large portion of cardiac tissue cellular mass, ranging from 40 to over 60% of the total cell population (Ivey and Tallquist 2016, Tallquist and Molkentin 2017). CFs are found throughout cardiac tissue and are closely connected to CMs (Pellman, Zhang et al. 2016). CFs synthesize extracellular matrix to contribute to cardiac development, myocardial structure, cell signaling, and electro-mechanical function as well as to replace damaged myocardium (Baudino, Carver et al. 2006). Cardiac fibrosis can occur after heart injury, inflammation, or during aging, resulting in the accumulation of extracellular matrix and stiffening of the heart (Kong, Christia et al. 2014, Travers, Kamal et al. 2016). In these cases, fibrotic areas in cardiac tissue create electrical obstacles to conduction and thus facilitate arrhythmic re-entry mechanisms (Platonov 2017). In neonatal *Scn1b* null atria, we were surprised to observe a high level of collagen staining, implying, that *Scn1b* deletion can contribute to myofibroblast dysregulation in pediatric patients. The role of Nav subunits in CFs and myofibroblasts is currently not understood. Na_v-α and -β subunits are expressed in cultured human atrial fibroblasts (Chatelier, Mercier et al. 2012). Upon differentiation to myofibroblasts, $Na_v1.5$, $Na_v1.3$, and Na_v-β1 are predominately expressed (Chatelier, Mercier et al. 2012). From this

work, it was hypothesized that I_{Na} in fibroblasts may modulate intracellular calcium via reverse mode of the sodium-calcium exchanger (Chatelier, Mercier et al. 2012). Additionally, several studies have suggested that cation conductance(s) may influence fibroblast mechano-electrical coupling in the heart (Kohl, Kamkin et al. 1992, Kiseleva, Kamkin et al. 1996, Kamkin, Kiseleva et al. 2003). Since the function of Na_v-β1 subunits goes beyond modulating ionic currents, we propose that *Scn1b* deletion may result in the loss of functional coupling between CFs and CMs. It will be important in the future to investigate isolated atrial CFs from *Scn1b* WT and null mice to determine whether *Scn1b* deletion affects activation and differentiation mechanisms. Myofibroblasts are not part of normal cardiac tissue and appear only following cardiac injury (Kong, Christia et al. 2014, Travers, Kamal et al. 2016), thus it is possible that *Scn1b* null CFs are more sensitive than WT to inflammatory mediators or growth factors such as interleukins or transforming growth factor beta. Alternatively, since CMs have limited proliferative capacity and scar formation is the only reparative mechanism to prevent cardiac rupture (Rog-Zielinska, Norris et al. 2016), it is feasible that the observed atrial fibrosis in *Scn1b* null atria is a result of CM apoptosis. It would be a rather straightforward experiment to stain *Scn1b* null atrial slices for markers of apoptosis. Interestingly, we observed cardiac fibrosis in *Scn1b* null atria but not ventricles. Determining the mechanisms of these chamber-specific changes is a critical therapeutic question. Lastly, it will be vital to determine the time course of fibrosis in *Scn1b* null mice. Specifically, do these animals develop fibrosis at developmental time-points earlier than P16? It is possible that fibrosis observed at P16 is secondary to the neurological phenotype that emerges at P10. Examining atrial tissues from P8 onward in *Scn1b* null mice will elucidate

whether there is a developmental progression of fibrosis. Overall, it is fascinating that P16 null mice undergo cardiac fibrosis and warrants future investigations to uncover the mechanism.

Electrophysiological characterization of *Scn1b* null cardiac neurons

Cardiac neurons play a key role in the regulation of cardiac function (Fedele and Brand 2020). Postganglionic cardiac sympathetic neurons have their cell bodies primarily in the stellate ganglion neurons and primarily utilize norepinephrine as their principal neurotransmitter (Gordan, Gwathmey et al. 2015). In contrast, parasympathetic cardiac neurons have their cell bodies predominately within cardiac atrial tissue and primarily utilize acetylcholine as their principal neurotransmitter (Gordan, Gwathmey et al. 2015). The mammalian cardiac neurons are arranged in distinct regions within the atrial tissue. The majority of cardiac ganglia are parasympathetic, and the projected axons are both parasympathetic and sympathetic (Rysevaite, Saburkina et al. 2011, Rysevaite, Saburkina et al. 2011, Pauza, Saburkina et al. 2013, Zarzoso, Rysevaite et al. 2013). In mice, neurons in right ganglionic cluster (RGC) are located close to the right cranial vein, while neurons in the left ganglionic cluster (LGC) are located near the base of the pulmonary vein (Pauza, Saburkina et al. 2013). Evidence suggests that neurons in the RGC are involved in the regulation of the SA node, while the AV node receives input from neurons located in the LGC (Pauza, Saburkina et al. 2013, Zarzoso, Rysevaite et al. 2013, Pauza, Rysevaite et al. 2014, Saburkina, Gukauskiene et al. 2014, Hanna, Dacey et al. 2021). Cardiac parasympathetic and sympathetic innervation starts prenatally in mice and undergo major

developmental changes during the first three weeks of postnatal life (Fregoso and Hoover 2012). Interestingly, parasympathetic innervation of the heart is functional before sympathetic innervation (Vegh, Duim et al. 2016, Fedele and Brand 2020), and occurs earlier at the atrioventricular node and bundle of His compared to the SA node (Fregoso and Hoover 2012). In chapter 2, using whole mount atrial preparation, we determined whether *Scn1b* deletion resulted in aberrant development of cardiac neurons. Whole mount atrial preparation technique has been used to the study the morphology of cardiac neurons in juvenile rats (Batulevicius, Pauziene et al. 2003), guinea pigs (Batulevicius, Pauziene et al. 2005), and rabbits (Saburkina, Gukauskiene et al. 2014), and our study is the first to describe the cardiac neuroanatomy in neonatal mice. Interestingly, we observed that null atria had an increased number of parasympathetic neurons found in the right ganglionic cluster (RGC) (Fregoso and Hoover 2012). Using *in vivo* techniques, treating *Scn1b* null mice with atropine reduced the incidence of bradycardia and the occurrence of atrial fibrillation (AF). Suggesting, that *Scn1b* deletion results in aberrant neonatal neuronal development which consequently alters CMs function (Zarzoso, Rysevaite et al. 2013, Hanna, Dacey et al. 2021) and creates a substrate for atria arrhythmias (Goldberger and Pavelec 1986, Wang, Page et al. 1992, Haissaguerre, Jais et al. 1998, Allessie, Boyden et al. 2001, Lemola, Chartier et al. 2008, Lu, Scherlag et al. 2009, Chen, Chen et al. 2014, Stavrakis, Nakagawa et al. 2015). The development of cardiac innervations begins with the migration of neural crest cells (NCCs) to the dorsal aorta (Fedele and Brand 2020). Then, the NCCs differentiate into neurons and form into the paravertebral sympathetic chain and parasympathetic cardiac ganglia (Fedele and Brand 2020). In the case of sympathetic neurons, nerve growth factor (NGF) and neurotrophin-3 (NT-3) are among the most important trophic factors (Zhou and

Rush 1996, Belliveau, Krivko et al. 1997, Kuruvilla, Zweifel et al. 2004). Deletion of neurturin (NRTN) results in functional and neuroanatomical deficiencies of parasympathetic neurons, implicating NRTN as an important trophic factor for parasympathetic neurons (Downs, Jalloh et al. 2016). Finally, both sympathetic and parasympathetic neurons require various factors released by CMs, vascular smooth muscle cells (VSMC), and glial cells to ensure the proper neuronal patterning and survival (Fedele and Brand 2020). The atrial RNA-Seq did not suggesting differential gene expression changes in trophic factor genes, thus, we hypothesis that improper cell signaling and mis-localization between cardiac neurons, CMs, VSMC, and glial cells promotes neuronal dysregulation. Future investigations are clearly needed to uncover the mechanism underlying the *Scn1b* null aberrant neuroanatomy.

To gain a deeper understanding of how cardiac neurons influence cardiac pathophysiology in *Scn1b*-linked DEE, several future experiments are required. For example, use of a peripherally restricted muscarinic antagonist instead of atropine would separate central from peripheral, including cardiac, autonomic blockade. Because *Scn1b* null mice have epilepsy in addition to cardiac arrhythmia, it will be important to define and dissect the influence of the central vs the peripheral nervous systems. Ultimately, central vs peripheral parasympathetic blockade may not offer differences in AF attenuation, as Scn1a +/- Dravet syndrome mice treated with either atropine or N-methyl scopolamine reduced the incidence of ictal bradycardia and SUDEP (Kalume 2013). Thus, bradycardia caused by hyperactivity of the parasympathetic nervous system might be a primary factor promoting sudden death in DEE mice. Characterization of intrinsic cardiac axons between genotypes will also be important. These

axons create an interconnecting circuit of neurons that influence the behavior of every CM (Rajendran, Challis et al. 2019). Techniques now exist to examine cardiac axons at high resolution to determine their arborization and fasciculation. Using tissue clearing techniques (Du, Hou et al. 2018), such as clarity, investigators can maintain a fully intact heart for imaging analysis. Use of this technology in the future would allow genotype specific analysis of axon projections from the right and left ganglionic clusters in both atrial and ventricular tissue.

Understanding the structure and localization of neurons informs their function. It remains unclear whether *Scn1b* null cardiac neurons have altered excitability. An initial straightforward experiment would be to study Langendorff perfused *Scn1b* null hearts, thereby, isolating them from CNS influences. Here, we could examine whether intrinsic cardiac neurons alone are sufficient to induce bradycardia and AF. Additionally, although technically challenging, once the hearts are cannulated, local stimulation could be used to induce firing of neurons in the RGC vs LGC. Alternatively, to local stimulation, optogenetic experiments would provide functional information on myocardial innervation at the cellular level. Gene delivery systems are currently being used to deliver opsins, e.g. channelrhodopsin 2 (ChR2), to select neuronal populations (Fenno, Yizhar et al. 2011, Britt, McDevitt et al. 2012). Recently, the Shivkumar group published a method to use AAV-based labeling and tracing to optically stimulate cholinergic neurons in the heart (Rajendran, Challis et al. 2019). These techniques should be used in the future to determine whether altered cardiac neuroanatomy in response to *Scn1b* deletion has functional consequences.

Electrophysiological characterization of isolated CNS neurons is an experimental technique that is critical and standard to the neuroscience field. However, in the cardiac field there is a scarcity of groups studying cardiac neurons, let alone isolating them for electrophysiological characterization. I have attempted to isolate cardiac neurons from 1 month old WT mice, in the hope of developing a way to isolate cardiac neurons from P16 *Scn1b* null mice. Admittedly, I was unsuccessful in producing neurons for the purposing of recording APs or I_{Na}. Nevertheless, I was able to isolate neurons for staining (Figure 4.1). The protocol was adapted from a study published in 2007 that was used to isolate cardiac neurons from 1-4 month old mice (Hoard, Hoover et al. 2007). Success in this area will require extensive troubleshooting in order to optimize this method for our younger mice. Characterizing excitability changes in *Scn1b* null cardiac neurons is an exciting area of study that will have significant impact on understanding autonomic influences contributing to cardiac disease.

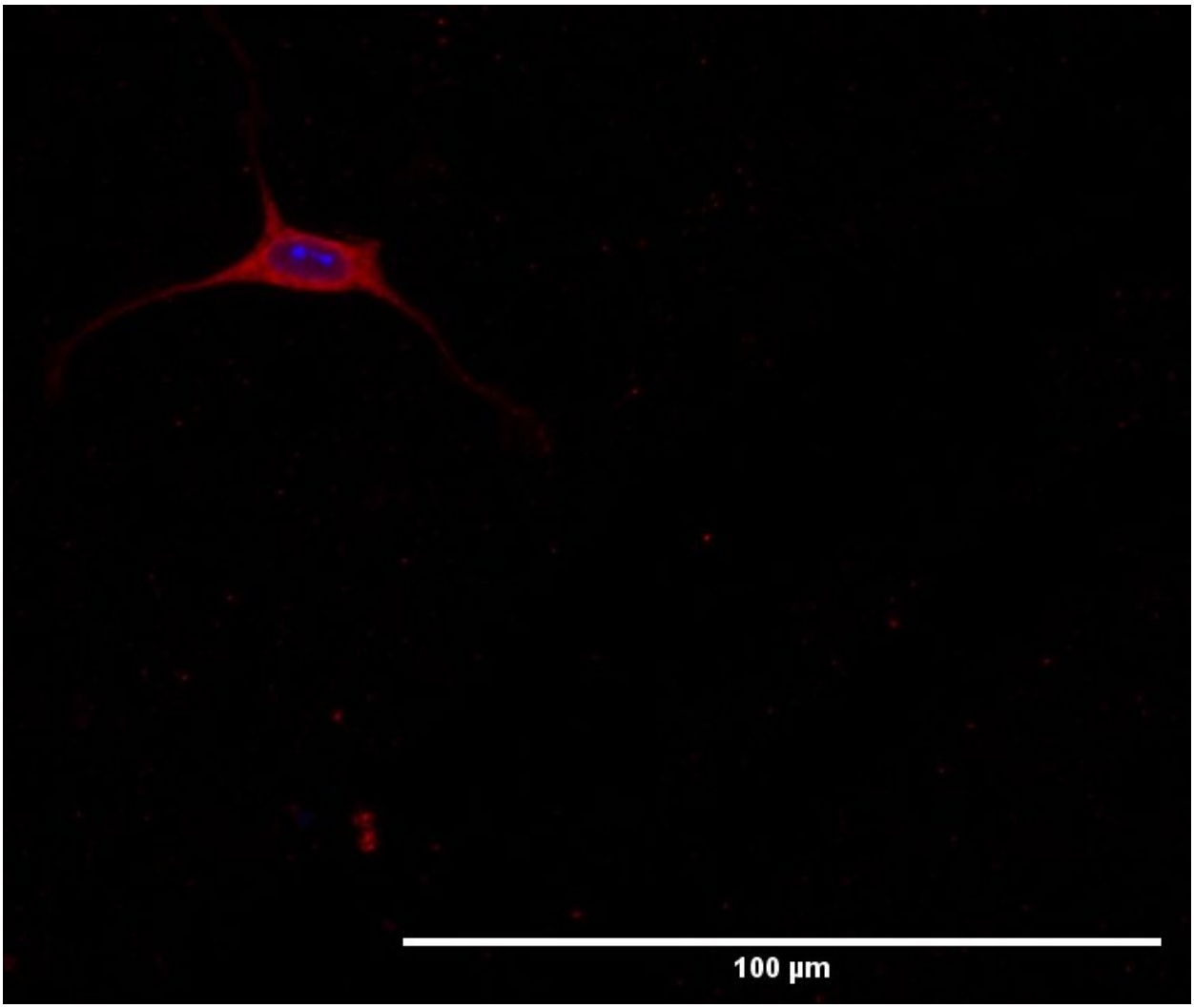

Figure 4.1 Dissociated ChAT+ neuron

Scn1b and SAN automaticity

Scn1b null mice begin to show characteristics of bradyarrhythmia compared to WT littermates around P12. In addition to bradycardia, we observed prolonged sinus node recovery time (SNRT), suggesting SA node dysfunction. The SA node displays intrinsic automaticity, and this intrinsic rhythm is primarily influenced by autonomic nerves. SA nodal cells generate regular spontaneous APs, and the depolarizing current is elicited by I_{Ca} instead of fast transient I_{Na}. Repolarization corresponds with increased I_K. At the end of repolarization and at very negative membrane potentials ion channels open that conduct slow, inward I_{Na}, termed "funny" currents, I_f. I_f is activated by hyperpolarization and causes the membrane potential to begin to spontaneously depolarize (Boyett, Honjo et al. 2000). The roles of Na_vs remain controversial in human SA node pacemaking and conduction. Some *SCN5A* variants have been linked to symptomatic SA node diseases (Benson, Wang et al. 2003), suggesting I_{Na} may be necessary for maintaining human SA node pacemaking and conduction. Interestingly, *Scn3b* null mice exhibit SA node and cardiac conduction dysfunction (Hakim, Brice et al. 2010). Similar to *Scn1b* null mice, *Scn3b* null mice have bradycardia, atrial arrhythmias, and prolonged SNRT. In contrast, *Scn2b* null mice have normal conduction and SNRT (Bao, Willis et al. 2016). Thus, Na_v-β subunits may have differential roles in SA nodal cells. *Scn1b* is expressed in human and mouse SA nodal cells (Domínguez, Navarro et al. 2005, Li, Kalyanasundaram et al. 2020), suggesting that *Scn1b* deletion may result in SA node dysfunction independent of autonomic influences. Isolating mouse SA nodal cells and investigating their cellular excitability would determine

whether SNRT prolongation in *Scn1b* null mice is attributed to increased autonomic tone or dysregulated SA nodal cell excitability.

β1-p.R89C-ICD transcriptional regulation

Na_v-β1 is a substrate for regulated intramembrane proteolysis (RIP) by BACE1 and γ-secretase (Wong, Sakurai et al. 2005, Bouza, Edokobi et al. 2021). The cleaved C-terminal fragment of β1 generated by RIP translocates to the nucleus where it is proposed to function as part of a transcriptional regulatory complex to reduce the expression of numerous genes, including those encoding ion channels (Bouza, Edokobi et al. 2021). Several *SCN1B* patient variants result in amino acid changes located in the protein's Ig domain. We predict that these changes may affect BACE1 and γ-secretase processing. However, for at least one variant, β1-p.R89C, we observed that the intermediary CTF product is accumulated similar to WT β1 upon γ-secretase inhibition, suggesting that BACE1 can recognize β1-p.R89C as a substrate and that the β1-p.R89C variant does not prevent RIP. These results also suggest that the β1-p.R89C-ICD is produced by γ-secretase, which has have significant implications for interpreting DEE52 disease mechanisms.

We performed RT-qPCR experiments to determine whether β1-p.R89C variant resulted in differential expression of ion channel genes in CMs, similar to what we observed for *Scn1b* null mice. Our results thus far, comparing control 1 and patient 1 iPSC-CMs, show increased *SCN1B* and decreased *SCN1A* mRNA expression in patient 1 (Figure 4.2). Increased *SCN1B*

expression may be an adaptive response by patient 1 cells to loss-of-function. Importantly, *SCN1A* haploinsufficiency is linked to DS (Escayg and Goldin 2010). We have reported abnormalities in the excitability of CMs in DS mice (Auerbach, Jones et al. 2013) and iPSC-CMs derived from DS patients (Frasier, Zhang et al. 2018) Hence, the severity of disease in patient 1 may be compounded by aberrant expression of multiple cardiac ion channel genes influenced by the β1-ICD. It will be interesting to determine whether patient 2 iPSC-CMs exhibit similar differential expression of ion channel genes. Because patient 2 has a milder disease than patient 1, it may be that cardiac ion channel gene expression will be less affected. In contrast, to *Scn1b* null mice, in which there are increases in the expression of *Scn5a* and *Scn3a* mRNA and protein in isolated ventricular myocytes (Lopez-Santiago, Meadows et al. 2007, Bouza, Edokobi et al. 2021), we did not observe significant changes in *SCN5A* or *SCN3A* expression in patient 1 iPSC-CMs (Figure 4.3). This result suggests that the effects of β1-p.R89C on genetic modulation are different than *Scn1b* deletion in CMs, which makes sense because β1 polypeptides are present in these patient cells. In addition, to completing the RT-qPCR analysis of patient 2, it will be important to ask whether patient 1- and 2-derived iPSC neurons exhibit a similar difference in gene expression as observed in CMs. Because *SCN1B* plays important roles in many tissue types, it will be critical to understand β1-p.R89C-ICD driven gene expression throughout development and differentiation.

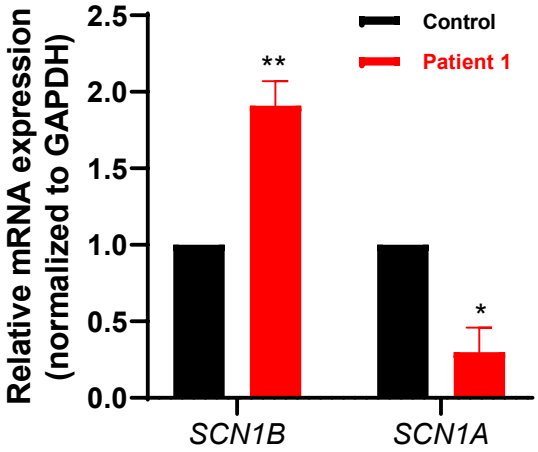

Figure 4.2. Increased expression of *SCN1B* and decreased expression of *SCN1A* in patient 1 iPSC-CMs.

qRT-PCR data from control iPSC-CM line and *SCN1B* patient iPSC-CMs. Data are presented as means ± SEM (n=4). *p < 0.05; **p < 0.01

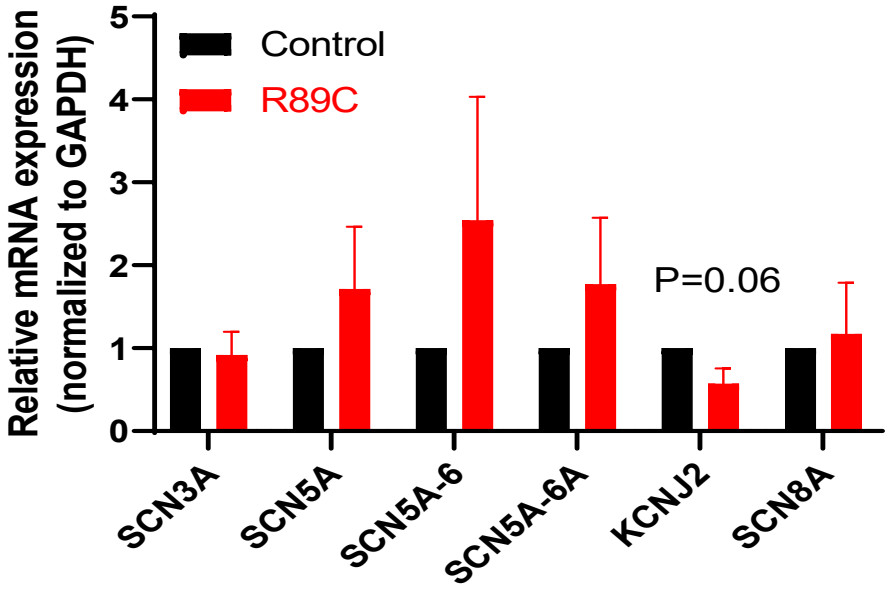

Figure 4.3. Expression of ion channels in iPSC-CMs

qRT-PCR results for *SCN1A, SCN3A, SCN8A, SCN5A and KCNJ2* in iPSC-CMs. Data are presented as means ± SEM.

Mechanism of SUDEP in *SCN1B*-linked DEE

Cardiac dysfunction is known to be associated with increased risk of premature mortality, including sudden cardiac death. We have proposed that DEE patients with variants in ion channel genes have a very high risk of SUDEP because of cardiac involvement in addition to neurological dysfunction. In this thesis, we suggest that the combination of intractable seizures with myocardial structure changes, genetic alteration of ion channels, and autonomic dysfunction in DEE52 due to *SCN1B* variants disrupts the complex inter-relationship between the brain and the heart and creates a pathophysiological environment that is permissive for SUDEP. We have a longstanding overall hypothesis that increased I_{Na} in cardiac cells may be a biomarker for increased SUDEP risk. In the case of β1-p.R89C, iPSC-CMs from two different patients with differing levels of disease severity showed increased I_{Na}. A critical next step will be to work with attending physicians to assess whether these patients have cardiac abnormalities. Thus, a cardiac work up with a resting or an exercise Holter monitor electrocardiogram, echocardiogram, and even additional genetic testing, will be necessary to further evaluate of our overall hypothesis.

SUDEP is a perfect storm of system wide organ failure. Importantly, we do not suggest that cardiac dysfunction is the sole cause of SUDEP. In fact, if epilepsy patients are first diagnosed with serious cardiac conduction disorders or exhibit signs of cardiac failure their cause of death may not be listed as SUDEP. The future of SUDEP research is promising as over the past decade there has been increased focus on the role of circadian rhythms, autonomic signaling, cardiac arrhythmias, and brain-stem respiratory dysfunction in the mechanism of SUDEP

(Elmali, Bebek et al. 2019, Mazzola and Rheims 2021). Interestingly, ion channels, including Na_v-β1 subunits, are expressed in cells that contribute to function of those organs systems. It is probable that high SUDEP risk in DEE52 is associated with coordinated ictal, peri-ictal, or post-ictal multi-systemic failure. Clinically, there is a close relationship between post-ictal respiratory dysfunction and cardiac conduction or rhythm disorders (Mazzola and Rheims 2021). Ictal and peri-ictal respiratory dysfunction might signify the beginning of the process leading up to a terminal apnea and asystole (Ryvlin, Nashef et al. 2013, Vilella, Lacuey et al. 2019). Additionally, seizure-induced apnea may contribute to hypoxemia of the heart, contributing to worsening cardiac function over time (Mazzola and Rheims 2021). For this reason, we have conducted preliminary experiments to characterize respiratory function in *Scn1b* null mice. In collaboration with Dr. Peng Li in the Life Science Institute at the University of Michigan, we have measured breathing frequency in 3 *Scn1b* null and 3 WT mice at normoxic and hypoxic levels (Figure 4.4). These data suggest that at P10, *Scn1b* null and WT have a similar tidal volume, the measure of the amount of air that displaced by the lungs during a respiratory cycle, as well as normal breathing response to normoxic and hypoxic conditions. However, similar to the neurological, failure to thrive, and cardiac phenotypes in *Scn1b* null mice, respiratory differences between genotypes begin to occur after P10. The data show that tidal volume in *Scn1b* null mice does not increase with age compared to the WT. Importantly, *Scn1b* null mice do exhibit an abnormal hypoxic response compared to WT. Breathing frequently in *Scn1b* null mice decreases under hypoxic conditions and does not fully return to baseline at the end of hypoxic treatment. It will be important to continue this study and validate this conclusion by increasing the number of animals. Additionally, next steps include determining whether lung

function is impaired or whether respiratory dysfunction is related to brainstem dysfunction. In summary, these preliminary results suggest that the *Scn1b* null mice have respiratory dysfunction.

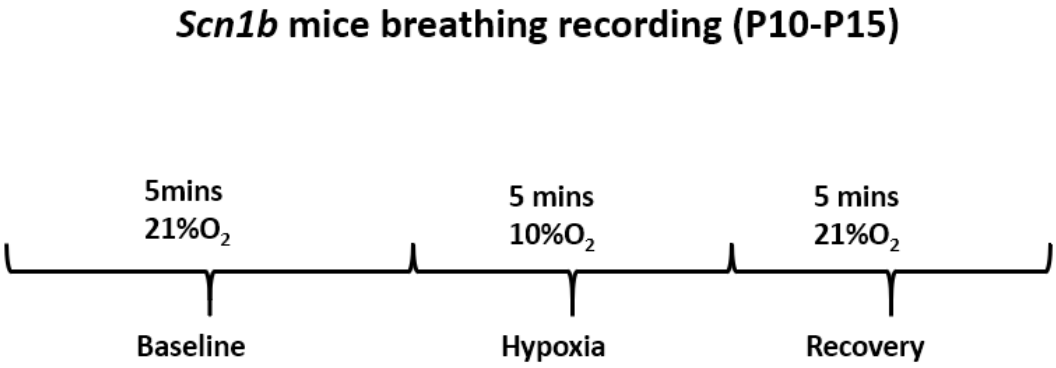

Figure 4.4 Experimental design for *Scn1b* null and WT plethysmography recordings

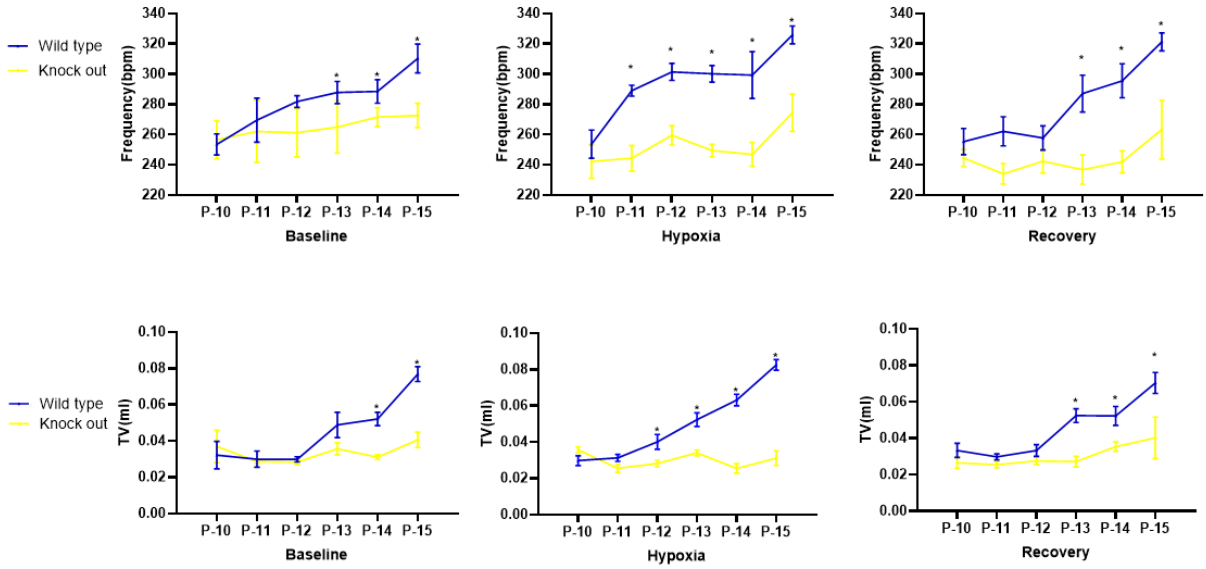

Figure 4.5 Plethysmograph results suggest abnormal breathing and lung function in *Scn1b* null mice

Overall Conclusion

At the end of the day, the question that stumps researchers, healthcare providers, parents, and patients is why this seizure on this day ends in SUDEP. Sadly, SUDEP risk is a reality faced by all patients with epilepsy. My graduate research has made considerable progress toward our understanding of the role of *SCN1B* in cardiac physiology and my contributions lay the groundwork to further our knowledge about neuro-cardiac mechanisms of SUDEP.

Methods

Cardiac Neuron Isolation and Immunohistochemistry

Prior to isolation glass cover slips (12 mm diameter) were passed briefly through a gas flame to enhance coating and then transferred to a 24-well culture plate where they were treated with 500 μg/ml poly-dl-ornithine (Sigma-Aldrich) for 72 h at 4°C followed by 5 μg/ml laminin (Invitrogen) for 3 h at 37°C. Cardiac neurons were isolated from the hearts of adult aged mice, as previously described (Hoard, Hoover et al. 2007).

mRNA expression analysis

Total RNA was isolated from differentiated iPSC-CMs using Trizol reagent (Invitrogen) and treated with RNase-free DNase I (Qiagen, Germany). RNA was stored at -80°C until converted to cDNA. 1-2 μg of RNA was converted to cDNA using Reverse Transcriptase SuperScript III (RT SS III), random primers, Salt buffers, RNase OUT, and dNTPs (Invitrogen). Primers, dNTPs, and RNA were initially incubated for 5 minutes at 65°C. Salt buffers, RNase OUT, and RT SS III were added to the initial mixture and incubated for 5 minutes at 25°C, 60 minutes at 50°C, and 15 minutes at 75°C. cDNA was either used directly or diluted 1:3 – 1:5 fold in molecular biology grade water. SYBR Green (Applied Biosystems) based comparative qPCR using gene-specific primers (Integrated DNA Technologies) was completed. ΔΔCt values were calculated by comparing ion channel genes to the housekeeping gene, *GAPDH,* and subsequently by normalizing to WT samples to determine fold-changes. Data are shown as gene expression ± SEM. Statistical significance (p-value < 0.05) was determined using Student's t-test.

Breathing monitoring and analysis

Neonatal mice were placed in a whole-body plethysmography chamber (Buxco) at room temperature (22C) in 21% O2 (for normoxia) or 10% O2 (for hypoxia). Mice were allowed to acclimate for 15-20 minutes in the chamber before beginning plethymography data collection.

References

Abecasis, B., P. Gomes-Alves, S. Rosa, P. J. Gouveia, L. Ferreira, M. Serra and P. M. Alves (2019). "Unveiling the molecular crosstalk in a human induced pluripotent stem cell-derived cardiac model." Biotechnol Bioeng **116**(5): 1245-1252.

Aeby, A., C. Sculier, A. A. Bouza, B. Askar, D. Lederer, A. S. Schoonjans, M. Vander Ghinst, B. Ceulemans, J. Offord, L. F. Lopez-Santiago and L. L. Isom (2019). "SCN1B-linked early infantile developmental and epileptic encephalopathy." Ann Clin Transl Neurol.

Aeby, A., C. Sculier, A. A. Bouza, B. Askar, D. Lederer, A. S. Schoonjans, M. Vander Ghinst, B. Ceulemans, J. Offord, L. F. Lopez-Santiago and L. L. Isom (2019). "SCN1B-linked early infantile developmental and epileptic encephalopathy." Ann Clin Transl Neurol **6**(12): 2354-2367.

Ahern, C. A., J. F. Zhang, M. J. Wookalis and R. Horn (2005). "Modulation of the cardiac sodium channel Nav1.5 by Fyn, a Src family tyrosine kinase." Circulation Research **96**(9): 991-998.

Ahmed, R. E., T. Anzai, N. Chanthra and H. Uosaki (2020). "A Brief Review of Current Maturation Methods for Human Induced Pluripotent Stem Cells-Derived Cardiomyocytes." Front Cell Dev Biol **8**: 178.

Akyuz, E., A. K. Uner, B. Koklu, A. Arulsamy and M. F. Shaikh (2021). "Cardiorespiratory findings in epilepsy: A recent review on outcomes and pathophysiology." J Neurosci Res.

Allessie, M. A., P. A. Boyden, A. J. Camm, A. G. Kleber, M. J. Lab, M. J. Legato, M. R. Rosen, P. J. Schwartz, P. M. Spooner, D. R. Van Wagoner and A. L. Waldo (2001). "Pathophysiology and prevention of atrial fibrillation." Circulation **103**(5): 769-777.

Allouis, M., F. Le Bouffant, R. Wilders, D. Péroz, J. J. Schott, J. Noireaud, H. Le Marec, J. Mérot, D. Escande and I. Baró (2006). "14-3-3 Is a regulator of the cardiac voltage-gated sodium channel Nav1.5." Circulation Research **98**(12): 1538-1546.

Audenaert, D., L. Claes, B. Ceulemans, A. Lofgren, C. Van Broeckhoven and P. De Jonghe (2003). "A deletion in SCN1B is associated with febrile seizures and early-onset absence epilepsy." Neurology **61**(6): 854-856.

Auerbach, D. S., J. Jones, B. C. Clawson, J. Offord, G. M. Lenk, I. Ogiwara, K. Yamakawa, M. H. Meisler, J. M. Parent and L. L. Isom (2013). "Altered Cardiac Electrophysiology and SUDEP in a Model of Dravet Syndrome." PLoS One **8**(10): e77843.

Bagnall, R. D., D. E. Crompton and C. Semsarian (2017). "Genetic Basis of Sudden Unexpected Death in Epilepsy." Front Neurol **8**: 348.

Bao, Y., B. C. Willis, C. R. Frasier, L. F. Lopez-Santiago, X. Lin, R. Ramos-Mondragon, D. S. Auerbach, C. Chen, Z. Wang, J. Anumonwo, H. H. Valdivia, M. Delmar, J. Jalife and L. L. Isom (2016). "Scn2b Deletion in Mice Results in Ventricular and Atrial Arrhythmias." Circ Arrhythm Electrophysiol **9**(12).

Baroni, D., C. Picco, R. Barbieri and O. Moran (2014). "Antisense-mediated post-transcriptional silencing of SCN1B gene modulates sodium channel functional expression." Biology of the Cell **106**(1): 13-29.

Bassil, G., M. Chang, A. Pauza, J. Diaz Vera, A. Tsalatsanis, B. G. Lindsey and S. F. Noujaim (2018). "Pulmonary Vein Ganglia Are Remodeled in the Diabetic Heart." J Am Heart Assoc **7**(23): e008919.

Batulevicius, D., N. Pauziene and D. H. Pauza (2003). "Topographic morphology and age-related analysis of the neuronal number of the rat intracardiac nerve plexus." Ann Anat **185**(5): 449-459.

Batulevicius, D., N. Pauziene and D. H. Pauza (2005). "Architecture and age-related analysis of the neuronal number of the guinea pig intrinsic cardiac nerve plexus." Ann Anat **187**(3): 225-243.

Baudino, T. A., W. Carver, W. Giles and T. K. Borg (2006). "Cardiac fibroblasts: friend or foe?" Am J Physiol Heart Circ Physiol **291**(3): H1015-1026.

Beghi, E. (2020). "The Epidemiology of Epilepsy." Neuroepidemiology **54**(2): 185-191.

Bell, G. S. and J. W. Sander (2001). "The epidemiology of epilepsy: the size of the problem." Seizure **10**(4): 306-314; quiz 315-306.

Belliveau, D. J., I. Krivko, J. Kohn, C. Lachance, C. Pozniak, D. Rusakov, D. Kaplan and F. D. Miller (1997). "NGF and neurotrophin-3 both activate TrkA on sympathetic neurons but differentially regulate survival and neuritogenesis." J Cell Biol **136**(2): 375-388.

Benson, D. W., D. W. Wang, M. Dyment, T. K. Knilans, F. A. Fish, M. J. Strieper, T. H. Rhodes and A. L. George, Jr. (2003). "Congenital sick sinus syndrome caused by recessive mutations in the cardiac sodium channel gene (SCN5A)." J Clin Invest **112**(7): 1019-1028.

Bezanilla, F. (2002). "Voltage sensor movements." J Gen Physiol **120**(4): 465-473.

Bouza, A. A., N. Edokobi, S. L. Hodges, A. M. Pinsky, J. Offord, L. Piao, Y. T. Zhao, A. N. Lopatin, L. F. Lopez-Santiago and L. L. Isom (2021). "Sodium channel beta1 subunits participate in regulated intramembrane proteolysis-excitation coupling." JCI Insight.

Bouza, A. A., J. M. Philippe, N. Edokobi, A. M. Pinsky, J. Offord, J. D. Calhoun, M. Lopez-Floran, L. F. Lopez-Santiago, P. M. Jenkins and L. L. Isom (2020). "Sodium channel beta1 subunits are post-translationally modified by tyrosine phosphorylation, S-palmitoylation, and regulated intramembrane proteolysis." J Biol Chem **295**(30): 10380-10393.

Boyett, M. R., H. Honjo and I. Kodama (2000). "The sinoatrial node, a heterogeneous pacemaker structure." Cardiovasc Res **47**(4): 658-687.

Brackenbury, W. J., J. D. Calhoun, C. Chen, H. Miyazaki, N. Nukina, F. Oyama, B. Ranscht and L. L. Isom (2010). "Functional reciprocity between Na+ channel Nav1.6 and beta1 subunits in the coordinated regulation of excitability and neurite outgrowth." Proc Natl Acad Sci U S A **107**(5): 2283-2288.

Brackenbury, W. J., T. H. Davis, C. Chen, E. A. Slat, M. J. Detrow, T. L. Dickendesher, B. Ranscht and L. L. Isom (2008). "Voltage-gated Na+ channel beta1 subunit-mediated neurite outgrowth requires Fyn kinase and contributes to postnatal CNS development in vivo." J Neurosci **28**(12): 3246-3256.

Brackenbury, W. J. and L. L. Isom (2011). "Na Channel beta Subunits: Overachievers of the Ion Channel Family." Front Pharmacol **2**: 53.

Brackenbury, W. J., Y. Yuan, H. A. O'Malley, J. M. Parent and L. L. Isom (2013). "Abnormal neuronal patterning occurs during early postnatal brain development of Scn1b-null mice and precedes hyperexcitability." Proc Natl Acad Sci U S A **110**(3): 1089-1094.

Britt, J. P., R. A. McDevitt and A. Bonci (2012). "Use of channelrhodopsin for activation of CNS neurons." Curr Protoc Neurosci **Chapter 2**: Unit2 16.

Buckley, U., K. Shivkumar and J. L. Ardell (2015). "Autonomic Regulation Therapy in Heart Failure." Curr Heart Fail Rep **12**(4): 284-293.

Burke, R. M., J. K. Lighthouse, P. Quijada, R. A. Dirkx, Jr., A. Rosenberg, C. S. Moravec, J. D. Alexis and E. M. Small (2018). "Small proline-rich protein 2B drives stress-dependent p53 degradation and fibroblast proliferation in heart failure." Proc Natl Acad Sci U S A **115**(15): E3436-E3445.

Calhoun, J. D. and L. L. Isom (2014). "The Role of Non-pore-Forming beta Subunits in Physiology and Pathophysiology of Voltage-Gated Sodium Channels." Handb Exp Pharmacol **221**: 51-89.

Calhoun, J. D. and L. L. Isom (2014). The Role of Non-pore-Forming β Subunits in Physiology and Pathophysiology of Voltage-Gated Sodium Channels. **221:** 51-89.

Camacho, P., H. Fan, Z. Liu and J. Q. He (2016). "Small mammalian animal models of heart disease." Am J Cardiovasc Dis **6**(3): 70-80.

Carregaro, F., A. C. Stefanini, T. Henrique and E. H. Tajara (2013). "Study of small proline-rich proteins (SPRRs) in health and disease: a review of the literature." Arch Dermatol Res **305**(10): 857-866.

Casini, S., H. L. Tan, I. Demirayak, C. A. Remme, A. S. Amin, B. P. Scicluna, H. Chatyan, J. M. Ruijter, C. R. Bezzina, A. C. van Ginneken and M. W. Veldkamp (2010). "Tubulin polymerization modifies cardiac sodium channel expression and gating." Cardiovasc Res **85**(4): 691-700.

Catterall, W. a. (2000). "From ionic currents to molecular mechanisms: the structure and function of voltage-gated sodium channels." Neuron **26**(1): 13-25.

Catterall, W. A. (2010). "Ion channel voltage sensors: structure, function, and pathophysiology." Neuron **67**(6): 915-928.

Catterall, W. A. (2012). "Voltage-gated sodium channels at 60: structure, function and pathophysiology." J Physiol **590**(Pt 11): 2577-2589.

Catterall, W. A. (2012). "Voltage-gated sodium channels at 60: structure, function and pathophysiology." J Physiol **590**(11): 2577-2589.

Catterall, W. a., A. L. Goldin and S. G. Waxman (2005). "International Union of Pharmacology. XLVII. Nomenclature and structure-function relationships of voltage-gated sodium channels." Pharmacological reviews **57**(4): 397-409.

Chatelier, A., A. Mercier, B. Tremblier, O. Theriault, M. Moubarak, N. Benamer, P. Corbi, P. Bois, M. Chahine and J. F. Faivre (2012). "A distinct de novo expression of Nav1.5 sodium channels in human atrial fibroblasts differentiated into myofibroblasts." J Physiol **590**(17): 4307-4319.

Chen, C. (2004). "Mice Lacking Sodium Channel 1 Subunits Display Defects in Neuronal Excitability, Sodium Channel Expression, and Nodal Architecture." Journal of Neuroscience **24**(16): 4030-4042.

Chen, C., J. D. Calhoun, Y. Zhang, L. Lopez-Santiago, N. Zhou, T. H. Davis, J. L. Salzer and L. L. Isom (2012). "Identification of the cysteine residue responsible for disulfide linkage of Na+channel α and β2 subunits." Journal of Biological Chemistry **287**(46): 39061-39069.

Chen, C., R. E. Westenbroek, X. Xu, C. A. Edwards, D. R. Sorenson, Y. Chen, D. P. McEwen, H. A. O'Malley, V. Bharucha, L. S. Meadows, G. A. Knudsen, A. Vilaythong, J. L. Noebels, T. L. Saunders, T. Scheuer, P. Shrager, W. A. Catterall and L. L. Isom (2004). "Mice lacking sodium channel beta1 subunits display defects in neuronal excitability, sodium channel expression, and nodal architecture." J Neurosci **24**(16): 4030-4042.

Chen, P. S., L. S. Chen, M. C. Fishbein, S. F. Lin and S. Nattel (2014). "Role of the autonomic nervous system in atrial fibrillation: pathophysiology and therapy." Circ Res **114**(9): 1500-1515.

Chugh, S. S., R. Havmoeller, K. Narayanan, D. Singh, M. Rienstra, E. J. Benjamin, R. F. Gillum, Y. H. Kim, J. H. McAnulty, Jr., Z. J. Zheng, M. H. Forouzanfar, M. Naghavi, G. A. Mensah, M.

Ezzati and C. J. Murray (2014). "Worldwide epidemiology of atrial fibrillation: a Global Burden of Disease 2010 Study." Circulation **129**(8): 837-847.

Chun, Y. W., D. A. Balikov, T. K. Feaster, C. H. Williams, C. C. Sheng, J. B. Lee, T. C. Boire, M. D. Neely, L. M. Bellan, K. C. Ess, A. B. Bowman, H. J. Sung and C. C. Hong (2015). "Combinatorial polymer matrices enhance in vitro maturation of human induced pluripotent stem cell-derived cardiomyocytes." Biomaterials **67**: 52-64.

Chyou, J. Y., D. Friedman, M. Cerrone, W. Slater, Y. Guo, D. Taupin, S. O'Rourke, S. G. Priori and O. Devinsky (2016). "Electrocardiographic features of sudden unexpected death in epilepsy." Epilepsia **57**(7): e135-139.

Clatot, J., M. Hoshi, X. Wan, H. Liu, A. Jain, K. Shinlapawittayatorn, C. Marionneau, E. Ficker, T. Ha and I. Deschênes (2017). "Voltage-gated sodium channels assemble and gate as dimers." Nature Communications **8**(1): 2077-2077.

Colilla, S., A. Crow, W. Petkun, D. E. Singer, T. Simon and X. Liu (2013). "Estimates of current and future incidence and prevalence of atrial fibrillation in the U.S. adult population." Am J Cardiol **112**(8): 1142-1147.

Costagliola, G., A. Orsini, M. Coll, R. Brugada, P. Parisi and P. Striano (2021). "The brain-heart interaction in epilepsy: implications for diagnosis, therapy, and SUDEP prevention." Ann Clin Transl Neurol **8**(7): 1557-1568.

Darras, N., T. K. Ha, S. Rego, P. M. Martin, E. Barroso, A. M. Slavotinek and M. R. Cilio (2019). "Developmental and epileptic encephalopathy in two siblings with a novel, homozygous missense variant in SCN1B." Am J Med Genet A **179**(11): 2190-2195.

Davis, T. H., C. Chen and L. L. Isom (2004). "Sodium channel beta1 subunits promote neurite outgrowth in cerebellar granule neurons." J Biol Chem **279**(49): 51424-51432.

Davis, T. H., C. Chen and L. L. Isom (2004). "Sodium Channel β1 Subunits Promote Neurite Outgrowth In Cerebellar Granule Neurons." J. Biol. Chem. **279**: 51424-51432.

de Lera Ruiz, M. and R. L. Kraus (2015). "Voltage-Gated Sodium Channels: Structure, Function, Pharmacology, and Clinical Indications." J Med Chem **58**(18): 7093-7118.

Deschênes, I., A. a. Armoundas, S. P. Jones and G. F. Tomaselli (2008). "Post-transcriptional gene silencing of KChIP2 and Navbeta1 in neonatal rat cardiac myocytes reveals a functional association between Na and Ito currents." Journal of molecular and cellular cardiology **45**(3): 336-346.

Deschenes, I. and G. F. Tomaselli (2002). "Modulation of Kv4.3 current by accessory subunits." FEBS Lett **528**(1-3): 183-188.

Deschênes, I. and G. F. Tomaselli (2002). "Modulation of Kv4.3 current by accessory subunits." FEBS Letters **528**(1-3): 183-188.

Dhar Malhotra, J., C. Chen, I. Rivolta, H. Abriel, R. Malhotra, L. N. Mattei, F. C. Brosius, R. S. Kass and L. L. Isom (2001). "Characterization of sodium channel alpha- and beta-subunits in rat and mouse cardiac myocytes." Circulation **103**(9): 1303-1310.

Domínguez, J. N., F. Navarro, D. Franco, R. P. Thompson and A. E. Aránega (2005). "Temporal and spatial expression pattern of beta1 sodium channel subunit during heart development." Cardiovascular research **65**(4): 842-850.

Donner, E. J., P. Camfield, L. Brooks, J. Buchhalter, C. Camfield, T. Loddenkemper and E. Wirrell (2017). "Understanding Death in Children With Epilepsy." Pediatr Neurol **70**: 7-15.

Downs, A. M., H. B. Jalloh, K. J. Prater, S. P. Fregoso, C. E. Bond, T. G. Hampton and D. B. Hoover (2016). "Deletion of neurturin impairs development of cholinergic nerves and heart rate control in postnatal mouse hearts." Physiol Rep **4**(9).

Du, H., P. Hou, W. Zhang and Q. Li (2018). "Advances in CLARITY-based tissue clearing and imaging." Exp Ther Med **16**(3): 1567-1576.

Dutta, S. and P. Sengupta (2016). "Men and mice: Relating their ages." Life Sci **152**: 244-248.

Dybkova, N., S. Ahmad, S. Pabel, P. Tirilomis, N. Hartmann, T. H. Fischer, P. Bengel, T. Tirilomis, S. Ljubojevic, A. Renner, J. Gummert, D. Ellenberger, S. Wagner, N. Frey, L. S. Maier, K. Streckfuss-Bomeke, G. Hasenfuss and S. Sossalla (2018). "Differential regulation of sodium channels as a novel proarrhythmic mechanism in the human failing heart." Cardiovasc Res **114**(13): 1728-1737.

Eaholtz, G., A. Colvin, D. Leonard, C. Taylor and W. A. Catterall (1999). "Block of brain sodium channels by peptide mimetics of the isoleucine, phenylalanine, and methionine (IFM) motif from the inactivation gate." J Gen Physiol **113**(2): 279-294.

Edokobi, N. and L. L. Isom (2018). "Voltage-Gated Sodium Channel beta1/beta1B Subunits Regulate Cardiac Physiology and Pathophysiology." Front Physiol **9**: 351.

El-Battrawy, I., J. Muller, Z. Zhao, L. Cyganek, R. Zhong, F. Zhang, M. Kleinsorge, H. Lan, X. Li, Q. Xu, M. Huang, Z. Liao, A. Moscu-Gregor, S. Albers, H. Dinkel, S. Lang, S. Diecke, W. H. Zimmermann, J. Utikal, T. Wieland, M. Borggrefe, X. Zhou and I. Akin (2019). "Studying Brugada Syndrome With an SCN1B Variants in Human-Induced Pluripotent Stem Cell-Derived Cardiomyocytes." Front Cell Dev Biol **7**: 261.

Elmali, A. D., N. Bebek and B. Baykan (2019). "Let's talk SUDEP." Noro Psikiyatr Ars **56**(4): 292-301.

Escayg, A. and A. L. Goldin (2010). "Sodium channel SCN1A and epilepsy: mutations and mechanisms." Epilepsia **51**(9): 1650-1658.

Fedele, L. and T. Brand (2020). "The Intrinsic Cardiac Nervous System and Its Role in Cardiac Pacemaking and Conduction." J Cardiovasc Dev Dis **7**(4).

Fendri-Kriaa, N., F. Kammoun, I. H. Salem, C. Kifagi, E. Mkaouar-Rebai, I. Hsairi, A. Rebai, C. Triki and F. Fakhfakh (2011). "New mutation c.374C>T and a putative disease-associated haplotype within SCN1B gene in Tunisian families with febrile seizures." European Journal of Neurology **18**(5): 695-702.

Fenno, L., O. Yizhar and K. Deisseroth (2011). "The development and application of optogenetics." Annu Rev Neurosci **34**: 389-412.

Fialho, G. L., P. Wolf, R. Walz and K. Lin (2021). "SUDEP - more attention to the heart? A narrative review on molecular autopsy in epilepsy." Seizure **87**: 103-106.

Frasier, C. R., J. L. Wagnon, Y. O. Bao, L. G. McVeigh, L. F. Lopez-Santiago, M. H. Meisler and L. L. Isom (2016). "Cardiac arrhythmia in a mouse model of sodium channel SCN8A epileptic encephalopathy." Proc Natl Acad Sci U S A **113**(45): 12838-12843.

Frasier, C. R., J. L. Wagnon, Y. O. Bao, L. G. McVeigh, L. F. Lopez-Santiago, M. H. Meisler and L. L. Isom (2016). "Cardiac arrhythmia in a mouse model of sodium channel SCN8A epileptic encephalopathy." Proc Natl Acad Sci U S A.

Frasier, C. R., H. Zhang, J. Offord, L. T. Dang, D. S. Auerbach, H. Shi, C. Chen, A. M. Goldman, L. L. Eckhardt, V. J. Bezzerides, J. M. Parent and L. L. Isom (2018). "Channelopathy as a SUDEP Biomarker in Dravet Syndrome Patient-Derived Cardiac Myocytes." Stem Cell Reports **11**(3): 626-634.

Freeman, S. A., A. Desmazières, D. Fricker, C. Lubetzki and N. Sol-Foulon (2016). Mechanisms of sodium channel clustering and its influence on axonal impulse conduction. **73:** 723-735.

Fregoso, S. P. and D. B. Hoover (2012). "Development of cardiac parasympathetic neurons, glial cells, and regional cholinergic innervation of the mouse heart." Neuroscience **221**: 28-36.

Fukuda, K., H. Kanazawa, Y. Aizawa, J. L. Ardell and K. Shivkumar (2015). "Cardiac innervation and sudden cardiac death." Circ Res **116**(12): 2005-2019.

Gabelli, S. B., A. Boto, V. H. Kuhns, M. A. Bianchet, F. Farinelli, S. Aripirala, J. Yoder, J. Jakoncic, G. F. Tomaselli and L. M. Amzel (2014). "Regulation of the NaV1.5 cytoplasmic domain by calmodulin." Nature Communications **5**.

Gellens, M. E., A. L. George, L. Q. Chen, M. Chahine, R. Horn, R. L. Barchi and R. G. Kallen (1992). "Primary structure and functional expression of the human cardiac tetrodotoxin-insensitive voltage-dependent sodium channel." Proceedings of the National Academy of Sciences of the United States of America **89**(2): 554-558.

Gilchrist, J., S. Das, F. Van Petegem and F. Bosmans (2013). "Crystallographic insights into sodium-channel modulation by the 4 subunit." Proceedings of the National Academy of Sciences **110**(51): E5016-E5024.

Goldberger, A. L. and R. S. Pavelec (1986). "Vagally-mediated atrial fibrillation in dogs: conversion with bretylium tosylate." Int J Cardiol **13**(1): 47-55.

Goldman, A. M., E. Glasscock, J. Yoo, T. T. Chen, T. L. Klassen and J. L. Noebels (2009). "Arrhythmia in heart and brain: KCNQ1 mutations link epilepsy and sudden unexplained death." Sci Transl Med **1**(2): 2ra6.

Gordan, R., J. K. Gwathmey and L. H. Xie (2015). "Autonomic and endocrine control of cardiovascular function." World J Cardiol **7**(4): 204-214.

Goversen, B., M. A. G. van der Heyden, T. A. B. van Veen and T. P. de Boer (2018). "The immature electrophysiological phenotype of iPSC-CMs still hampers in vitro drug screening: Special focus on IK1." Pharmacol Ther **183**: 127-136.

Green, L. C., S. R. Anthony, S. Slone, L. Lanzillotta, M. L. Nieman, X. Wu, N. Robbins, S. M. Jones, S. Roy, A. P. Owens, 3rd, J. Aube, L. Xu, J. N. Lorenz, B. C. Blaxall, J. Rubinstein, J. B. Benoit and M. Tranter (2019). "Human antigen R as a therapeutic target in pathological cardiac hypertrophy." JCI Insight **4**(4).

Gutstein, D. E., G. E. Morley, H. Tamaddon, D. Vaidya, M. D. Schneider, J. Chen, K. R. Chien, H. Stuhlmann and G. I. Fishman (2001). "Conduction Slowing and Sudden Arrhythmic Death in Mice With Cardiac-Restricted Inactivation of Connexin43." Circulation Research **88**(3): 333-339.

Haissaguerre, M., P. Jais, D. C. Shah, A. Takahashi, M. Hocini, G. Quiniou, S. Garrigue, A. Le Mouroux, P. Le Metayer and J. Clementy (1998). "Spontaneous initiation of atrial fibrillation by ectopic beats originating in the pulmonary veins." N Engl J Med **339**(10): 659-666.

Hakim, P., N. Brice, R. Thresher, J. Lawrence, Y. Zhang, A. P. Jackson, A. A. Grace and C. L. Huang (2010). "Scn3b knockout mice exhibit abnormal sino-atrial and cardiac conduction properties." Acta Physiol (Oxf) **198**(1): 47-59.

Hanna, P., M. J. Dacey, J. Brennan, A. Moss, S. Robbins, S. Achanta, N. P. Biscola, M. A. Swid, P. S. Rajendran, S. Mori, J. E. Hadaya, E. H. Smith, S. G. Peirce, J. Chen, L. A. Havton, Z. J. Cheng, R. Vadigepalli, J. Schwaber, R. L. Lux, I. Efimov, J. D. Tompkins, D. B. Hoover, J. L. Ardell and K. Shivkumar (2021). "Innervation and Neuronal Control of the Mammalian Sinoatrial Node a Comprehensive Atlas." Circ Res **128**(9): 1279-1296.

Hartmann, H. A., L. V. Colom, M. L. Sutherland and J. L. Noebels (1999). "Selective localization of cardiac SCN5A sodium channels in limbic regions of rat brain." Nat Neurosci **2**(7): 593-595.

Hayashi, K., T. Konno, H. Tada, S. Tani, L. Liu, N. Fujino, A. Nohara, A. Hodatsu, T. Tsuda, Y. Tanaka, M. A. Kawashiri, H. Ino, N. Makita and M. Yamagishi (2015). "Functional Characterization of Rare Variants Implicated in Susceptibility to Lone Atrial Fibrillation." Circ Arrhythm Electrophysiol **8**(5): 1095-1104.

Heinemann, S. H., H. Terlau, W. Stuhmer, K. Imoto and S. Numa (1992). "Calcium channel characteristics conferred on the sodium channel by single mutations." Nature **356**(6368): 441-443.

Helms, A. S., V. T. Tang, T. S. O'Leary, S. Friedline, M. Wauchope, A. Arora, A. H. Wasserman, E. D. Smith, L. M. Lee, X. W. Wen, J. A. Shavit, A. P. Liu, M. J. Previs and S. M. Day (2020). "Effects of MYBPC3 loss-of-function mutations preceding hypertrophic cardiomyopathy." JCI Insight **5**(2).

Herron, T. J., A. M. Rocha, K. F. Campbell, D. Ponce-Balbuena, B. C. Willis, G. Guerrero-Serna, Q. Liu, M. Klos, H. Musa, M. Zarzoso, A. Bizy, J. Furness, J. Anumonwo, S. Mironov and J. Jalife (2016). "Extracellular Matrix-Mediated Maturation of Human Pluripotent Stem Cell-Derived Cardiac Monolayer Structure and Electrophysiological Function." Circ Arrhythm Electrophysiol **9**(4): e003638.

Hoard, J. L., D. B. Hoover and R. Wondergem (2007). "Phenotypic properties of adult mouse intrinsic cardiac neurons maintained in culture." Am J Physiol Cell Physiol **293**(6): C1875-1883.

Holst, A. G., S. Saber, M. Houshmand, E. V. Zaklyazminskaya, Y. Wang, H. K. Jensen, L. Refsgaard, S. Haunsø, J. H. Svendsen, M. S. Olesen and J. Tfelt-Hansen (2012). "Sodium Current and Potassium Transient Outward Current Genes in Brugada Syndrome: Screening and Bioinformatics." Canadian Journal of Cardiology **28**(2): 196-200.

Hu, D., H. Barajas-Martinez, A. Medeiros-Domingo, L. Crotti, C. Veltmann, R. Schimpf, J. Urrutia, A. Alday, O. Casis, R. Pfeiffer, E. Burashnikov, G. Caceres, D. J. Tester, C. Wolpert, M. Borggrefe, P. Schwartz, M. J. Ackerman and C. Antzelevitch (2012). "A novel rare variant in SCN1Bb linked to Brugada syndrome and SIDS by combined modulation of Na(v)1.5 and K(v)4.3 channel currents." Heart Rhythm **9**(5): 760-769.

Hu, D., H. Barajas-Martínez, A. Medeiros-Domingo, L. Crotti, C. Veltmann, R. Schimpf, J. Urrutia, A. Alday, O. Casis, R. Pfeiffer, E. Burashnikov, G. Caceres, D. J. Tester, C. Wolpert, M. Borggrefe, P. Schwartz, M. J. Ackerman and C. Antzelevitch (2012). "A novel rare variant in SCN1Bb linked to Brugada syndrome and SIDS by combined modulation of Nav1.5 and Kv4.3 channel currents." Heart Rhythm **9**(5): 760-769.

Hund, T. J., O. M. Koval, J. Li, P. J. Wright, L. Qian, J. S. Snyder, H. Gudmundsson, C. F. Kline, N. P. Davidson, N. Cardona, M. N. Rasband, M. E. Anderson and P. J. Mohler (2010). "A β IV -spectrin / CaMKII signaling complex is essential for membrane excitability in mice." The Journal of Clinical Investigation **120**(10): 3508-3519.

Hunter, A. W. (2005). "Zonula Occludens-1 Alters Connexin43 Gap Junction Size and Organization by Influencing Channel Accretion." Molecular Biology of the Cell **16**(12): 5686-5698.

Isom, L. L., K. S. De Jongh, D. E. Patton, B. F. Reber, J. Offord, H. Charbonneau, K. Walsh, A. L. Goldin and W. A. Catterall (1992). "Primary structure and functional expression of the beta 1 subunit of the rat brain sodium channel." Science (New York, N.Y.) **256**(5058): 839-842.

Isom, L. L., T. Scheuer, A. B. Brownstein, D. S. Ragsdale, B. J. Murphy and W. A. Catterall (1995). "Functional co-expression of the beta 1 and type IIA alpha subunits of sodium channels in a mammalian cell line." J Biol Chem **270**(7): 3306-3312.

Ivey, M. J. and M. D. Tallquist (2016). "Defining the Cardiac Fibroblast." Circ J **80**(11): 2269-2276.

Jain, P., S. Sharma and M. Tripathi (2013). "Diagnosis and management of epileptic encephalopathies in children." Epilepsy Res Treat **2013**: 501981.

Jansen, J. A., M. Noorman, H. Musa, M. Stein, S. De Jong, R. Van Der Nagel, T. J. Hund, P. J. Mohler, M. A. Vos, T. A. Van Veen, J. M. De Bakker, M. Delmar and H. V. Van Rijen (2012). "Reduced heterogeneous expression of Cx43 results in decreased Nav1.5 expression and reduced sodium current that accounts for arrhythmia vulnerability in conditional Cx43 knockout mice." Heart Rhythm **9**(4): 600-607.

Jin, X., Y. Jiang, G. Xue, Y. Yuan, H. Zhu, L. Zhan, Y. Zhuang, Q. Huang, L. Shi, Y. Zhao, P. Li, Y. Sun, W. Su, Y. Zhang, B. Yang, Y. Lu, Z. Wang and Z. Pan (2019). "Increase of late sodium current contributes to enhanced susceptibility to atrial fibrillation in diabetic mice." Eur J Pharmacol **857**: 172444.

Johnson, D., M. L. Montpetit, P. J. Stocker and E. S. Bennett (2004). "The sialic acid component of the beta1 subunit modulates voltage-gated sodium channel function." The Journal of biological chemistry **279**(43): 44303-44310.

Kamakura, T., T. Makiyama, K. Sasaki, Y. Yoshida, Y. Wuriyanghai, J. Chen, T. Hattori, S. Ohno, T. Kita, M. Horie, S. Yamanaka and T. Kimura (2013). "Ultrastructural maturation of human-induced pluripotent stem cell-derived cardiomyocytes in a long-term culture." Circ J **77**(5): 1307-1314.

Kamkin, A., I. Kiseleva and G. Isenberg (2003). "Activation and inactivation of a non-selective cation conductance by local mechanical deformation of acutely isolated cardiac fibroblasts." Cardiovasc Res **57**(3): 793-803.

Kanai, M., K. Toyohara and M. Shoda (2021). "Familial atrial rapid fibrillation associated with double mutations of SCN5A and KCNQ1." Cardiol Young: 1-3.

Kane, C., L. Couch and C. M. Terracciano (2015). "Excitation-contraction coupling of human induced pluripotent stem cell-derived cardiomyocytes." Front Cell Dev Biol **3**: 59.

Karbassi, E., A. Fenix, S. Marchiano, N. Muraoka, K. Nakamura, X. Yang and C. E. Murry (2020). "Cardiomyocyte maturation: advances in knowledge and implications for regenerative medicine." Nat Rev Cardiol **17**(6): 341-359.

Kaufmann, S. G., R. E. Westenbroek, C. Zechner, A. H. Maass, S. Bischoff, J. Muck, E. Wischmeyer, T. Scheuer and S. K. G. Maier (2010). "Functional protein expression of multiple sodium channel alpha- and beta-subunit isoforms in neonatal cardiomyocytes." Journal of molecular and cellular cardiology **48**(1): 261-269.

Kazen-Gillespie, K. a., D. S. Ragsdale, M. R. D'Andrea, L. N. Mattei, K. E. Rogers and L. L. Isom (2000). "Cloning, localization, and functional expression of sodium channel beta1A subunits." The Journal of biological chemistry **275**(2): 1079-1088.

Kazen-Gillespie, K. A., D. S. Ragsdale, M. R. D'Andrea, L. N. Mattei, K. E. Rogers and L. L. Isom (2000). "Cloning, localization, and functional expression of sodium channel b1A subunits." J. Biol. Chem. **275**: 1079-1088.

Kim, D. Y., B. W. Carey, H. Wang, L. A. M. Ingano, A. M. Binshtok, M. H. Wertz, W. H. Pettingell, P. He, V. M. Y. Lee, C. J. Woolf and D. M. Kovacs (2007). "BACE1 regulates voltage-gated sodium channels and neuronal activity." Nature Cell Biology **9**(7): 755-764.

Kim, J., S. Ghosh, H. Liu, M. Tateyama, R. S. Kass and G. S. Pitt (2004). "Calmodulin mediates Ca2+ sensitivity of sodium channels." Journal of Biological Chemistry **279**(43): 45004-45012.

Kiseleva, I., A. Kamkin, P. Kohl and M. J. Lab (1996). "Calcium and mechanically induced potentials in fibroblasts of rat atrium." Cardiovasc Res **32**(1): 98-111.

Kohl, P., A. G. Kamkin, I. S. Kiseleva and T. Streubel (1992). "Mechanosensitive cells in the atrium of frog heart." Exp Physiol **77**(1): 213-216.

Koivumaki, J. T., N. Naumenko, T. Tuomainen, J. Takalo, M. Oksanen, K. A. Puttonen, S. Lehtonen, J. Kuusisto, M. Laakso, J. Koistinaho and P. Tavi (2018). "Structural Immaturity of Human iPSC-Derived Cardiomyocytes: In Silico Investigation of Effects on Function and Disease Modeling." Front Physiol **9**: 80.

Kong, P., P. Christia and N. G. Frangogiannis (2014). "The pathogenesis of cardiac fibrosis." Cell Mol Life Sci **71**(4): 549-574.

Kontis, K. J., A. Rounaghi and A. L. Goldin (1997). "Sodium channel activation gating is affected by substitutions of voltage sensor positive charges in all four domains." J Gen Physiol **110**(4): 391-401.

Kruger, L. C., H. A. O'Malley, J. M. Hull, A. Kleeman, G. A. Patino and L. L. Isom (2016). "beta1-C121W Is Down But Not Out: Epilepsy-Associated Scn1b-C121W Results in a Deleterious Gain-of-Function." J Neurosci **36**(23): 6213-6224.

Kuruvilla, R., L. S. Zweifel, N. O. Glebova, B. E. Lonze, G. Valdez, H. Ye and D. D. Ginty (2004). "A neurotrophin signaling cascade coordinates sympathetic neuron development through differential control of TrkA trafficking and retrograde signaling." Cell **118**(2): 243-255.

Lal, M. and M. Caplan (2011). "Regulated intramembrane proteolysis: signaling pathways and biological functions." Physiology (Bethesda) **26**(1): 34-44.

Laxer, K. D., E. Trinka, L. J. Hirsch, F. Cendes, J. Langfitt, N. Delanty, T. Resnick and S. R. Benbadis (2014). "The consequences of refractory epilepsy and its treatment." Epilepsy Behav **37**: 59-70.

Lemola, K., D. Chartier, Y. H. Yeh, M. Dubuc, R. Cartier, A. Armour, M. Ting, M. Sakabe, A. Shiroshita-Takeshita, P. Comtois and S. Nattel (2008). "Pulmonary vein region ablation in experimental vagal atrial fibrillation: role of pulmonary veins versus autonomic ganglia." Circulation **117**(4): 470-477.

Lewandowski, J., N. Rozwadowska, T. J. Kolanowski, A. Malcher, A. Zimna, A. Rugowska, K. Fiedorowicz, W. Labedz, L. Kubaszewski, K. Chojnacka, K. Bednarek-Rajewska, P. Majewski

and M. Kurpisz (2018). "The impact of in vitro cell culture duration on the maturation of human cardiomyocytes derived from induced pluripotent stem cells of myogenic origin." Cell Transplant **27**(7): 1047-1067.

Li, M. C. H., T. J. O'Brien, M. Todaro and K. L. Powell (2019). "Acquired cardiac channelopathies in epilepsy: Evidence, mechanisms, and clinical significance." Epilepsia **60**(9): 1753-1767.

Li, N., A. Kalyanasundaram, B. J. Hansen, E. J. Artiga, R. Sharma, S. H. Abudulwahed, K. M. Helfrich, G. Rozenberg, P. J. Wu, S. Zakharkin, S. Gyorke, P. M. Janssen, B. A. Whitson, N. A. Mokadam, B. J. Biesiadecki, F. Accornero, J. D. Hummel, P. J. Mohler, H. Dobrzynski, J. Zhao and V. V. Fedorov (2020). "Impaired neuronal sodium channels cause intranodal conduction failure and reentrant arrhythmias in human sinoatrial node." Nat Commun **11**(1): 512.

Lian, X., C. Hsiao, G. Wilson, K. Zhu, L. B. Hazeltine, S. M. Azarin, K. K. Raval, J. Zhang, T. J. Kamp and S. P. Palecek (2012). "Robust cardiomyocyte differentiation from human pluripotent stem cells via temporal modulation of canonical Wnt signaling." Proc Natl Acad Sci U S A **109**(27): E1848-1857.

Lin, X., N. Liu, J. Lu, J. Zhang, J. M. B. Anumonwo, L. L. Isom, G. I. Fishman and M. Delmar (2011). "Subcellular heterogeneity of sodium current properties in adult cardiac ventricular myocytes." Heart Rhythm **8**(12): 1923-1930.

Lin, X., H. O'Malley, C. Chen, D. Auerbach, M. Foster, A. Shekhar, M. Zhang, W. Coetzee, J. Jalife, G. I. Fishman, L. Isom and M. Delmar (2015). "Scn1b deletion leads to increased tetrodotoxin-sensitive sodium current, altered intracellular calcium homeostasis and arrhythmias in murine hearts." The Journal of Physiology **593**(6): 1389-1407.

Lin, X., H. O'Malley, C. Chen, D. Auerbach, M. Foster, A. Shekhar, M. Zhang, W. Coetzee, J. Jalife, G. I. Fishman, L. Isom and M. Delmar (2015). "Scn1b deletion leads to increased tetrodotoxin-sensitive sodium current, altered intracellular calcium homeostasis and arrhythmias in murine hearts." J Physiol **593**(6): 1389-1407.

Lipkind, G. M. and H. A. Fozzard (2008). "Voltage-gated Na channel selectivity: the role of the conserved domain III lysine residue." J Gen Physiol **131**(6): 523-529.

Liu, C., D. J. Tester, Y. Hou, W. Wang, G. Lv, M. J. Ackerman, J. C. Makielski and J. Cheng (2014). "Is sudden unexplained nocturnal death syndrome in Southern China a cardiac sodium channel dysfunction disorder?" Forensic Science International **236**: 38-45.

Liu, C. j., S. D. Dib-Hajj, M. Renganathan, T. R. Cummins and S. G. Waxman (2003). "Modulation of the cardiac sodium channel Nav1.5 by fibroblast growth factor homologous factor 1B." Journal of Biological Chemistry **278**(2): 1029-1036.

Liu, G., B. T. David, M. Trawczynski and R. G. Fessler (2020). "Advances in Pluripotent Stem Cells: History, Mechanisms, Technologies, and Applications." Stem Cell Rev Rep **16**(1): 3-32.

Liu, J., Z. Laksman and P. H. Backx (2016). "The electrophysiological development of cardiomyocytes." Adv Drug Deliv Rev **96**: 253-273.

Lopez-Santiago, L. F., W. J. Brackenbury, C. Chen and L. L. Isom (2011). "Na+ channel Scn1b gene regulates dorsal root ganglion nociceptor excitability in vivo." J Biol Chem **286**(26): 22913-22923.

Lopez-Santiago, L. F., L. S. Meadows, S. J. Ernst, C. Chen, J. D. Malhotra, D. P. McEwen, A. Speelman, J. L. Noebels, S. K. Maier, A. N. Lopatin and L. L. Isom (2007). "Sodium channel Scn1b null mice exhibit prolonged QT and RR intervals." J Mol Cell Cardiol **43**(5): 636-647.

Lopez-Santiago, L. F., L. S. Meadows, S. J. Ernst, C. Chen, J. D. Malhotra, D. P. McEwen, A. Speelman, J. L. Noebels, S. K. G. Maier, A. N. Lopatin and L. L. Isom (2007). "Sodium channel Scn1b null mice exhibit prolonged QT and RR intervals." Journal of Molecular and Cellular Cardiology **43**(5): 636-647.

Lowe, J. S., O. Palygin, N. Bhasin, T. J. Hund, P. A. Boyden, E. Shibata, M. E. Anderson and P. J. Mohler (2008). "Voltage-gated Nav channel targeting in the heart requires an ankyrin-G-dependent cellular pathway." Journal of Cell Biology **180**(1): 173-186.

Lu, Z., B. J. Scherlag, J. Lin, L. Yu, J. H. Guo, G. Niu, W. M. Jackman, R. Lazzara, H. Jiang and S. S. Po (2009). "Autonomic mechanism for initiation of rapid firing from atria and pulmonary veins: evidence by ablation of ganglionated plexi." Cardiovasc Res **84**(2): 245-252.

Lundy, S. D., W. Z. Zhu, M. Regnier and M. A. Laflamme (2013). "Structural and functional maturation of cardiomyocytes derived from human pluripotent stem cells." Stem Cells Dev **22**(14): 1991-2002.

Maier, S. K. G., R. E. Westenbroek, K. A. McCormick, R. Curtis, T. Scheuer and W. A. Catterall (2004). "Distinct Subcellular Localization of Different Sodium Channel α and β Subunits in Single Ventricular Myocytes from Mouse Heart." Circulation **109**(11): 1421-1427.

Maier, S. K. G., R. E. Westenbroek, K. A. Schenkman, E. O. Feigl, T. Scheuer and W. A. Catterall (2002). "An unexpected role for brain-type sodium channels in coupling of cell surface depolarization to contraction in the heart." Proceedings of the National Academy of Sciences **99**(6): 4073-4078.

Makara, M. A., J. Curran, S. C. Little, H. Musa, I. Polina, S. A. Smith, P. J. Wright, S. D. Unudurthi, J. Snyder, V. Bennett, T. J. Hund and P. J. Mohler (2014). "Ankyrin-G coordinates intercalated disc signaling platform to regulate cardiac excitability in vivo." Circulation Research **115**(11): 929-938.

Makita, N., P. B. Bennett and A. L. George (1994). "Voltage-gated Na+ channel beta 1 subunit mRNA expressed in adult human skeletal muscle, heart, and brain is encoded by a single gene." J Biol Chem **269**(10): 7571-7578.

Malek Mohammadi, M., A. Abouissa, I. Azizah, Y. Xie, J. Cordero, A. Shirvani, A. Gigina, M. Engelhardt, F. A. Trogisch, R. Geffers, G. Dobreva, J. Bauersachs and J. Heineke (2019). "Induction of cardiomyocyte proliferation and angiogenesis protects neonatal mice from pressure overload-associated maladaptation." JCI Insight **5**.

Malhotra, J. D., K. Kazen-Gillespie, M. Hortsch and L. L. Isom (2000). "Sodium channel beta subunits mediate homophilic cell adhesion and recruit ankyrin to points of cell-cell contact." J Biol Chem **275**(15): 11383-11388.

Malhotra, J. D., K. Kazen-Gillespie, M. Hortsch and L. L. Isom (2000). "Sodium channel β subunits mediate homophilic cell adhesion and recruit ankyrin to points of cell-cell contact." Journal of Biological Chemistry **275**(15): 11383-11388.

Malhotra, J. D., V. Thyagarajan, C. Chen and L. L. Isom (2004). "Tyrosine-phosphorylated and nonphosphorylated sodium channel β1 subunits are differentially localized in cardiac myocytes." Journal of Biological Chemistry **279**(39): 40748-40754.

Marban, E., T. Yamagishi and G. F. Tomaselli (1998). "Structure and function of voltage-gated sodium channels." J Physiol **508 (Pt 3)**: 647-657.

Marionneau, C., Y. Carrasquillo, A. J. Norris, R. R. Townsend, L. L. Isom, A. J. Link and J. M. Nerbonne (2012). "The sodium channel accessory subunit Navβ1 regulates neuronal excitability through modulation of repolarizing voltage-gated K^+ channels." The Journal of neuroscience : the official journal of the Society for Neuroscience **32**(17): 5716-5727.

Martinez-Moreno, R., E. Selga, H. Riuro, D. Carreras, M. Parnes, C. Srinivasan, M. F. Wangler, G. J. Perez, F. S. Scornik and R. Brugada (2020). "An SCN1B Variant Affects Both Cardiac-Type (NaV1.5) and Brain-Type (NaV1.1) Sodium Currents and Contributes to Complex Concomitant Brain and Cardiac Disorders." Front Cell Dev Biol **8**: 528742.

Massey, C. A., L. P. Sowers, B. J. Dlouhy and G. B. Richerson (2014). "Mechanisms of sudden unexpected death in epilepsy: the pathway to prevention." Nature Reviews Neurology **10**(5): 271-282.

Matamoros, M., M. Perez-Hernández, G. Guerrero-Serna, I. Amorós, A. Barana, M. Núñez, D. Ponce-Balbuena, S. Sacristán, R. Gómez, J. Tamargo, R. Caballero, J. Jalife and E. Delpón (2016). "Nav1.5 N-terminal domain binding to α1-syntrophin increases membrane density of human Kir2.1, Kir2.2 and Nav1.5 channels." Cardiovascular Research **110**(2): 279-290.

Matsumoto, M., A. Fujikawa, R. Suzuki, H. Shimizu, K. Kuboyama, T. Y. Hiyama, R. A. Hall and M. Noda (2012). "SAP97 promotes the stability of Nax channels at the plasma membrane." FEBS Letters **586**(21): 3805-3812.

Mazzola, L. and S. Rheims (2021). "Ictal and Interictal Cardiac Manifestations in Epilepsy. A Review of Their Relation With an Altered Central Control of Autonomic Functions and With the Risk of SUDEP." Front Neurol **12**: 642645.

McCain, M. L., H. Yuan, F. S. Pasqualini, P. H. Campbell and K. K. Parker (2014). "Matrix elasticity regulates the optimal cardiac myocyte shape for contractility." Am J Physiol Heart Circ Physiol **306**(11): H1525-1539.

McCormick, K. A., L. L. Isom, D. Ragsdale, D. Smith, T. Scheuer and W. A. Catterall (1998). "Molecular determinants of Na+ channel function in the extracellular domain of the beta1 subunit." Journal of Biological Chemistry **273**(7): 3954-3962.

McEwen, D. P., C. Chen, L. S. Meadows, L. Lopez-Santiago and L. L. Isom (2009). "The voltage-gated Na+channel β3 subunit does not mediate trans homophilic cell adhesion or associate with the cell adhesion molecule contactin." Neuroscience Letters **462**(3): 272-275.

Meadows, L., J. D. Malhotra, a. Stetzer, L. L. Isom and D. S. Ragsdale (2001). "The intracellular segment of the sodium channel beta 1 subunit is required for its efficient association with the channel alpha subunit." Journal of neurochemistry **76**(6): 1871-1878.

Meadows, L. S., J. Malhotra, A. Loukas, V. Thyagarajan, K. A. Kazen-Gillespie, M. C. Koopman, S. Kriegler, L. L. Isom and D. S. Ragsdale (2002). "Functional and biochemical analysis of a sodium channel beta1 subunit mutation responsible for generalized epilepsy with febrile seizures plus type 1." J Neurosci **22**(24): 10699-10709.

Mercier, A., R. Clément, T. Harnois, N. Bourmeyster, J. F. Faivre, I. Findlay, M. Chahine, P. Bois and A. Chatelier (2012). "The β1-Subunit of Nav1.5 Cardiac Sodium Channel Is Required for a Dominant Negative Effect through α -α Interaction." PLoS ONE **7**(11).

Miller, J. D., Y. M. Ganat, S. Kishinevsky, R. L. Bowman, B. Liu, E. Y. Tu, P. K. Mandal, E. Vera, J. W. Shim, S. Kriks, T. Taldone, N. Fusaki, M. J. Tomishima, D. Krainc, T. A. Milner, D. J. Rossi and L. Studer (2013). "Human iPSC-based modeling of late-onset disease via progerin-induced aging." Cell Stem Cell **13**(6): 691-705.

Mizuguchi, Y., S. Specht, J. G. Lunz, 3rd, K. Isse, N. Corbitt, T. Takizawa and A. J. Demetris (2012). "SPRR2A enhances p53 deacetylation through HDAC1 and down regulates p21 promoter activity." BMC Mol Biol **13**: 20.

Mohler, P. J., I. Rivolta, C. Napolitano, G. LeMaillet, S. Lambert, S. G. Priori and V. Bennett (2004). "Nav1.5 E1053K mutation causing Brugada syndrome blocks binding to ankyrin-G and expression of Nav1.5 on the surface of cardiomyocytes." Proceedings of the National Academy of Sciences **101**(50): 17533-17538.

Morgan, K., E. B. Stevens, B. Shah, P. J. Cox, a. K. Dixon, K. Lee, R. D. Pinnock, J. Hughes, P. J. Richardson, K. Mizuguchi and a. P. Jackson (2000). "Beta 3: an Additional Auxiliary Subunit of the Voltage-Sensitive Sodium Channel That Modulates Channel Gating With Distinct Kinetics." Proceedings of the National Academy of Sciences of the United States of America **97**(5): 2308-2313.

Nerbonne, J. M. and R. S. Kass (2005). "Molecular physiology of cardiac repolarization." Physiol Rev **85**(4): 1205-1253.

Neubauer, J., J.-S. Rougier, H. Abriel and C. Haas (2018). "Functional implications of a rare variant in the sodium channel β1B subunit (SCN1B) in a five-month old male sudden infant death syndrome (SIDS) case." HeartRhythm Case Reports.

Nguyen, H. M., H. Miyazaki, N. Hoshi, B. J. Smith, N. Nukina, A. L. Goldin and K. G. Chandy (2012). "Modulation of voltage-gated K+ channels by the sodium channel beta1 subunit." Proc Natl Acad Sci U S A **109**(45): 18577-18582.

Nguyen, H. M., H. Miyazaki, N. Hoshi, B. J. Smith, N. Nukina, A. L. Goldin and K. G. Chandy (2012). "Modulation of voltage-gated K+ channels by the sodium channel β1 subunit." Proceedings of the National Academy of Sciences of the United States of America **109**(45): 18577-18582.

Noda, M., S. Shimizu, T. Tanabe, T. Takai, T. Kayano, T. Ikeda, H. Takahashi, H. Nakayama, Y. Kanaoka, N. Minamino and et al. (1984). "Primary structure of Electrophorus electricus sodium channel deduced from cDNA sequence." Nature **312**(5990): 121-127.

O'Malley, H. A. and L. L. Isom (2015). "Sodium Channel beta Subunits: Emerging Targets in Channelopathies." Annu Rev Physiol **77**: 481-504.

O'Malley, H. A. and L. L. Isom (2015). "Sodium Channel β Subunits: Emerging Targets in Channelopathies." Annual Review of Physiology **77**(1): 481-504.

Odening, K. E. (2019). "The Role of Nav1.8 in Cardiac Electrophysiology-a Matter of the Heart or the Nerve?" Cardiovasc Drugs Ther **33**(6): 645-647.

Ogasawara, T., S. Okano, H. Ichimura, S. Kadota, Y. Tanaka, I. Minami, M. Uesugi, Y. Wada, N. Saito, K. Okada, K. Kuwahara and Y. Shiba (2017). "Impact of extracellular matrix on engraftment and maturation of pluripotent stem cell-derived cardiomyocytes in a rat myocardial infarct model." Sci Rep **7**(1): 8630.

Ogiwara, I., T. Nakayama, T. Yamagata, H. Ohtani, E. Mazaki, S. Tsuchiya, Y. Inoue and K. Yamakawa (2012). "A homozygous mutation of voltage-gated sodium channel beta(I) gene SCN1B in a patient with Dravet syndrome." Epilepsia **53**(12): e200-203.

Olesen, M. S., A. G. Holst, J. H. Svendsen, S. Haunso and J. Tfelt-Hansen (2012). "SCN1Bb R214Q found in 3 patients: 1 with Brugada syndrome and 2 with lone atrial fibrillation." Heart Rhythm **9**(5): 770-773.

Orrico, A., L. Galli, S. Grosso, S. Buoni, R. Pianigiani, P. Balestri and D. Sorrentino (2009). Mutational analysis of the SCN1A, SCN1B and GABRG2 genes in 150 Italian patients with idiopathic childhood epilepsies. **75:** 579-581.

Palatinus, J. A., M. P. O'Quinn, R. J. Barker, B. S. Harris, J. Jourdan and R. G. Gourdie (2010). "ZO-1 Determines Adherens and Gap Junction Localization at Intercalated Disks." Am J Physiol Heart Circ Physiol: 583-594.

Parikh, S. S., D. J. Blackwell, N. Gomez-Hurtado, M. Frisk, L. Wang, K. Kim, C. P. Dahl, A. Fiane, T. Tonnessen, D. O. Kryshtal, W. E. Louch and B. C. Knollmann (2017). "Thyroid and Glucocorticoid Hormones Promote Functional T-Tubule Development in Human-Induced Pluripotent Stem Cell-Derived Cardiomyocytes." Circ Res **121**(12): 1323-1330.

Patino, G. A., W. J. Brackenbury, Y. Bao, L. F. Lopez-Santiago, H. A. O'Malley, C. Chen, J. D. Calhoun, R. G. Lafreniere, P. Cossette, G. A. Rouleau and L. L. Isom (2011). "Voltage-gated Na+ channel beta1B: a secreted cell adhesion molecule involved in human epilepsy." J Neurosci **31**(41): 14577-14591.

Patino, G. A., L. R. Claes, L. F. Lopez-Santiago, E. A. Slat, R. S. Dondeti, C. Chen, H. A. O'Malley, C. B. Gray, H. Miyazaki, N. Nukina, F. Oyama, P. De Jonghe and L. L. Isom (2009). "A functional null mutation of SCN1B in a patient with Dravet syndrome." J Neurosci **29**(34): 10764-10778.

Patino, G. A., L. R. F. Claes, L. F. Lopez-Santiago, E. A. Slat, R. S. R. Dondeti, C. Chen, H. A. O'Malley, C. B. B. Gray, H. Miyazaki, N. Nukina, F. Oyama, P. De Jonghe and L. L. Isom (2009). "A Functional Null Mutation of SCN1B in a Patient with Dravet Syndrome." Journal of Neuroscience **29**(34): 10764-10778.

Pauza, D. H., K. Rysevaite, H. Inokaitis, M. Jokubauskas, A. G. Pauza, K. E. Brack and N. Pauziene (2014). "Innervation of sinoatrial nodal cardiomyocytes in mouse. A combined approach using immunofluorescent and electron microscopy." J Mol Cell Cardiol **75**: 188-197.

Pauza, D. H., I. Saburkina, K. Rysevaite, H. Inokaitis, M. Jokubauskas, J. Jalife and N. Pauziene (2013). "Neuroanatomy of the murine cardiac conduction system: a combined stereomicroscopic and fluorescence immunohistochemical study." Auton Neurosci **176**(1-2): 32-47.

Pellman, J., J. Zhang and F. Sheikh (2016). "Myocyte-fibroblast communication in cardiac fibrosis and arrhythmias: Mechanisms and model systems." J Mol Cell Cardiol **94**: 22-31.

Pensel, M. C., R. D. Nass, E. Tauboll, D. Aurlien and R. Surges (2020). "Prevention of sudden unexpected death in epilepsy: current status and future perspectives." Expert Rev Neurother **20**(5): 497-508.

Peters, N. S., N. J. Severs, S. M. Rothery, C. Lincoln, M. H. Yacoub and C. R. Green (1994). "Spatiotemporal relation between gap junctions and fascia adherens junctions during postnatal development of human ventricular myocardium." Circulation **90**(2): 713-725.

Petitprez, S., A. F. Zmoos, J. Ogrodnik, E. Balse, N. Raad, S. El-Haou, M. Albesa, P. Bittihn, S. Luther, S. E. Lehnart, S. N. Hatem, A. Coulombe and H. Abriel (2011). "SAP97 and dystrophin macromolecular complexes determine two pools of cardiac sodium channels Nav1.5 in cardiomyocytes." Circulation Research **108**(3): 294-304.

Petrucci, A. N., K. G. Joyal, B. S. Purnell and G. F. Buchanan (2020). "Serotonin and sudden unexpected death in epilepsy." Exp Neurol **325**: 113145.

Platonov, P. G. (2017). "Atrial fibrosis: an obligatory component of arrhythmia mechanisms in atrial fibrillation?" J Geriatr Cardiol **14**(4): 233-237.

Poulet, C., E. Wettwer, M. Grunnet, T. Jespersen, L. Fabritz, K. Matschke, M. Knaut and U. Ravens (2015). "Late Sodium Current in Human Atrial Cardiomyocytes from Patients in Sinus Rhythm and Atrial Fibrillation." PLoS One **10**(6): e0131432.

Pradervand, S., H. Yasukawa, O. G. Muller, H. Kjekshus, T. Nakamura, T. R. St Amand, T. Yajima, K. Matsumura, H. Duplain, M. Iwatate, S. Woodard, T. Pedrazzini, J. Ross, D. Firsov, B. C. Rossier, M. Hoshijima and K. R. Chien (2004). "Small proline-rich protein 1A is a gp130 pathway- and stress-inducible cardioprotective protein." EMBO J **23**(22): 4517-4525.

Qu, Y., L. L. Isom, R. E. Westenbroek, J. C. Rogers, T. N. Tanada, K. A. McCormick, T. Scheuer and W. A. Catterall (1995). "Modulation of cardiac Na+ channel expression in Xenopus oocytes by beta 1 subunits." J Biol Chem **270**(43): 25696-25701.

Rajendran, P. S., R. C. Challis, C. C. Fowlkes, P. Hanna, J. D. Tompkins, M. C. Jordan, S. Hiyari, B. A. Gabris-Weber, A. Greenbaum, K. Y. Chan, B. E. Deverman, H. Munzberg, J. L. Ardell, G. Salama, V. Gradinaru and K. Shivkumar (2019). "Identification of peripheral neural circuits that regulate heart rate using optogenetic and viral vector strategies." Nat Commun **10**(1): 1944.

Ramadan, W., N. Patel, S. Anazi, A. Y. Kentab, F. A. Bashiri, M. H. Hamad, L. Jad, M. A. Salih, H. Alsaif, M. Hashem, E. Faqeih, H. E. Shamseddin and F. S. Alkuraya (2017). "Confirming the recessive inheritance of SCN1B mutations in developmental epileptic encephalopathy." Clin Genet **92**(3): 327-331.

Ramadan, W., N. Patel, S. Anazi, A. Y. Kentab, F. A. Bashiri, M. H. Hamad, L. Jad, M. A. Salih, H. Alsaif, M. Hashem, E. Faqeih, H. E. Shamseddin and F. S. Alkuraya (2017). "Confirming the recessive inheritance of SCN1B mutations in developmental epileptic encephalopathy." Clin Genet.

Ravindran, K., K. L. Powell, M. Todaro and T. J. O'Brien (2016). "The pathophysiology of cardiac dysfunction in epilepsy." Epilepsy Res **127**: 19-29.

Rhett, J. M., J. Jourdan and R. G. Gourdie (2011). "Connexin 43 connexon to gap junction transition is regulated by zonula occludens-1." Mol Biol Cell **22**(9): 1516-1528.

Rhett, J. M., E. L. Ongstad, J. Jourdan and R. G. Gourdie (2012). "Cx43 associates with Nav1.5 in the cardiomyocyte perinexus." Journal of Membrane Biology **245**(7): 411-422.

Rhett, J. M., R. Veeraraghavan, S. Poelzing and R. G. Gourdie (2013). The perinexus: Sign-post on the path to a new model of cardiac conduction? **23:** 222-228.

Ribeiro, A. J., Y. S. Ang, J. D. Fu, R. N. Rivas, T. M. Mohamed, G. C. Higgs, D. Srivastava and B. L. Pruitt (2015). "Contractility of single cardiomyocytes differentiated from pluripotent stem cells depends on physiological shape and substrate stiffness." Proc Natl Acad Sci U S A **112**(41): 12705-12710.

Ripplinger, C. M., S. F. Noujaim and D. Linz (2016). "The nervous heart." Prog Biophys Mol Biol **120**(1-3): 199-209.

Riuró, H., O. Campuzano, E. Arbelo, A. Iglesias, M. Batlle, F. Pérez-Villa, J. Brugada, G. J. Pérez, F. S. Scornik and R. Brugada (2014). "A missense mutation in the sodium channel β1b subunit reveals SCN1B as a susceptibility gene underlying long QT syndrome." Heart Rhythm **11**(7): 1202-1209.

Rog-Zielinska, E. A., R. A. Norris, P. Kohl and R. Markwald (2016). "The Living Scar--Cardiac Fibroblasts and the Injured Heart." Trends Mol Med **22**(2): 99-114.

Rogart, R. B., L. L. Cribbs, L. K. Muglia, D. D. Kephart and M. W. Kaiser (1989). "Molecular Cloning of a Putative Tetrodotoxin-Resistant Rat Heart Na+ Channel Isoform." Proc Natl Acad Sci USA **86**(20): 8170-8174.

Rougier, J.-S., M. X. van Bemmelen, M. C. Bruce, T. Jespersen, B. Gavillet, F. Apothéloz, S. Cordonier, O. Staub, D. Rotin and H. Abriel (2005). "Molecular determinants of voltage-gated sodium channel regulation by the Nedd4/Nedd4-like proteins." American journal of physiology. Cell physiology **288**(3): C692-701.

Rysevaite, K., I. Saburkina, N. Pauziene, S. F. Noujaim, J. Jalife and D. H. Pauza (2011). "Morphologic pattern of the intrinsic ganglionated nerve plexus in mouse heart." Heart Rhythm **8**(3): 448-454.

Rysevaite, K., I. Saburkina, N. Pauziene, R. Vaitkevicius, S. F. Noujaim, J. Jalife and D. H. Pauza (2011). "Immunohistochemical characterization of the intrinsic cardiac neural plexus in whole-mount mouse heart preparations." Heart Rhythm **8**(5): 731-738.

Ryvlin, P., L. Nashef, S. D. Lhatoo, L. M. Bateman, J. Bird, A. Bleasel, P. Boon, A. Crespel, B. A. Dworetzky, H. Hogenhaven, H. Lerche, L. Maillard, M. P. Malter, C. Marchal, J. M. Murthy, M. Nitsche, E. Pataraia, T. Rabben, S. Rheims, B. Sadzot, A. Schulze-Bonhage, M. Seyal, E. L. So, M. Spitz, A. Szucs, M. Tan, J. X. Tao and T. Tomson (2013). "Incidence and mechanisms of cardiorespiratory arrests in epilepsy monitoring units (MORTEMUS): a retrospective study." Lancet Neurol **12**(10): 966-977.

Saburkina, I., L. Gukauskiene, K. Rysevaite, K. E. Brack, A. G. Pauza, N. Pauziene and D. H. Pauza (2014). "Morphological pattern of intrinsic nerve plexus distributed on the rabbit heart and interatrial septum." J Anat **224**(5): 583-593.

Satin, J., J. W. Kyle, M. Chen, P. Bell, L. L. Cribbs, H. A. Fozzard and R. B. Rogart (1992). "A mutant of TTX-resistant cardiac sodium channels with TTX-sensitive properties." Science **256**(5060): 1202-1205.

Savio-Galimberti, E., M. H. Gollob and D. Darbar (2012). "Voltage-gated sodium channels: biophysics, pharmacology, and related channelopathies." Front Pharmacol **3**: 124.

Scala, M., S. Efthymiou, T. Sultan, J. De Waele, M. Panciroli, V. Salpietro, R. Maroofian, P. Striano, F. Van Petegem, H. Houlden and F. Bosmans (2021). "Homozygous SCN1B variants causing early infantile epileptic encephalopathy 52 affect voltage-gated sodium channel function." Epilepsia **62**(6): e82-e87.

Scheffer, I. E., L. A. Harkin, B. E. Grinton, L. M. Dibbens, S. J. Turner, M. A. Zielinski, R. Xu, G. Jackson, J. Adams, M. Connellan, S. Petrou, R. M. Wellard, R. S. Briellmann, R. H. Wallace, J. C. Mulley and S. F. Berkovic (2006). "Temporal lobe epilepsy and GEFS+ phenotypes associated with SCN1B mutations." Brain **130**(1): 100-109.

Shi, Y., H. Inoue, J. C. Wu and S. Yamanaka (2017). "Induced pluripotent stem cell technology: a decade of progress." Nat Rev Drug Discov **16**(2): 115-130.

Shy, D., L. Gillet, J. Ogrodnik, M. Albesa, A. O. Verkerk, R. Wolswinkel, J. S. Rougier, J. Barc, M. C. Essers, N. Syam, R. F. Marsman, A. M. Van Mil, S. Rotman, R. Redon, C. R. Bezzina, C. A. Remme and H. Abriel (2014). "PDZ domain-binding motif regulates cardiomyocyte compartment-specific nav1.5 channel expression and function." Circulation **130**(2): 147-160.

Silva, J. (2014). "Slow inactivation of Na(+) channels." Handb Exp Pharmacol **221**: 33-49.

Sinnecker, D., K. L. Laugwitz and A. Moretti (2014). "Induced pluripotent stem cell-derived cardiomyocytes for drug development and toxicity testing." Pharmacol Ther **143**(2): 246-252.

Smith, A. S., J. Macadangdang, W. Leung, M. A. Laflamme and D. H. Kim (2017). "Human iPSC-derived cardiomyocytes and tissue engineering strategies for disease modeling and drug screening." Biotechnol Adv **35**(1): 77-94.

Snyders, D. J. (1999). "Structure and function of cardiac potassium channels." Cardiovascular research **42**(2): 377-390.

Sossalla, S., B. Kallmeyer, S. Wagner, M. Mazur, U. Maurer, K. Toischer, J. D. Schmitto, R. Seipelt, F. A. Schondube, G. Hasenfuss, L. Belardinelli and L. S. Maier (2010). "Altered Na(+) currents in atrial fibrillation effects of ranolazine on arrhythmias and contractility in human atrial myocardium." J Am Coll Cardiol **55**(21): 2330-2342.

Sreedhar, R., S. Arumugam, R. A. Thandavarayan, V. V. Giridharan, V. Karuppagounder, V. Pitchaimani, R. Afrin, M. Harima, M. Nakamura, K. Suzuki, N. Gurusamy, P. Krishnamurthy and K. Watanabe (2016). "Depletion of cardiac 14-3-3η protein adversely influences pathologic cardiac remodeling during myocardial infarction after coronary artery ligation in mice." International Journal of Cardiology **202**: 146-153.

Srinivasan, J., M. Schachner and W. a. Catterall (1998). "Interaction of voltage-gated sodium channels with the extracellular matrix molecules tenascin-C and tenascin-R." Proceedings of the National Academy of Sciences of the United States of America **95**(26): 15753-15757.

Stavrakis, S., H. Nakagawa, S. S. Po, B. J. Scherlag, R. Lazzara and W. M. Jackman (2015). "The role of the autonomic ganglia in atrial fibrillation." JACC Clin Electrophysiol **1**(1-2): 1-13.

Stuhmer, W., F. Conti, H. Suzuki, X. D. Wang, M. Noda, N. Yahagi, H. Kubo and S. Numa (1989). "Structural parts involved in activation and inactivation of the sodium channel." Nature **339**(6226): 597-603.

Szurhaj, W., A. Leclancher, A. Nica, B. Perin, P. Derambure, P. Convers, L. Mazzola, B. Godet, M. Faucanie, M. C. Picot and J. De Jonckheere (2021). "Cardiac Autonomic Dysfunction and Risk of Sudden Unexpected Death in Epilepsy." Neurology **96**(21): e2619-e2626.

Takahashi, K., K. Tanabe, M. Ohnuki, M. Narita, T. Ichisaka, K. Tomoda and S. Yamanaka (2007). "Induction of pluripotent stem cells from adult human fibroblasts by defined factors." Cell **131**(5): 861-872.

Takahashi, K. and S. Yamanaka (2006). "Induction of pluripotent stem cells from mouse embryonic and adult fibroblast cultures by defined factors." Cell **126**(4): 663-676.

Tallquist, M. D. and J. D. Molkentin (2017). "Redefining the identity of cardiac fibroblasts." Nat Rev Cardiol **14**(8): 484-491.

Tan, H. L., S. Kupershmidt, R. Zhang, S. Stepanovic, D. M. Roden, A. A. M. Wilde, M. E. Anderson and J. R. Balser (2002). "A calcium sensor in the sodium channel modulates cardiac excitability." Nature **415**(6870): 442-447.

Terlau, H., S. H. Heinemann, W. Stuhmer, M. Pusch, F. Conti, K. Imoto and S. Numa (1991). "Mapping the site of block by tetrodotoxin and saxitoxin of sodium channel II." FEBS Lett **293**(1-2): 93-96.

Tohyama, S., F. Hattori, M. Sano, T. Hishiki, Y. Nagahata, T. Matsuura, H. Hashimoto, T. Suzuki, H. Yamashita, Y. Satoh, T. Egashira, T. Seki, N. Muraoka, H. Yamakawa, Y. Ohgino, T. Tanaka, M. Yoichi, S. Yuasa, M. Murata, M. Suematsu and K. Fukuda (2013). "Distinct metabolic flow enables large-scale purification of mouse and human pluripotent stem cell-derived cardiomyocytes." Cell Stem Cell **12**(1): 127-137.

Tomson, T., L. Nashef and P. Ryvlin (2008). "Sudden unexpected death in epilepsy: current knowledge and future directions." Lancet Neurol **7**(11): 1021-1031.

Travers, J. G., F. A. Kamal, J. Robbins, K. E. Yutzey and B. C. Blaxall (2016). "Cardiac Fibrosis: The Fibroblast Awakens." Circ Res **118**(6): 1021-1040.

Tsan, Y.-C., Y.-T. Zhao, S. J. DePalma, A. Capilnasiu, Y.-W. Wu, B. Elder, I. Panse, S. Friedline, T. S. O'Leary, N. Wubshet, K. K. Y. Ho, M. J. Previs, D. Nordsletten, B. M. Baker, L. L. Isom, A. P. Liu and A. S. Helms (2021). "Biomechanics and Myofibrillar Alignment Enhance Contractile Development and Reproducibility in Stem Cell Derived Cardiac Muscle." bioRxiv: 2021.2005.2023.445330.

Tu, C., B. S. Chao and J. C. Wu (2018). "Strategies for Improving the Maturity of Human Induced Pluripotent Stem Cell-Derived Cardiomyocytes." Circ Res **123**(5): 512-514.

Ufford, K., S. Friedline, Z. Tong, V. T. Tang, A. S. Dobbs, Y. C. Tsan, S. L. Bielas, A. P. Liu and A. S. Helms (2021). "Myofibrillar Structural Variability Underlies Contractile Function in Stem Cell-Derived Cardiomyocytes." Stem Cell Reports **16**(3): 470-477.

Ulbricht, W. (2005). "Sodium channel inactivation: molecular determinants and modulation." Physiol Rev **85**(4): 1271-1301.

Vaidyanathan, R., Y. S. Markandeya, T. J. Kamp, J. C. Makielski, C. T. January and L. L. Eckhardt (2016). "IK1-enhanced human-induced pluripotent stem cell-derived cardiomyocytes: an improved cardiomyocyte model to investigate inherited arrhythmia syndromes." Am J Physiol Heart Circ Physiol **310**(11): H1611-1621.

Vaidyanathan, R., A. L. Vega, C. Song, Q. Zhou, B. Tan, S. Berger, J. C. Makielski and L. L. Eckhardt (2013). "The interaction of caveolin 3 protein with the potassium inward rectifier channel Kir2.1: Physiology and pathology related to long QT syndrome 9 (LQT9)." Journal of Biological Chemistry **288**(24): 17472-17480.

Van Bemmelen, M. X., J. S. Rougier, B. Gavillet, F. Apothéloz, D. Daidié, M. Tateyama, I. Rivolta, M. A. Thomas, R. S. Kass, O. Staub and H. Abriel (2004). "Cardiac voltage-gated sodium channel Nav1.5 is regulated by Nedd4-2 mediated ubiquitination." Circulation Research **95**(3): 284-291.

Vassilev, P., T. Scheuer and W. A. Catterall (1989). "Inhibition of inactivation of single sodium channels by a site-directed antibody." Proc Natl Acad Sci U S A **86**(20): 8147-8151.

Vassilev, P. M., T. Scheuer and W. A. Catterall (1988). "Identification of an intracellular peptide segment involved in sodium channel inactivation." Science **241**(4873): 1658-1661.

Veeraraghavan, R., G. S. Hoeker, A. Alvarez-Laviada, D. Hoagland, X. Wan, D. R. King, J. Sanchez-Alonso, C. Chen, J. Jourdan, L. L. Isom, I. Deschenes, J. W. Smyth, J. Gorelik, S. Poelzing and R. G. Gourdie (2018). "The adhesion function of the sodium channel beta subunit (beta1) contributes to cardiac action potential propagation." Elife **7**.

Vegh, A. M. D., S. N. Duim, A. M. Smits, R. E. Poelmann, A. D. J. Ten Harkel, M. C. DeRuiter, M. J. Goumans and M. R. M. Jongbloed (2016). "Part and Parcel of the Cardiac Autonomic Nerve System: Unravelling Its Cellular Building Blocks during Development." J Cardiovasc Dev Dis **3**(3).

Vermij, S. H., H. Abriel and T. A. B. van Veen (2017). Refining the molecular organization of the cardiac intercalated disc. **113:** 259-275.

Vilella, L., N. Lacuey, J. P. Hampson, M. R. S. Rani, R. K. Sainju, D. Friedman, M. Nei, K. Strohl, C. Scott, B. K. Gehlbach, B. Zonjy, N. J. Hupp, A. Zaremba, N. Shafiabadi, X. Zhao, V. Reick-Mitrisin, S. Schuele, J. Ogren, R. M. Harper, B. Diehl, L. Bateman, O. Devinsky, G. B. Richerson,

P. Ryvlin and S. D. Lhatoo (2019). "Postconvulsive central apnea as a biomarker for sudden unexpected death in epilepsy (SUDEP)." Neurology **92**(3): e171-e182.

Vreeker, A., L. van Stuijvenberg, T. J. Hund, P. J. Mohler, P. G. Nikkels and T. A. van Veen (2014). "Assembly of the cardiac intercalated disk during pre- and postnatal development of the human heart." PLoS One **9**(4): e94722.

Vreeker, A., L. van Stuijvenberg, T. J. Hund, P. J. Mohler, P. G. J. Nikkels and T. A. B. van Veen (2014). "Assembly of the cardiac intercalated disk during pre- and postnatal development of the human heart." PloS one **9**(4): e94722-e94722.

Vuorenpaa, H., K. Penttinen, T. Heinonen, M. Pekkanen-Mattila, J. R. Sarkanen, T. Ylikomi and K. Aalto-Setala (2017). "Maturation of human pluripotent stem cell derived cardiomyocytes is improved in cardiovascular construct." Cytotechnology **69**(5): 785-800.

Wallace, R. H., I. E. Scheffer, G. Parasivam, S. Barnett, G. B. Wallace, G. R. Sutherland, S. F. Berkovic and J. C. Mulley (2002). "Generalized epilepsy with febrile seizures plus: mutation of the sodium channel subunit SCN1B." Neurology **58**(9): 1426-1429.

Wallace, R. H., D. W. Wang, R. Singh, I. E. Scheffer, A. L. George, Jr., H. A. Phillips, K. Saar, A. Reis, E. W. Johnson, G. R. Sutherland, S. F. Berkovic and J. C. Mulley (1998). "Febrile seizures and generalized epilepsy associated with a mutation in the Na+-channel beta1 subunit gene SCN1B." Nat Genet **19**(4): 366-370.

Wang, L., Z. Han, J. Dai and K. Cao (2020). "Brugada Syndrome Caused by Sodium Channel Dysfunction Associated with a SCN1B Variant A197V." Arch Med Res **51**(3): 245-253.

Wang, Z., P. Page and S. Nattel (1992). "Mechanism of flecainide's antiarrhythmic action in experimental atrial fibrillation." Circ Res **71**(2): 271-287.

Watanabe, H., D. Darbar, D. W. Kaiser, K. Jiramongkolchai, S. Chopra, B. S. Donahue, P. J. Kannankeril and D. M. Roden (2009). "Mutations in sodium channel beta1- and beta2-subunits associated with atrial fibrillation." Circ Arrhythm Electrophysiol **2**(3): 268-275.

Watanabe, H., D. Darbar, D. W. Kaiser, K. Jiramongkolchai, S. Chopra, B. S. Donahue, P. J. Kannankeril and D. M. Roden (2009). "Mutations in Sodium Channel β1- and β2-Subunits

Associated With Atrial Fibrillation." Circulation: Arrhythmia and Electrophysiology **2**(3): 268-275.

Watanabe, H., T. T. Koopmann, S. Le Scouarnec, T. Yang, C. R. Ingram, J. J. Schott, S. Demolombe, V. Probst, F. Anselme, D. Escande, A. C. Wiesfeld, A. Pfeufer, S. Kaab, H. E. Wichmann, C. Hasdemir, Y. Aizawa, A. A. Wilde, D. M. Roden and C. R. Bezzina (2008). "Sodium channel beta1 subunit mutations associated with Brugada syndrome and cardiac conduction disease in humans." J Clin Invest **118**(6): 2260-2268.

West, J. W., D. E. Patton, T. Scheuer, Y. Wang, A. L. Goldin and W. A. Catterall (1992). "A cluster of hydrophobic amino acid residues required for fast Na(+)-channel inactivation." Proc Natl Acad Sci U S A **89**(22): 10910-10914.

Wong, H. K., T. Sakurai, F. Oyama, K. Kaneko, K. Wada, H. Miyazaki, M. Kurosawa, B. De Strooper, P. Saftig and N. Nukina (2005). "beta Subunits of voltage-gated sodium channels are novel substrates of beta-site amyloid precursor protein-cleaving enzyme (BACE1) and gamma-secretase." J Biol Chem **280**(24): 23009-23017.

Wong, H. K., T. Sakurai, F. Oyama, K. Kaneko, K. Wada, H. Miyazaki, M. Kurosawa, B. De Strooper, P. Saftig and N. Nukina (2005). "β subunits of voltage-gated sodium channels are novel substrates of β-site amyloid precursor protein-cleaving enzyme (BACE1) and γ-secretase." Journal of Biological Chemistry **280**(24): 23009-23017.

Xiao, Z. C., D. S. Ragsdale, J. D. Malhotra, L. N. Mattei, P. E. Braun, M. Schachner and L. L. Isom (1999). "Tenascin-R is a functional modulator of sodium channel β subunits." Journal of Biological Chemistry **274**(37): 26511-26517.

Xu, R., E. A. Thomas, E. V. Gazina, K. L. Richards, M. Quick, R. H. Wallace, L. A. Harkin, S. E. Heron, S. F. Berkovic, I. E. Scheffer, J. C. Mulley and S. Petrou (2007). "Generalized epilepsy with febrile seizures plus-associated sodium channel beta1 subunit mutations severely reduce beta subunit-mediated modulation of sodium channel function." Neuroscience **148**(1): 164-174.

Yamanaka, S. (2020). "Pluripotent Stem Cell-Based Cell Therapy-Promise and Challenges." Cell Stem Cell **27**(4): 523-531.

Yang, C., J. Al-Aama, M. Stojkovic, B. Keavney, A. Trafford, M. Lako and L. Armstrong (2015). "Concise Review: Cardiac Disease Modeling Using Induced Pluripotent Stem Cells." Stem Cells **33**(9): 2643-2651.

Yang, K. C., N. C. Foeger, C. Marionneau, P. Y. Jay, J. R. McMullen and J. M. Nerbonne (2010). "Homeostatic regulation of electrical excitability in physiological cardiac hypertrophy." J Physiol **588**(Pt 24): 5015-5032.

Yang, N., A. L. George, Jr. and R. Horn (1996). "Molecular basis of charge movement in voltage-gated sodium channels." Neuron **16**(1): 113-122.

Yang, N. and R. Horn (1995). "Evidence for voltage-dependent S4 movement in sodium channels." Neuron **15**(1): 213-218.

Yang, X., M. Rodriguez, L. Pabon, K. A. Fischer, H. Reinecke, M. Regnier, N. J. Sniadecki, H. Ruohola-Baker and C. E. Murry (2014). "Tri-iodo-l-thyronine promotes the maturation of human cardiomyocytes-derived from induced pluripotent stem cells." J Mol Cell Cardiol **72**: 296-304.

Yang, Y., Y. Ogawa, K. L. Hedstrom and M. N. Rasband (2007). "βIV spectrin is recruited to axon initial segments and nodes of Ranvier by ankyrinG." Journal of Cell Biology **176**(4): 509-519.

Yereddi, N. R., F. S. Cusdin, S. Namadurai, L. C. Packman, T. P. Monie, P. Slavny, J. J. Clare, A. J. Powell and A. P. Jackson (2013). "The immunoglobulin domain of the sodium channel beta3 subunit contains a surface-localized disulfide bond that is required for homophilic binding." FASEB J **27**(2): 568-580.

Yoshida, S., S. Miyagawa, S. Fukushima, T. Kawamura, N. Kashiyama, F. Ohashi, T. Toyofuku, K. Toda and Y. Sawa (2018). "Maturation of Human Induced Pluripotent Stem Cell-Derived Cardiomyocytes by Soluble Factors from Human Mesenchymal Stem Cells." Mol Ther **26**(11): 2681-2695.

Young, K. A. and J. H. Caldwell (2005). "Modulation of skeletal and cardiac voltage-gated sodium channels by calmodulin." Journal of Physiology **565**(2): 349-370.

Yu, J., M. A. Vodyanik, K. Smuga-Otto, J. Antosiewicz-Bourget, J. L. Frane, S. Tian, J. Nie, G. A. Jonsdottir, V. Ruotti, R. Stewart, Slukvin, II and J. A. Thomson (2007). "Induced pluripotent stem cell lines derived from human somatic cells." Science **318**(5858): 1917-1920.

Yuan, L., J. T. Koivumaki, B. Liang, L. G. Lorentzen, C. Tang, M. N. Andersen, J. H. Svendsen, J. Tfelt-Hansen, M. Maleckar, N. Schmitt, M. S. Olesen and T. Jespersen (2014). "Investigations

of the Navbeta1b sodium channel subunit in human ventricle; functional characterization of the H162P Brugada syndrome mutant." Am J Physiol Heart Circ Physiol **306**(8): H1204-1212.

Yuan, Y., H. A. O'Malley, M. A. Smaldino, A. A. Bouza, J. M. Hull and L. L. Isom (2019). "Delayed maturation of GABAergic signaling in the Scn1a and Scn1b mouse models of Dravet Syndrome." Sci Rep **9**(1): 6210.

Zaidi, A., P. Clough, P. Cooper, B. Scheepers and A. P. Fitzpatrick (2000). "Misdiagnosis of epilepsy: many seizure-like attacks have a cardiovascular cause." J Am Coll Cardiol **36**(1): 181-184.

Zarzoso, M., K. Rysevaite, M. L. Milstein, C. J. Calvo, A. C. Kean, F. Atienza, D. H. Pauza, J. Jalife and S. F. Noujaim (2013). "Nerves projecting from the intrinsic cardiac ganglia of the pulmonary veins modulate sinoatrial node pacemaker function." Cardiovasc Res **99**(3): 566-575.

Zhou, X. F. and R. A. Rush (1996). "Functional roles of neurotrophin 3 in the developing and mature sympathetic nervous system." Mol Neurobiol **13**(3): 185-197.

Zhu, W., W. Wang, P. Angsutararux, R. L. Mellor, L. L. Isom, J. M. Nerbonne and J. R. Silva (2021). "Modulation of the effects of Class-Ib antiarrhythmics on cardiac NaV1.5-encoded channels by accessory NaVbeta subunits." JCI Insight.